

Potential Determinants in Malignancy Growth, Angiogenesis and Metastasis

Hui Liu

ISBN	978-94-6361-438-2
Cover	Erwin Timmerman and Hui Liu
Layout	Hui Liu
Printing	Optima Grafische Communicatie, Rotterdam, The Netherlands

© Hui Liu, 2020

No part of this thesis may be reproduced, stored or transmitted in any form by any means without prior written permission from the author.

Potential Determinants in Malignancy Growth, Angiogenesis and Metastasis

Potentiële determinanten in de groei,
angiogenese en metastase van maligniteiten

Thesis

to obtain the degree of Doctor from the
Erasmus University Rotterdam
by command of the rector magnificus
Prof.dr. R.C.M.E. Engels
and in accordance with the decision of the Doctorate Board.

The public defence shall be held on
Thursday 9th July 2020 at 13:30 hrs

by

Hui Liu

born in Liaocheng, Shandong, China

Doctoral Committee:

Promotor: Prof. dr. A.B. Houtsmuller

Other members: Prof. dr. M.P. Peppelenbosch
Prof. dr. C.R.M. Rüegg
Prof. dr. N.J. Galjart

Co-promotor: Dr. T.L.M. ten Hagen

Contents

Chapter 1	General introduction	7
Chapter 2	A microcarrier-based spheroid 3D invasion assay to monitor dynamic cell movement in extracellular matrix	25
Chapter 3	CREPT promotes melanoma progression through accelerated proliferation and enhanced migration by RhoA-mediated actin filaments and focal adhesion formation	51
Chapter 4	Melanoma promotes pericyte survival under restrictive conditions and in vitro migration	81
Chapter 5	HOXA9 mediates and marks premalignant compartment size expansion in colonic adenomas	111
Chapter 6	General discussion	143
Chapter 7	Summary	163
	Samenvatting	165
Appendix	List of abbreviations	171
	PhD portfolio	175
	List of publications	177
	Acknowledgments	179
	Curriculum vitae	183

Chapter 1

General introduction

General background of cancer

Cancer is one of the leading causes of death worldwide. In 2018, it was estimated to be 18.1 million new cases and 9.6 million deaths of 36 cancer types combined in 185 countries globally [1]. The term cancer represents a collection of diseases which may affect any part of the body. They have different names on the basis of the affected organ and the main feature. Accordingly, the clinical manifestation is varying for diverse tumor types, or even within the same type, patients may have distinct outcome. For this reason, hundreds of thousands of researchers are engaged in cancer research, trying to understand more about the process of tumorigenesis and to find ways to block or inhibit tumor progression.

Although cancers show a diversity of features, they also have some in common. Hanahan and Weinberg have summarized eight hallmarks of cancer for the shared characteristics [2, 3]:

- 1) Cell growth and division with self-sufficiency of signals;
- 2) Uncontrolled growth and division regardless of antigrowth signals;
- 3) Avoidance of programmed cell death;
- 4) Limitless cell mitogenesis;
- 5) Inducing new blood vessel construction;
- 6) Tissue invasion and formation of metastases;
- 7) Metabolic reprogramming;
- 8) Evasion of the immune system.

In this thesis we described our work which correlated with several of the above hallmarks. It is simple to consider these hallmarks as individual processes, supposing oncogenic agents and signaling pathways have a one-to-one relationship with these events. In fact, cancer itself is a complicated, coordinated, organic entity. One oncogenic agent always influences several events through different signaling pathways. For instance, distinct p53 activities can regulate DNA damage responses and tumor suppression [4, 5], repress epithelial-mesenchymal transition and stem cell properties [6, 7], and inhibit angiogenesis through regulating proangiogenic and antiangiogenic factors [8-10]. Hypoxia is a situation with a lack of oxygen supply in tissues. This hypoxic condition could: 1) promote cell mobility and migration by inducing epithelial-mesenchymal transition [11]; 2) cause metabolic reprogramming to adapt to the restricted condition and reduce cell death [12, 13]; 3) induce cell cycle arrest resulting in chemoresistance because rapid mitotic cells are the target of some anti-tumor drugs [14]. The immune system contributes to recognizing and eliminating incipient cancer cells. However, there is increasing evidence to show the tumor-promoting effect of immune cells. Inflammation can contribute to several tumor

progressing events by providing bioactive molecules to tumor microenvironment. So many findings suggest that the cancer phenotype is the outcome of a combination of stimuli, inducers and suppressors, signal transduction pathways, and the resulting events, interweaving a function network. Taken this into account, research of tumorigenesis mechanism will be held under a wide perspective, resulting in a better translation from bench to bedside. Abnormal tumor cell growth and cell death

Normal cell growth is controlled by precisely programmed cell cycle to maintain homeostasis, which is not the case for cancer cells. They are capable of sustaining growth factors, which are produced by stromal cells and cancer cells themselves, to keep continuous proliferation [15-18]. Growth factor receptors at cell surface may be overexpressed, activated or structurally altered, making cells hyper-responsive to growth factor ligands [19]. Receptors react with ligands operating distinct downstream pathways, leading to crucial cellular activities like cell proliferation, survival and differentiation (Figure 1). Ras GTPase, in the center of its tumorigenic web, is involved in two independent pathways of proliferation: one is MAPK/ERK and PI3K/AKT/mTOR; the other includes activation of YAP1 and c-Myc [20-22]. Ras is often activated by ras gene missense mutation, disrupting the natural negative-feedback loop for excessive cell proliferation. In addition to activating pro-proliferative pathways, inactivation of tumor suppressor genes also plays a central role in tumor growth. Rb and TP53 have long been known as potent tumor suppressors. Retinoblastoma (Rb) protein, encoded by RB gene, is commonly inactivated in several tumor types. The defective RB pathway in cancer cells lack the gatekeeper of cell cycle process, resulting in persistent cell proliferation [23, 24]. The TP53 gene has almost the highest mutation frequency in human cancer [25]. The majority of TP53 alterations are missense mutations causing the production of mutant p53 protein. p53 is sensitive to stresses and abnormality sensors intracellularly, and responds by pausing cell cycle or even triggering apoptosis [26, 27].

Apoptosis, defined as programmed cell death, is the intrinsic barrier to prevent limitless tumor expansion [28]. The two well-known apoptosis cascades are the mitochondrial pathway and the extrinsic pathway. Requiring external stimulation, the extrinsic pathway is activated by death receptor family members, namely tumor necrosis factor receptor 1, FAS, tumor necrosis factor-related apoptosis-inducing ligand (TRAIL) receptor 1 and 2. After binding with ligands, the death receptor activates caspases, inducing extensive cleavage of caspase substrates and swift cell death [29]. The mitochondrial pathway, also known as intrinsic pathway, is triggered by intracellular stimuli such as DNA damage, endoplasmic reticulum stress and cytokine deprivation [30]. These apoptotic stimuli lead to increasing mitochondrial outer membrane permeabilization (MOMP), followed with caspase activation via the apoptosome [31].

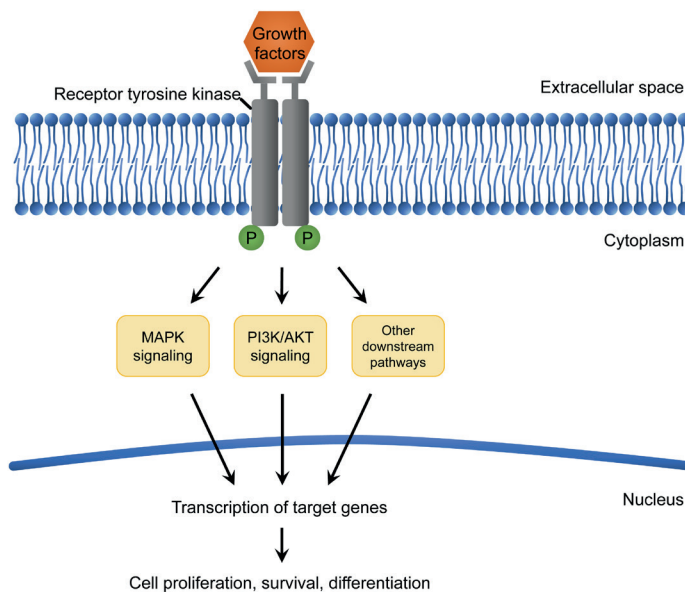


Figure 1. Receptor tyrosine kinase signaling in cell growth. Growth factors bind to receptor tyrosine kinases to activate them through dimerization and phosphorylation at the intracellular part. Further, several downstream signaling pathways can be triggered, leading to regulation of a series of cellular processes including cell proliferation, survival and differentiation.

The tumor growth is the result of dynamic equilibrium between cell division and cell death. Cancer cells have various ways to surpass the apoptotic process [28, 32]. In spite of downregulating and inactivating the tumor suppressors like p53, many tumors may upregulate anti-apoptotic proteins (Bcl-2) or downregulate pro-apoptotic proteins (BAX and BAK) to inhibit apoptotic cascade activation. While tumor cells try to evade apoptosis, we can also reversely use this mechanism to kill tumors. Many drugs have been developed to target both the extrinsic and intrinsic pathways [33-35]. The treatment targets include the Bcl-2 family anti-apoptotic proteins [36, 37], X-linked inhibitor of apoptosis protein (XIAP) [38], survivin [39] and other inhibitors of apoptosis.

Angiogenesis in tumors

As tumor cells grow rapidly, there is not enough oxygen and nutrients supply in local areas over $1\sim 2\text{ mm}^3$ [40]. Tumors need vasculature to transport “food” supply and metabolic waste to sustain their expansion. Angiogenesis is a process of new blood vessel formation from preexistent vessels. It occurs in normal physiological events including

vasculature development during embryogenesis, wound healing, chronic inflammation and the reproductive cycle in females [41, 42]. In these events angiogenesis is transiently switched on, but most of the time it remains quiescent. However during tumor progression, the “angiogenic switch” can be activated continuously to grow vessels for tumor cell metabolism [43-45].

Angiogenesis occurs in two ways: sprouting or splitting. Sprouting angiogenesis is featured by recruiting cells to form sprouts on preexisting vessels for new vessel formation (Figure 2). Pro-angiogenic growth factors activate endothelial cells to release proteases for basement membrane degradation. Next, the endothelial cells proliferate and migrate in surrounding matrix to form sprouts and grow to a mature vessel lumen. Unlike sprouting angiogenesis to form an entirely new vessel, splitting angiogenesis uses the existing vessel and divided it into two. The main mechanism is to reorganize basic structures so that growth factors can penetrate into the lumen for further cell recruitment and lumen growth. In both ways pro-angiogenic factors play a key role in stimulating cells to grow a vessel.

Pro-angiogenic factors can be produced by tumor cells or many tumor-associated stromal cells. Infiltrating leukocytes and tissue-resident cells including endothelial cells (EC), pericytes, fibroblasts and adipocytes are recruited to form a tumor microenvironment together with the extracellular matrix they are embedded in [46]. Macrophages are found associated with elevated vascular density in some tumor types [47-49]. Tumor-associated macrophages can produce growth factors and cytokines, including vascular endothelial

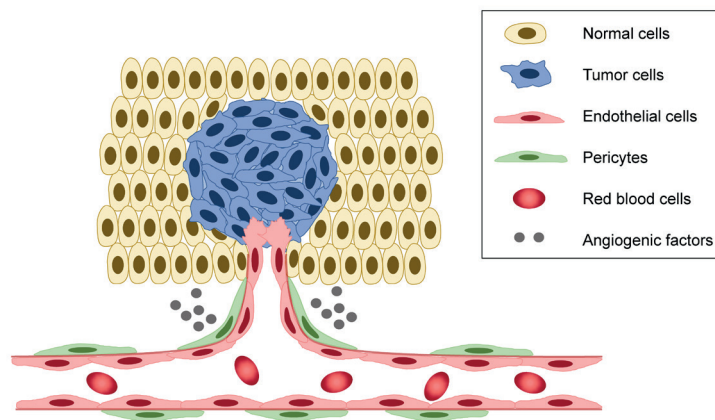


Figure 2. Schematic diagram of the sprouting angiogenic process.

growth factor A (VEGFA), placental growth factor (PlGF), tumor necrosis factor (TNF), fibroblast growth factor 2 (FGF2), interleukin-1 β (IL-1 β), IL-6 and IL-8, to support angiogenic process by inducing endothelial cell proliferation and survival [50-53]. The contribution of neutrophils in the early stages of tumor was highlighted in a mouse model through MMP9 mediating angiogenesis switch [54, 55]. B cells promote tumor angiogenesis by expressing pro-angiogenic mediators regulated by signal transducer and activator of transcription 3 (STAT3) [56]. Pericytes derived angiopoietin 1 (ANGPT1) binds to TIE2 on ECs to tighten EC junctions and stabilize new vessels [57, 58]. Pericytes can also express NG2 proteoglycan and neural cell adhesion molecule 1 (NCAM1) to induce pericyte recruitment for vasculature maturation [59, 60]. Although cancer associated fibroblasts are the main source of VEGFA, they can also produce platelet-derived growth factor C (PDGFC) to stimulate secretion of pro-angiogenic FGF2 and osteopontin [61-63].

As a result of prolonged pro-angiogenic signaling, the tumor vasculature has aberrant characteristics with multi-layered endothelial, redundant branching, loose cellular junctions and pericyte coverage. All these features lead to vascular immaturity, dysfunction and incoherent tumor perfusion [64-67]. The limited blood flow resulting in hypoxic and acidosis areas, which may obstruct therapeutic effectiveness and cause resistance to conventional therapies.

Tumor metastatic cascade

The main feature to distinguish benign and malignant tumor is metastasis. Malignant cells gain capability to invade adjacent tissue, transfer through circulation and seed in distant sites for a secondary growth (Figure 3). Metastasis is the major cause of tumor patient death, but current therapeutic strategies are not effective for most metastatic diseases. Therefore, determining cellular and molecular features of metastatic tumor cells is very important.

Epithelial cells, either normal or neoplastic, lack movement and often adhere to each other or extracellular matrix (ECM). To conquer this obstacle for invasion and metastatic dissemination, the epithelial-mesenchymal transition (EMT) occurs, remarkably increasing cell motility, invasiveness and the ability to degrade ECM components [68, 69]. EMT used to be considered as a complete transition between two cell states. However, the perspective has been expanded nowadays, with the introduction of partial EMT representing an intermediate phenotype of epithelial and mesenchymal hybrid [70-72]. Classical EMT regulation centers on suppression of E-cadherin transcription [73]. This process is triggered by a series of master EMT transcription factors including Twist, Snail,

Slug and Zeb [73, 74]. The transcripts are processed by multiple miRNAs (e.g. miR-200 and miR-34) or alternative splicing [75-77].

Migrating cells have a leading edge polarized in the direction of movement. At the leading edge, different plasma membrane protrusions were observed together with the dynamics of actin filaments [78]. The formation of actin filaments in the front is considered to provide the main motile forces for cell migration, based on the fact that actin filaments connect adhesions and cell membrane. Besides, microtubules also contribute to the formation and maintenance of membrane protrusions through their ability to resist high compressive loads and generate pushing forces [79]. Importantly, microtubules provide an intracellular transport network for the transport of membrane vesicles, signaling molecules and other cytoskeletal components, which are essential to maintain polarity and directional persistence of cell migration.

Tumor cells show a great diversity of migration morphologies and modes *in vivo* [80]. Motile tumor cells can migrate individually, either in an amoeboid-like way or as mesenchymal phenotype depending on cell contractility regulated by the Rho signaling pathway [81, 82]. Other cells may migrate as loosely attached stream following the same paths,

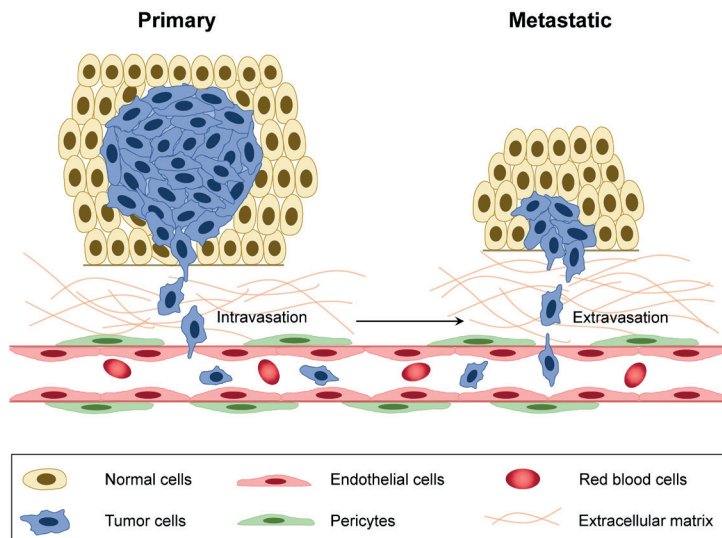


Figure 3. Main steps of the tumor metastatic process. Primary tumor cells invade basement membrane and extracellular matrix for migrating. Some cells further pass through vascular wall (intravasation) and travel with blood flow to a distant site where cells may extravasate. If local microenvironment is appropriate, tumor cells can grow to form a metastatic tumor.

or move as a cluster with cells attaching to each other. The collectively migrating cells have enhanced cell-cell interaction through cadherins and cell-ECM binding through integrins [83]. The mode of cell migration is not always fixed, which in some cases, can be changed. Treating MDCK epithelial cells with hepatocyte growth factor induces a transition from individual to collective migration through upregulation of N-cadherin [84]. In epithelial cancers invasive cells tend to migrate collectively and form scattered clusters [85, 86]. This may cause the presence of circulating tumor cell clusters rather than single cells [87, 88]. Instead of aggregating after intravasation, the clusters were found before entry of vessels and they are much easier to form colonies at secondary sites than single circulating tumor cells [89].

Two tumor types to study cancer hallmarks

To delineate the process of malignancy affected by intrinsic modulators and events, we performed biological studies in melanoma and colorectal carcinoma. Here we described the development and biology of these two tumor types.

Melanoma pathogenesis and biology

Melanoma derives from melanocytes which can produce the pigment melanin. The main location of malignancy occurrence is skin, but it can also be found in other tissues that contain melanocytes, e.g. eyes and intestines. According to clinical and epidemiologic evidence, people frequently exposed to intense or intermittent sunlight have a higher risk of melanoma [90]. This risk is much influenced by skin color. Populations with dark skin have a lower incidence than populations with light skin even exposed to equivalent amount of sunlight [91]. Although the mechanism by which ultraviolet (UV) induces melanoma occurrence is not fully delineated, the role of UV as the main mutagen in cutaneous melanoma is corroborated by genomic studies. Next generation sequencing shows increasing somatic mutation burdens in patients with UV exposure [92].

In general, the progression model follows a linear path from melanocytes, nevus, dysplastic nevus, melanoma *in situ*, to invasive melanoma. However, multiple melanoma types may not pass through all steps and only be linked with some of the precursor lesions [93]. The BRAF^{V600E} mutation exists as early in nevi without other pathogenic mutations found, suggesting a single pathogenic mutation is ample for nevus formation [94, 95]. Dysplastic nevi most likely occur *de novo* rather than from preexistent nevi according to histological observations [96]. Among them syndromic dysplastic nevi tend to have a high penetrance of melanoma with germline variants like cyclin-dependent kinase 4 (CDK4), protection of telomeres 1 (POT1), cyclin-dependent kinase inhibitor 2A (CDKN2A) and

telomerase reverse transcriptase (TERT); whereas sporadic dysplastic nevi are enriched with NRAS and BRAF^{nonV600E} mutations, both differing from typical nevi mutation [94, 97-99]. As to form a melanoma at the end, *in situ* or metastatic, the heterogeneous nature makes it complex featured by genomic instability, epigenomic alterations and epigenetic dysregulation [100]. The driver mutations, BRAF, NRAS and neurofibromatosis type 1 (NF1), activate the mitogen-activated protein kinase (MAPK) signaling pathway which controls cell cycle, proliferation, differentiation and transcription [101]. Unlike in precursor lesions, loss or inactivation of CDKN2A is found frequently in melanoma [102]. The CDKN2A locus encodes p16^{INK4A} and p14^{ARF}, two tumor suppressors with function of arresting cell cycle. To this end, inactivation or deletion of CDKN2A conduce to uncontrolled cell proliferation. At late stage of melanoma progression, mutations of TP53 and phosphatase and tensin homolog (PTEN) arise, leading to further malignant properties [103, 104].

Colorectal carcinoma malignant development

Colorectal carcinoma (CRC) is the 2nd most common cancer in women and 3rd most in men, accounting for 10% of the cancer deaths worldwide [1]. Lifestyle risk factors and hereditary factors contribute in part to CRC development. People with long-term inflammatory bowel diseases like ulcerative colitis and Crohn's disease have increasing risk for CRC [105, 106]. Currently CRC is presumed to be originated from stem cells or cells with stemness. These cells are found to possess genetic and epigenetic alterations which activate oncogenes and inhibit tumor suppressors for a progressive activity [107, 108]. Although the molecular characterization of CRC is complex with remarkable genetic heterogeneity, they have some features in common.

Three main histopathological trajectories are involved in the development of CRC, with various genetic and epigenetic events in a relatively sequential order [109]. First, the conventional adenoma-carcinoma pathway contributes to a big portion of CRC. It is typically initiated by adenomatous polyposis coli (APC) mutation, followed by RAS activation, SMAD deactivation or TP53 dysfunction. The APC protein usually prevents β -catenin accumulation. When APC alters genetically, β -catenin accumulates and translocates into the nucleus, activating the transcription of proto-oncogenes [110]. Another cascade referred to as serrated neoplasia pathway is correlated with BRAF mutation and that the CpG island methylation phenotype (CIMP). CIMP is characterized by global hypermethylation of CpG island sites in the promoter region, causing the inactivation of several tumor suppressor genes or other tumor-related genes [111]. CRC matching serrated lesions show a poor outcome compared to adenoma-carcinoma pathway related CRC [112]. Not limited to one phenotype, CIMP can also occurred in microsatellite

instability (MSI) pathway. MSI results from the inactivation of mismatch repair (MMR) genes, which is critical in genetic stability maintenance by repairing DNA replication and recombination errors, and responding to DNA damage. MSI tumors usually have abundant tumor-infiltrating T cells and result in a favorable patient outcome [113]. The detection of different precursor phenotypes and developing trajectories guide following intervention, which provides a promising strategy to prevent malignant transformation.

To standardize CRC classification based on clinical and molecular characteristics for more precise treatment, Guinney et al analyzed data from 4151 patients and categorized four consensus molecular subtypes (CMS) [114]. CMS1 (MSI immune) is characterized by high MSI, high CIMP, hypermutation, immune activation and worse prognosis. CMS2 (canonical) accounts for 37%, the biggest proportion of all subtypes. This type has epithelial features, high somatic copy number alterations (SCNA) together with Wnt and Myc signaling activation. CMS3 (metabolic) has mixed MSI status and evident metabolic dysregulation. CMS4 (mesenchymal) is featured by high TGF β signaling activation, stromal infiltration and angiogenesis. A fifth subtype was also found with mixed features of the above four types. It may represent a transition phenotype or intratumoral heterogeneity. The molecular classification of CRC may be the foundation of disease stratification and subtype-based targeted therapy.

Aims and scope of this thesis

The tumorigenesis and progression of malignancy is intricate with composition of various genetic alterations and pathways regulating cell growth and death, differentiation, migration, invasion and interaction with tumor microenvironment. The objective of this thesis is to link phenotypic features with genetic modulators in melanoma and colorectal carcinoma to find potential intrinsic drivers of tumor progression, which may serve as a target or inspire further development of therapeutic strategies in melanoma and colorectal carcinoma.

In **Chapter 2**, a microcarrier-based spheroid invasion assay is introduced to explore the dynamics of adherent cell behaviors including cell invasion in a three-dimensional model. This assay is described in detail and reckoned to be a fast and highly reproducible method for guidance of cell biology studies.

In **Chapter 3**, we elucidated the role of the oncoprotein CREPT in positive regulation of melanoma cell proliferation, migration and invasion *in vitro*. Its function in malignant process appears to be associated with RhoA-induced actin organization and focal adhesion assembly.

In **Chapter 4**, we evaluated the melanoma angiogenic potential through the effect of melanoma cell productions on promoting pericytes survival under hypoxia and migration *in vitro*.

In **Chapter 5**, we investigated the function of HOXA9 in colorectal cancer. The close correlation with adenoma growth and reduction in migration suggests that HOXA9 is a marker and driver of premalignant polyp growth.

In **Chapter 6**, the results of above chapters are discussed comprehensively together with future perspectives.

REFERENCES

1. Bray F, Ferlay J, Soerjomataram I, Siegel R.L., Torre L.A., Jemal A. Global cancer statistics 2018: GLOBOCAN estimates of incidence and mortality worldwide for 36 cancers in 185 countries. *Ca-Cancer J Clin.* 2018;68(6):394-424.
2. Hanahan D., Weinberg R.A. The hallmarks of cancer. *Cell.* 2000;100(1):57-70.
3. Hanahan D., Weinberg R.A. Hallmarks of Cancer: The Next Generation. *Cell.* 2011;144(5):646-74.
4. Brady C.A., Jiang D., Mello S.S., Johnson T.M., Jarvis L.A., Kozak M.M., et al. Distinct p53 Transcriptional Programs Dictate Acute DNA-Damage Responses and Tumor Suppression. *Cell.* 2011;145(4):571-83.
5. Aubrey B.J., Kelly G.L., Janic A., Herold M.J., Strasser A. How does p53 induce apoptosis and how does this relate to p53-mediated tumour suppression? *Cell Death Differ.* 2018;25(1):104-13.
6. Pinho A.V., Rooman I., Real F.X. p53-dependent regulation of growth, epithelial-mesenchymal transition and stemness in normal pancreatic epithelial cells. *Cell Cycle.* 2011;10(8):1312-21.
7. Chang C.J., Chao C.H., Xia W.Y., Yang J.Y., Xiong Y., Li C.W., et al. p53 regulates epithelial-mesenchymal transition and stem cell properties through modulating miRNAs. *Nat Cell Biol.* 2011;13(3):317-U296.
8. Teodoro J.G., Evans S.K., Green M.R. Inhibition of tumor angiogenesis by p53: a new role for the guardian of the genome. *J Mol Med-Jmm.* 2007;85(11):1175-86.
9. Assadian S., El-Assaad W., Wang X.Q.D., Gannon P.O., Barres V., Latour M., et al. p53 Inhibits Angiogenesis by Inducing the Production of Arresten. *Cancer Res.* 2012;72(5):1270-9.
10. Teodoro J.G., Parker A.E., Zhu X.C., Green M.R. p53-mediated inhibition of angiogenesis through up-regulation of a collagen prolyl hydroxylase. *Science.* 2006;313(5789):968-71.
11. Joseph J.P., Harishankar M.K., Pillai A.A., Devi A. Hypoxia induced EMT: A review on the mechanism of tumor progression and metastasis in OSCC. *Oral Oncol.* 2018;80:23-32.
12. Aragones J., Fraisl P., Baes M., Carmeliet P. Oxygen Sensors at the Crossroad of Metabolism. *Cell Metab.* 2009;9(1):11-22.
13. Ferreira L.M.R., Hebrant A., Dumont J.E. Metabolic reprogramming of the tumor. *Oncogene.* 2012;31(36):3999-4011.
14. Milane L., Duan Z.F., Amiji M. Role of hypoxia and glycolysis in the development of multi-drug resistance in human tumor cells and the establishment of an orthotopic multi-drug resistant tumor model in nude mice using hypoxic pre-conditioning. *Cancer Cell Int.* 2011;11.
15. Witsch E., Sela M., Yarden Y. Roles for Growth Factors in Cancer Progression. *Physiology.* 2010;25(2):85-101.
16. Strnad H., Lacina L., Kolar M., Cada Z., Vlcek C., Dvorankova B., et al. Head and neck squamous cancer stromal fibroblasts produce growth factors influencing phenotype of normal human keratinocytes. *Histochem Cell Biol.* 2010;133(2):201-11.
17. Kruslin B., Ulamec M., Tomas D. Prostate cancer stroma: an important factor in cancer growth and progression. *Bosnian J Basic Med.* 2015;15(2):1-8.
18. Mullen M., Gonzalez-Perez R.R. Leptin-Induced JAK/STAT Signaling and Cancer Growth. *Vaccines-Basel.* 2016;4(3).
19. Lemmon M.A., Schlessinger J. Cell Signaling by Receptor Tyrosine Kinases. *Cell.* 2010;141(7):1117-34.
20. Nussinov R., Tsai C.J., Jang H., Korcsmaros T., Csermely P. Oncogenic KRAS signaling and YAP1/beta-catenin: Similar cell cycle control in tumor initiation. *Semin Cell Dev Biol.* 2016;58:79-85.
21. Ratner N., Miller S.J. A RASopathy gene commonly mutated in cancer: the neurofibromatosis type 1 tumour suppressor. *Nature Reviews Cancer.* 2015;15(5):290-301.

22. Pylayeva-Gupta Y., Grabocka E., Bar-Sagi D. RAS oncogenes: weaving a tumorigenic web. *Nature Reviews Cancer*. 2011;11(11):761-74.
23. Dick F.A., Rubin S.M. Molecular mechanisms underlying RB protein function. *Nat Rev Mol Cell Bio*. 2013;14(5):297-306.
24. Weinberg R.A. The Retinoblastoma Protein and Cell-Cycle Control. *Cell*. 1995;81(3):323-30.
25. Kim M.P., Zhang Y., Lozano G. Mutant p53: Multiple Mechanisms Define Biologic Activity in Cancer. *Front Oncol*. 2015;5.
26. Kruijswijk F., Labuschagne C.F., Vousden K.H. p53 in survival, death and metabolic health: a lifeguard with a licence to kill. *Nat Rev Mol Cell Bio*. 2015;16(7):393-405.
27. Haupt S., Raghu D., Haupt Y. Mutant p53 Drives Cancer by Subverting Multiple Tumor Suppression Pathways. *Front Oncol*. 2016;6.
28. Lopez J., Tait S.W.G. Mitochondrial apoptosis: killing cancer using the enemy within. *Br J Cancer*. 2015;112(6):957-62.
29. Taylor R.C., Cullen S.P., Martin S.J. Apoptosis: controlled demolition at the cellular level. *Nat Rev Mol Cell Bio*. 2008;9(3):231-41.
30. Czabotar P.E., Lessene G., Strasser A., Adams J.M. Control of apoptosis by the BCL-2 protein family: implications for physiology and therapy. *Nat Rev Mol Cell Bio*. 2014;15(1):49-63.
31. Tait S.W.G., Green D.R. Mitochondria and cell death: outer membrane permeabilization and beyond. *Nat Rev Mol Cell Bio*. 2010;11(9):621-32.
32. Koff J.L., Ramachandiran S., Bernal-Mizrachi L. A Time to Kill: Targeting Apoptosis in Cancer. *Int J Mol Sci*. 2015;16(2):2942-55.
33. Liu Y., Zhu X. Endoplasmic reticulum-mitochondria tethering in neurodegenerative diseases. *Transl Neurodegener*. 2017;6:21.
34. Villa-Pulgarín J.A., Gajate C., Botet J., Jimenez A., Justies N., Varela-M R.E., et al. Mitochondria and lipid raft-located FoF1-ATP synthase as major therapeutic targets in the antileishmanial and anticancer activities of ether lipid edelfosine. *PLoS Negl Trop Dis*. 2017;11:e0005805.
35. Bao H., Zhang Q., Zhu Z., Xu H., Ding F., Wang M., et al. BHX, a novel pyrazoline derivative, inhibits breast cancer cell invasion by reversing the epithelial-mesenchymal transition and down-regulating Wnt/ β -catenin signaling. *Sci Rep*. 2017;7:9153.
36. Albershardt TC, Salerni BL, Soderquist RS, Bates DJ, Pletnev AA, Kisselev AF, Eastman A. Multiple BH3 mimetics antagonize antiapoptotic MCL1 protein by inducing the endoplasmic reticulum stress response and upregulating BH3-only protein NOXA. *J Biol Chem*. 2011;286(28):24882-24895.
37. Wu X, Liu X, Sengupta J, Bu Y, Yi F, Wang C, et al. Silencing of Bmi-1 gene by RNA interference enhances sensitivity to doxorubicin in breast cancer cells. *Indian J Exp Biol*. 2011;49(2):105-112.
38. Lopez J., Tait S.W.G. Mitochondrial apoptosis: Killing cancer using the enemy within. *Br J Cancer*. 2015;112:957-962.
39. Li D, Hu C, Li H. Survivin as a novel target protein for reducing the proliferation of cancer cells. *Biomed Rep*. 2018;8(5):399-406.
40. Spill F, Guerrero P, Alarcon T., Maini P.K., Byrne H.M. Mesoscopic and continuum modelling of angiogenesis. *J Math Biol*. 2015;70(3):485-532.
41. Carmeliet P. Mechanisms of angiogenesis and arteriogenesis. *Nat Med*. 2000;6(4):389-95.
42. Ribatti D., Nico B., Crivellato E. The development of the vascular system: a historical overview. *Methods Mol Biol*. 2015;1214:1-14.
43. Hanahan D, Folkman J. Patterns and emerging mechanisms of the angiogenic switch during tumorigenesis. *Cell*. 1996;86(3):353-64.
44. Carmeliet P., Jain R.K. Angiogenesis in cancer and other diseases. *Nature*. 2000;407(6801):249-57.

45. Baeriswyl V., Christofori G. The angiogenic switch in carcinogenesis. *Semin Cancer Biol.* 2009;19(5):329-37.
46. Egeblad M., Nakasone E.S., Werb Z. Tumors as Organs: Complex Tissues that Interface with the Entire Organism. *Dev Cell.* 2010;18(6):884-901.
47. Koh Y.W., Park C.S., Yoon D.H., Suh C., Huh J. CD163 Expression Was Associated with Angiogenesis and Shortened Survival in Patients with Uniformly Treated Classical Hodgkin Lymphoma. *PLoS One.* 2014;9(1).
48. Clear A.J., Lee A.M., Calaminici M., Ramsay A.G., Morris K.J., Hallam S., et al. Increased angiogenic sprouting in poor prognosis FL is associated with elevated numbers of CD163(+) macrophages within the immediate sprouting microenvironment. *Blood.* 2010;115(24):5053-6.
49. Halin S., Rudolfsson S.H., van Rooijen N., Bergh A. Extratumoral Macrophages Promote Tumor and Vascular Growth in an Orthotopic Rat Prostate Tumor Model. *Neoplasia.* 2009;11(2):177-86.
50. Hughes R., Qian B.Z., Rowan C., Muthana M., Keklikoglou I., Olson O.C., et al. Perivascular M2 Macrophages Stimulate Tumor Relapse after Chemotherapy. *Cancer Res.* 2015;75(17):3479-91.
51. Squadrito M.L., De Palma M. Macrophage regulation of tumor angiogenesis: Implications for cancer therapy. *Mol Aspects Med.* 2011;32(2):123-45.
52. Baer C., Squadrito M.L., Iruela-Arispe M.L., De Palma M. Reciprocal interactions between endothelial cells and macrophages in angiogenic vascular niches. *Exp Cell Res.* 2013;319(11):1626-34.
53. Murdoch C., Muthana M., Coffelt S.B., Lewis C.E. The role of myeloid cells in the promotion of tumour angiogenesis. *Nature Reviews Cancer.* 2008;8(8):618-31.
54. Nozawa H., Chiu C., Hanahan D. Infiltrating neutrophils mediate the initial angiogenic switch in a mouse model of multistage carcinogenesis. *Proc Natl Acad Sci U S A.* 2006;103(33):12493-8.
55. Bergers G., Brekken R., McMahon G., Vu T.H., Itoh T., Tamaki K., et al. Matrix metalloproteinase-9 triggers the angiogenic switch during carcinogenesis. *Nat Cell Biol.* 2000;2(10):737-44.
56. Yang C.M., Lee H., Pal S., Jove V., Deng J.H., Zhang W., et al. B Cells Promote Tumor Progression via STAT3 Regulated-Angiogenesis. *PLoS One.* 2013;8(5).
57. Huang H.H., Bhat A., Woodnutt G., Lappe R. Targeting the ANGPT-TIE2 pathway in malignancy. *Nature Reviews Cancer.* 2010;10(8):575-85.
58. Thurston G., Suri C., Smith K., McClain J., Sato T.N., Yancopoulos G.D., et al. Leakage-resistant blood vessels in mice transgenically overexpressing angiopoietin-1. *Science.* 1999;286(5449):2511-4.
59. You W.K., Yotsumoto F., Sakimura K., Adams R.H., Stallcup W.B. NG2 proteoglycan promotes tumor vascularization via integrin-dependent effects on pericyte function. *Angiogenesis.* 2014;17(1):61-76.
60. Er E.E., Valiente M., Ganesh K., Zou Y.L., Agrawal S., Hu J., et al. Pericyte-like spreading by disseminated cancer cells activates YAP and MRTF for metastatic colonization. *Nat Cell Biol.* 2018;20(8):966-+.
61. Gerber H.P., Kowalski J., Sherman D., Eberhard D.A., Ferrara N. Complete inhibition of rhabdomyosarcoma xenograft growth and neovascularization requires blockade of both tumor and host vascular endothelial growth factor. *Cancer Res.* 2000;60(22):6253-8.
62. Anderberg C., Li H., Fredriksson L., Andrae J., Betsholtz C., Li X.R., et al. Paracrine Signaling by Platelet-Derived Growth Factor-CC Promotes Tumor Growth by Recruitment of Cancer-Associated Fibroblasts. *Cancer Res.* 2009;69(1):369-78.
63. Hou X., Kumar A., Lee C., Wang B., Arjunan P., Dong L.J., et al. PDGF-CC blockade inhibits pathological angiogenesis by acting on multiple cellular and molecular targets. *Proc Natl Acad Sci U S A.* 2010;107(27):12216-21.
64. Hida K., Maishi N., Torii C., Hida Y. Tumor angiogenesis-characteristics of tumor endothelial cells. *Int J Clin Oncol.* 2016;21(2):206-12.
65. Bergers G., Benjamin L.E. Tumorigenesis and the angiogenic switch. *Nature Reviews Cancer.*

- 2003;3(6):401-10.
66. Morikawa S., Baluk P., Kaidoh T., Haskell A., Jain R.K., McDonald D.M. Abnormalities in pericytes on blood vessels and endothelial sprouts in tumors. *Am J Pathol.* 2002;160(3):985-1000.
 67. Aird W.C. Endothelial Cell Heterogeneity. *Cold Spring Harb Perspect Med.* 2012;2(1).
 68. Nieto M.A., Huang R.Y.J., Jackson R.A., Thiery J.P. EMT: 2016. *Cell.* 2016;166(1):21-45.
 69. Kalluri R., Weinberg R.A. The basics of epithelial-mesenchymal transition. *J Clin Invest.* 2009;119(6):1420-8.
 70. Grigore A.D., Jolly M.K., Jia D.Y., Farach-Carson M.C., Levine H. Tumor Budding: The Name is EMT. Partial EMT. *J Clin Med.* 2016;5(5):51.
 71. Yu M., Bardia A., Wittner B., Stott S., Smas M., Ting D., et al. Circulating tumor cells in human breast cancer exhibit dynamic changes in epithelial and mesenchymal composition. *Cancer Res.* 2013;73.
 72. Grande M.T., Sanchez-Laorden B., Lopez-Blau C., De Frutos C.A., Boutet A., Arevalo M., et al. Snail1-induced partial epithelial-to-mesenchymal transition drives renal fibrosis in mice and can be targeted to reverse established disease (vol 21, pg 989, 2015). *Nat Med.* 2015;21(9).
 73. Lamouille S., Xu J., Derynck R. Molecular mechanisms of epithelial-mesenchymal transition. *Nat Rev Mol Cell Bio.* 2014;15(3):178-96.
 74. De Craene B., Berx G. Regulatory networks defining EMT during cancer initiation and progression. *Nature Reviews Cancer.* 2013;13(2):97-110.
 75. Diaz-Lopez A., Moreno-Bueno G., Cano A. Role of microRNA in epithelial to mesenchymal transition and metastasis and clinical perspectives. *Cancer Manag Res.* 2014;6:205-16.
 76. Warzecha C.C., Carstens R.P. Complex changes in alternative pre-mRNA splicing play a central role in the epithelial-to-mesenchymal transition (EMT). *Semin Cancer Biol.* 2012;22(5-6):417-27.
 77. Braeutigam C., Rago L., Rolke A., Waldmeier L., Christofori G., Winter J. The RNA-binding protein Rbfox2: an essential regulator of EMT-driven alternative splicing and a mediator of cellular invasion. *Oncogene.* 2014;33(9):1082-92.
 78. Ridley A.J. Life at the leading edge. *Cell.* 2011;145(7):1012-22.
 79. Laan L., Husson J., Munteanu E.L., Kerssemakers J.W., Dogterom M. Force-generation and dynamic instability of microtubule bundles. *Proc Natl Acad Sci U S A.* 2008;105(26):8920-5.80. Clark A.G., Vignjevic D.M. Modes of cancer cell invasion and the role of the microenvironment. *Curr Opin Cell Biol.* 2015;36:13-22.
 81. Bergert M., Chandradoss S.D., Desai R.A., Paluch E. Cell mechanics control rapid transitions between blebs and lamellipodia during migration. *Proc Natl Acad Sci U S A.* 2012;109(36):14434-9.
 82. Sanz-Moreno V., Gadea G., Ahn J., Paterson H., Marra P., Pinner S., et al. Rac Activation and Inactivation Control Plasticity of Tumor Cell Movement. *Cell.* 2008;135(3):510-23.
 83. Friedl P., Alexander S. Cancer Invasion and the Microenvironment: Plasticity and Reciprocity. *Cell.* 2011;147(5):992-1009.
 84. Shih W.T., Yamada S. N-cadherin-mediated cell-cell adhesion promotes cell migration in a three-dimensional matrix. *J Cell Sci.* 2012;125(15):3661-70.
 85. Bronsert P., Enderle-Ammour K., Bader M., Timme S., Kuehs M., Csanadi A., et al. Cancer cell invasion and EMT marker expression: a three-dimensional study of the human cancer-host interface. *J Pathol.* 2014;234(3):410-22.
 86. Prall F. Tumour budding in colorectal carcinoma. *Histopathology.* 2007;50(1):151-62.
 87. Khoja L., Shenjere P., Hodgson C., Hodgetts J., Clack G., Hughes A., et al. Prevalence and heterogeneity of circulating tumour cells in metastatic cutaneous melanoma. *Melanoma Res.* 2014;24(1):40-6.
 88. Hou J.M., Krebs M.G., Lancashire L., Sloane R., Backen A., Swain R.K., et al. Clinical Significance and Molecular Characteristics of Circulating Tumor Cells and Circulating Tumor Microemboli in Patients

- With Small-Cell Lung Cancer. *J Clin Oncol*. 2012;30(5):525-32.
89. Aceto N., Bardia A., Miyamoto D.T., Donaldson M.C., Wittner B.S., Spencer J.A., et al. Circulating Tumor Cell Clusters Are Oligoclonal Precursors of Breast Cancer Metastasis. *Cell*. 2014;158(5):1110-22.
 90. Liu-Smith F., Farhat A.M., Arce A., Ziogas A., Taylor T., Wang Z., et al. Sex differences in the association of cutaneous melanoma incidence rates and geographic ultraviolet light exposure. *J Am Acad Dermatol*. 2017;76(3):499-+.
 91. Gilchrest B.A., Eller M.S., Geller A.C., Yaar M. The pathogenesis of melanoma induced by ultraviolet radiation. *N Engl J Med*. 1999;340(17):1341-8.
 92. Melamed R.D., Aydin I.T., Rajan G.S., Phelps R., Silvers D.N., Emmett K.J., et al. Genomic Characterization of Dysplastic Nevi Unveils Implications for Diagnosis of Melanoma. *J Invest Dermatol*. 2017;137(4):905-9.
 93. Shain A.H., Bastian B.C. From melanocytes to melanomas. *Nature Reviews Cancer*. 2016;16(6):345-58.
 94. Shain A.H., Yeh I., Kovalyshyn I., Sriharan A., Talevich E., Gagnon A., et al. The Genetic Evolution of Melanoma from Precursor Lesions. *N Engl J Med*. 2015;373(20):1926-36.
 95. Yeh I., von Deimling A., Bastian B.C. Clonal BRAF Mutations in Melanocytic Nevi and Initiating Role of BRAF in Melanocytic Neoplasia. *Jnci-J Natl Cancer I*. 2013;105(12):917-9.
 96. Duffy K., Grossman D. The dysplastic nevus: From historical perspective to management in the modern era. *J Am Acad Dermatol*. 2012;67(1).
 97. Robles-Espinoza C.D., Harland M., Ramsay A.J., Aoude L.G., Quesada V., Ding Z.H., et al. POT1 loss-of-function variants predispose to familial melanoma. *Nat Genet*. 2014;46(5):478-81.
 98. Goldstein A.M., Chan M., Harland M., Hayward N.K., Demenais F., Bishop D.T., et al. Features associated with germline CDKN2A mutations: a GenoMEL study of melanoma-prone families from three continents. *J Med Genet*. 2007;44(2):99-106.
 99. Law M.H., Bishop D.T., Lee J.E., Brossard M., Martin N.G., Moses E.K., et al. Genome-wide meta-analysis identifies five new susceptibility loci for cutaneous malignant melanoma. *Nat Genet*. 2015;47(9):987-+.
 100. Grzywa T.M., Paskal W., Wlodarski P.K. Intratumor and Intertumor Heterogeneity in Melanoma. *Transl Oncol*. 2017;10(6):956-75.
 101. Abildgaard C., Guldberg P. Molecular drivers of cellular metabolic reprogramming in melanoma. *Trends Mol Med*. 2015;21(3):164-71.
 102. Liu J.L., Fukunaga-Kalabis M., Li L., Herlyn M. Developmental pathways activated in melanocytes and melanoma. *Arch Biochem Biophys*. 2014;563:13-21.
 103. Birck A., Ahrenkiel V., Zeuthen J., Hou-Jensen K., Guldberg P. Mutation and allelic loss of the PTEN/MMAC1 gene in primary and metastatic melanoma biopsies. *J Invest Dermatol*. 2000;114(2):277-80.
 104. Papp T., Jafari M., Schiffmann D. Lack of p53 mutations and loss of heterozygosity in non-cultured human melanocytic lesions. *J Cancer Res Clin Oncol*. 1996;122(9):541-8.
 105. Jess T., Rungoe C., Peyrin-Biroulet L. Risk of Colorectal Cancer in Patients With Ulcerative Colitis: A Meta-analysis of Population-Based Cohort Studies. *Clin Gastroenterol Hepatol*. 2012;10(6):639-45.
 106. Hu T., Li L.F., Shen J., Zhang L., Cho C.H. Chronic Inflammation and Colorectal Cancer: The Role of Vascular Endothelial Growth Factor. *Curr Pharm Des*. 2015;21(21):2960-7.
 107. Medema J.P. Cancer stem cells: The challenges ahead. *Nat Cell Biol*. 2013;15(4):338-44.
 108. Nassar D., Blanpain C. Cancer Stem Cells: Basic Concepts and Therapeutic Implications. *Annu Rev Pathol-Mech*. 2016;11:47-76.
 109. Muzny D.M., Bainbridge M.N., Chang K., Dinh H.H., Drummond J.A., Fowler G., et al. Comprehensive molecular characterization of human colon and rectal cancer. *Nature*. 2012;487(7407):330-7.
 110. Markowitz S.D., Bertagnolli M.M. Molecular Origins of Cancer: Molecular Basis of Colorectal Cancer.

- N Engl J Med.* 2009;361(25):2449-60.
111. Mitchell E.P, Catalano P.J., Giantonio B.J., O'Dwyer P.J., Meropol N.J., Benson A., et al. CpG island methylator phenotype (CIMP) and outcome differences for African Americans (AA) and Caucasians (C) treated with FOLFOX4 or the combination with bevacizumab (B) in patients (pts) with metastatic colorectal cancer (MCRC): Results from the Eastern Cooperative Oncology Group study E3200. *J Clin Oncol.* 2014;32(15).
 112. De Sousa E Melo F, Wang X., Jansen M., Fessler E., Trinh A., de Rooij L.P.M.H., et al. Poor-prognosis colon cancer is defined by a molecularly distinct subtype and develops from serrated precursor lesions. *Nat Med.* 2013;19(5):614-8.
 113. Wu C., Bekaii-Saab T. CpG Island Methylation, Microsatellite Instability, and BRAF Mutations and Their Clinical Application in the Treatment of Colon Cancer. *Chemother Res Pract.* 2012;2012:359041.
 114. Guinney J, Dienstmann R., Wang X., de Reyniès A., Schlicker A., Soneson C., et al. The consensus molecular subtypes of colorectal cancer. *Nat Med.* 2015;21(11):1350-6.

Chapter 2

A microcarrier-based spheroid 3D invasion assay to monitor dynamic cell movement in extracellular matrix

Hui Liu, Tao Lu, Gert-Jan Kremers, Ann L.B. Seynhaeve,
Timo L.M. ten Hagen

Biological Procedures Online 2020.

ABSTRACT

Background: Cell invasion through extracellular matrix (ECM) is a critical step in tumor metastasis. To study cell invasion in vitro, the internal microenvironment can be simulated via the application of 3D models.

Results: This study presents a method for 3D invasion examination using microcarrier-based spheroids. Cell invasiveness can be evaluated by quantifying cell dispersion in matrices or tracking cell movement through time-lapse imaging. It allows measuring of cell invasion and monitoring of dynamic cell behavior in three dimensions. Here we show different invasive capacities of several cell types using this method. The content and concentration of matrices can influence cell invasion, which should be optimized before large scale experiments. We also introduce further analysis methods of this 3D invasion assay, including manual measurements and homemade semi-automatic quantification. Finally, our results indicate that the position of spheroids in a matrix has a strong impact on cell moving paths, which may be easily overlooked by researchers and may generate false invasion results.

Conclusions: In all, the microcarrier-based spheroids 3D model allows exploration of adherent cell invasion in a fast and highly reproducible way, and provides informative results on dynamic cell behavior in vitro.

Keywords: cell invasion, 3D, microcarrier beads, spheroids, time-lapse microscopy, quantification

INTRODUCTION

Malignant tumors have the potential to metastasize from the original tissue to a distant site, which is the main cause of morbidity and mortality in tumor patients. During this process, the basic but decisive step is migration of tumor cells through the extracellular matrix (ECM) either towards lymph and blood vessels, or to a secondary site after survival in circulation [1]. To disseminate in tissue, cells require adhesion, proteolysis of ECM components and migration, which also occurs in normal physiological processes like embryonic morphogenesis and wound healing [2]. There is a diversity of strategies for cells movement, either individually (e.g. amoeboid or mesenchymal migration) or collectively (multicellular streaming, cluster, strand or sheet), which are based on cell-cell adhesion and cell-matrix interaction [3-5]. This activity can be simulated and observed by *in vitro* models and optical imaging to study cellular and molecular mechanisms. Unlike 2D migration, a 3D matrix provides both a substructure and obstacles to all surfaces of cells during movement through the surroundings, which simulates cell movement through tissues. Importantly, 3D models provide more information on the process of cell migration and invasion, including cell morphological alterations, cell-cell interaction, cell-matrix interaction, and matrix remodeling. Therefore, 3D models can serve as a supplement or an advanced alternative to 2D assays.

To examine cell invasive potential, a variety of *in vitro* assays are developed in a 3D format. Among them the Transwell invasion assay, or Boyden chamber assay, is widely used. Basically, it includes seeding cells on a layer of ECM gel pre-coated on top of a porous membrane, and assessing cell invasion by measuring the number of cells passing through the ECM gel. The chamber invasion assay is straightforward to quantify invading cells induced by chemoattractants [6] or internal gene regulation [7]. Despite the advantages, this assay counts vertically invading cell numbers at the endpoint but neglects the whole invasion process. How cells move in matrix and interact with surroundings remains unclear. As a substitute, a matrix embedding cell culture offers more possibilities. Cell aggregates, such as multicellular spheroids, can be embedded in a 3D matrix and cells moving away from spheroids into the matrix are monitored by microscopy. This approach allows cells migrating in any direction and many migratory parameters can be detected, including cell trajectories, migration distance, and velocity. However, establishing spheroids has met with challenges such as absence of formation, lack of size and uniformity control, difficulty in manipulation, requirements of special equipment and training, and is time consuming [8, 9]. Most importantly, not all cells are capable to form tight and regular-shaped spheroids, but some end up as friable and loose aggregates, or aggregation does not occur at all, which complicates manipulation and use in an invasion assay [10-12]. Therefore, we choose microcarriers as a core to grow spheroids and to standardize the invasion assay in a simple and highly reproducible way. Adherent cells which

do not aggregate spontaneously, can attach to microcarriers and thus form spheroids. Interestingly, introduction of carriers also enables co-culture of different cell types in close proximity [13]. Although microcarrier-based spheroids, because of the core, do not mimic fully the *in vivo* situation of solid tumors, they are faster to establish and stabilize experimental conditions allowing easy duplication compared to cell-only spheroids. In this study, we describe a microcarrier-based spheroid model to investigate dynamic cell behavior in three dimensional matrices.

RESULTS

In this study we present a method for 3D invasion examination and introduce various measurements according to different experimental settings and requirements. The whole workflow and schematic diagram are shown in **Fig. 1**.

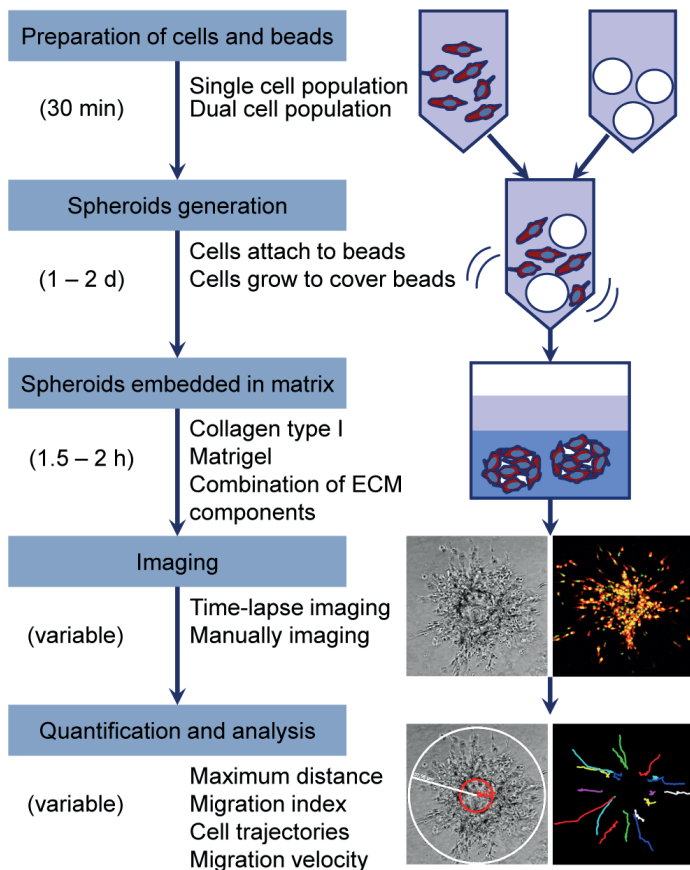


Fig. 1 Workflow diagram of the whole assay with schematic drawings and example results.

Different cell dispersions in matrix show invasiveness

This method can be used to monitor invasiveness of adherent cells in vitro. Here we performed the 3D invasion assay with melanoma cell lines (BLM, M14 and MEL57) and colorectal cancer cell lines (SW480 and CACO2) in 1.6 mg/ml collagen I gel. These cell lines were chosen because of difference in cell dispersion in the matrix allowing us show typical invasiveness patterns which may be visible. Images of cell dispersion were obtained every day and the maximum migration distances were measured. Within 4 days BLM cells migrated 285 μm away from the microcarrier core. M14 and MEL57 cells migrated slower than BLM cells, with dispersion of 270 μm and 110 μm in 6 days respectively. All melanoma cells moved collectively in the matrix, but single cells were visible in the front of migrating cells. In comparison, colorectal cancer cells SW480 show less invasive and remained more connected than melanoma cell lines. CACO2 cells grew around the core to multi-layers without any sign of migration into matrices (Fig. 2). The results indicate that this 3D assay can be used to examine cell invasive capacity and the way cells move.

The content and concentration of matrix influence cell invasion

To investigate the effect of matrix composition on cell invasion, we tried three different types of matrices. Here we use LLC cells because of the individual movement these cells show in collagen. Collagen type I and reconstituted basement membrane (Matrigel) are most commonly used matrices for 3D culture. Agar is a mixture of polysaccharides and can solidify at 32~40 °C for biological use. Fluorescently labeled LLC cells disperse collectively in Matrigel, spread individually in collagen, while no migration was observed in agar (Fig. 3a). Further, to test if the concentration of matrix would influence cell invasion, we used M14 cells in a gradient of collagen matrices and monitored cell invasion in 6 days. We selected M14 cells for the moderate migration speed this cell line shows; not too fast like LLC and BLM, which would move out of the imaging field, or too slow like MEL57, SW480 and CACO2 which demand long culture time causing cell proliferation to affect the migration. The results show a visible descending of migration distances in 4 to 6 days when collagen concentration was increased (Fig. 3b,c). These data demonstrate that different content and concentration of matrix influence cell invasion, so matrix can be adjusted for different experimental design.

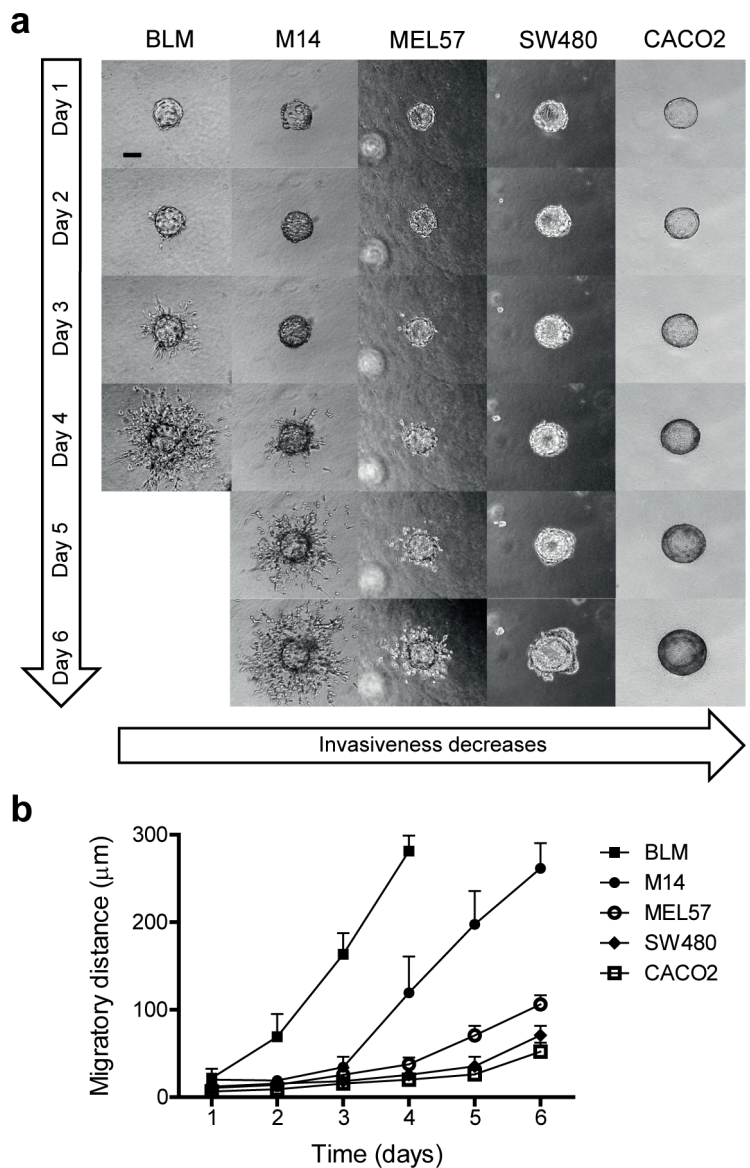
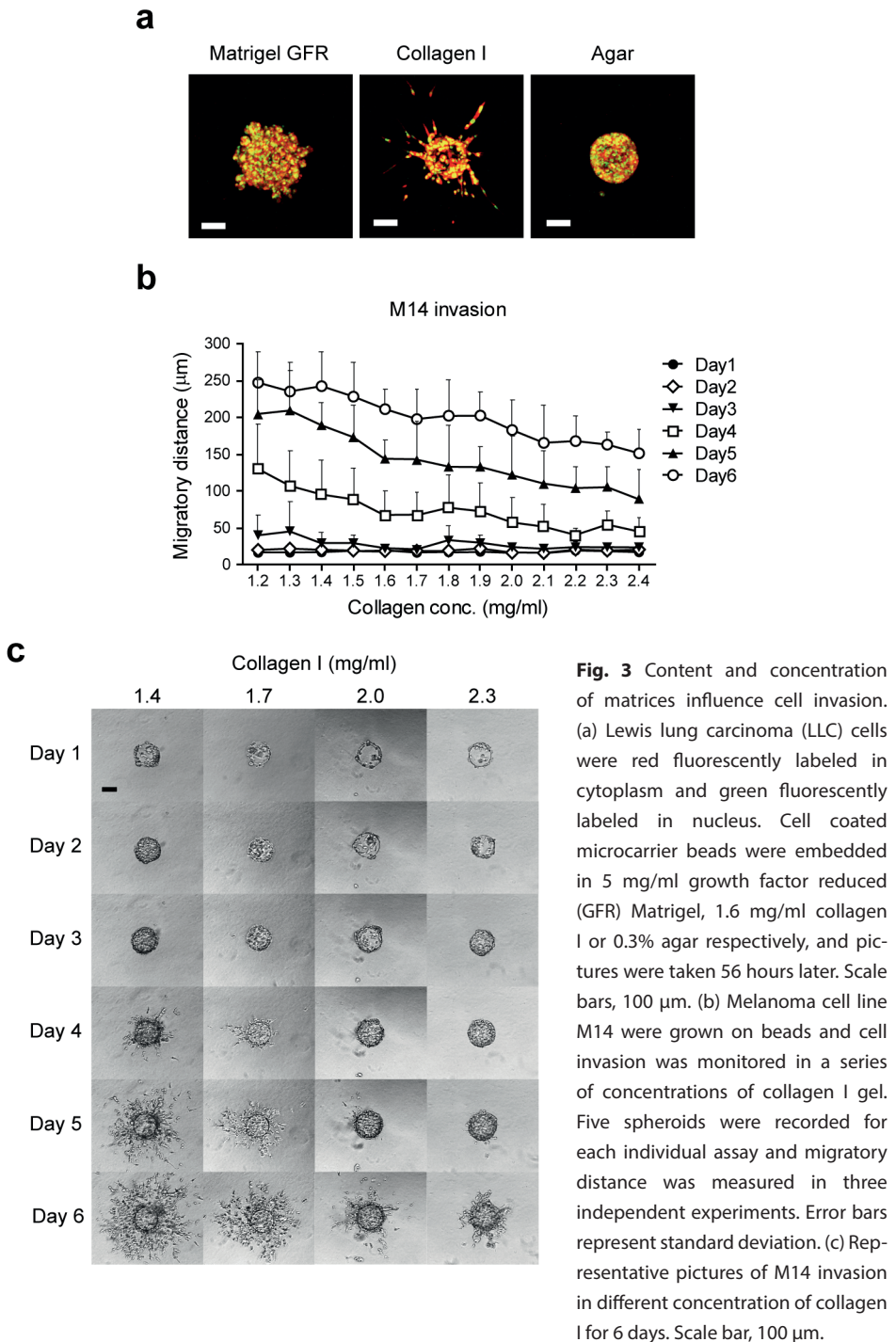


Fig. 2 Cell invasion/dispersion in collagen I. Melanoma cells (BLM, M14 and MEL57) and colorectal cancer cells (SW480 and CACO2) were cultured on microcarrier beads and embedded in collagen I gel (1.6 mg/ml). Cell invasion was monitored and recorded daily, and three independent experiments were performed. This assay lasted for 6 days and was ended when cells started to move out of frame. (a) Representative pictures of cell invasion of each cell line. All three melanoma cell lines displayed invasive behavior at different levels, while two colorectal cancer cell lines appeared less invasive, especially CACO2, which showed non-invasive growth. Scale bar, 100 μm . (b) Line graphs show maximum migration distances measured every day of each cell line.



Evaluating the effect of treatment on cell invasion using the migration index

To study the effect of a certain treatment on cell invasion, we added extra 10% FBS to a final concentration of 20% in culture medium as treatment, while using DMEM supplemented with 10%FBS as control. To reduce the interference factor of cell division, instead of using collectively migrating cells, we fluorescently labeled LLC cells, which move individually, for confocal time-lapse imaging in three dimensions. Because LLC cells move individually and are scattered in collagen, measuring maximum migration distance, i.e. the distance travelled by one cell furthest from the bead, may exaggerate the real invasiveness and may cause deviation in the data analysis. Therefore we defined a migration index considering the weights of all fast and slowly migrating cells. The migration index is calculated as the sum of all migrating cells multiplied with the distance from the bead. In this setting, fast migrating cells add more values than slowly migrating cells to the migration index, which shows the invasive capacity of the cells together. The cell number is difficult to obtain from images, so cell areas are used to represent cell numbers. Here we used homemade macros (Supplementary File 1) in Fiji to measure migrating cell areas at every 10 μm away from the core. In Fig. 4a, the red circle shows the microcarrier core and green areas indicate migrating cells included in data analysis. At 72 hours, cells with 20% FBS supplemented in medium seem to have larger migration areas at all distance ranges than cells in 10% medium, while the maximum distances in both groups are very close, around 350 μm (Fig. 4b). This result indicates the necessity of introducing the migration index. After computing the migration index of all time points, we found no significant difference between 10% and 20% medium, although an increasing trend was observed in 20% medium (Fig. 4c). The data reveal that the migration index calculation may be affected by increased cell proliferation, and reducing nutrients in the medium will make results of cell invasion more convincing.

The position of spheroids in 3D matrix influences cell invasion

During experiments using this 3D assay, we observed that spheroids might settle at the bottom of the culture plate because of the softness of the gel. When spheroids touch the bottom, most cells prefer migrating along the bottom instead of invading the collagen scaffold (Fig. 5a). This is possibly due to the low resistance in the interface between gel and bottom surface. The spheroids at the bottom cannot be included in data analysis because of exaggerated cell migration distances. If this settlement of beads at the bottom of the well occurs to most spheroids, the matrix concentration might be too low. Normally, increasing the concentration by 0.1~0.2 mg/ml can improve the viscosity of matrix during gel preparation but not reduce migration distance too much (Fig. 3b). In order to avoid beads to settle at the bottom, and to keep the matrix concentration as low as required, we tried to make a sandwich gel consisting of a bottom gel without spheroids

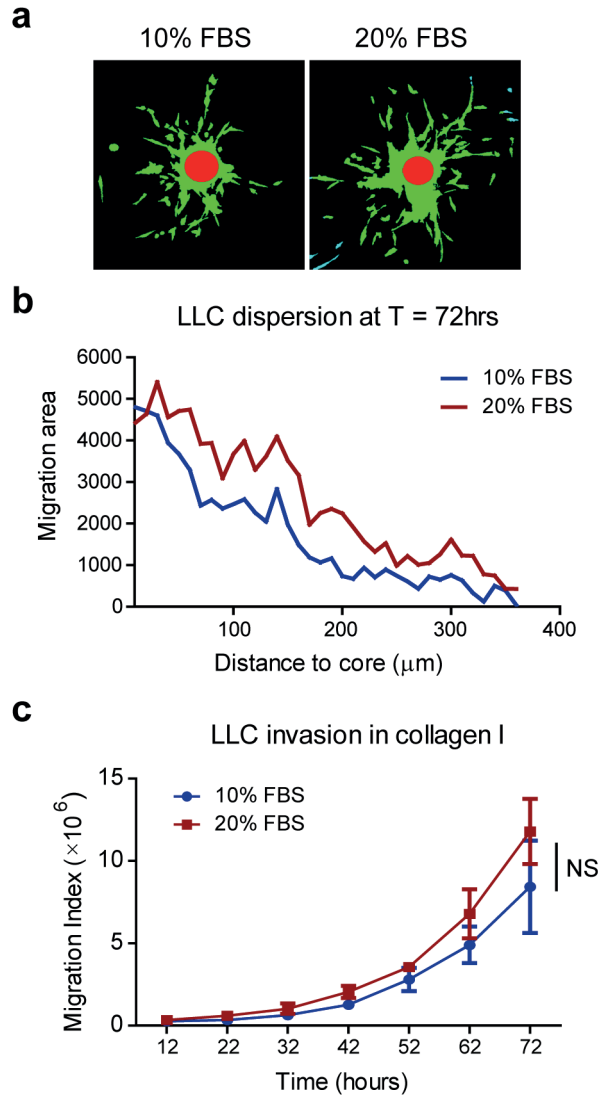


Fig. 4 Migration index shows cell invasive capacity. Fluorescently labeled LLC cells were used for invasion test in this 3D assay to compare the effect of 20% FBS vs. 10% FBS. (a) Representative pictures of LLC cell dispersion at 72 hours. Cell were color coded for analysis after running additional macros in Fiji. Red circles show microcarrier beads in spheroids, and green areas show distribution of migrating cells at 72 hours. (b) Line graph shows migration area changes based on the distance to core at T = 72 hours. (c) Calculation of migration index using data of each time point. Data represent mean \pm standard deviation (N=3). NS, not significant.

and a top gel with spheroids. Interestingly, spheroids could be found in the interface between the two layers of gel and most cells appeared to move in this interface (Fig. 5b). A possible solution could be inverting the culture plate for 1-2 min at room temperature (Fig. 5c), which can, however, only be applied to 96-well format as the well is small enough to retain the viscous liquid. Making use of fluidity of the gel at a certain temperature is another solution. When a low matrix concentration is used, the gel mixed with the cell-coated beads may be pipetted carefully at room temperature to keep the beads in the gel by increasing the viscosity. A proper position of spheroids in the matrix will allow cells to migrate evenly to all directions (Fig. 5d), which shows the innate cell invasion capacity in matrix. Here we show incorrect positions of spheroids in matrices and possible solutions to obtain proper positions for good experiments.

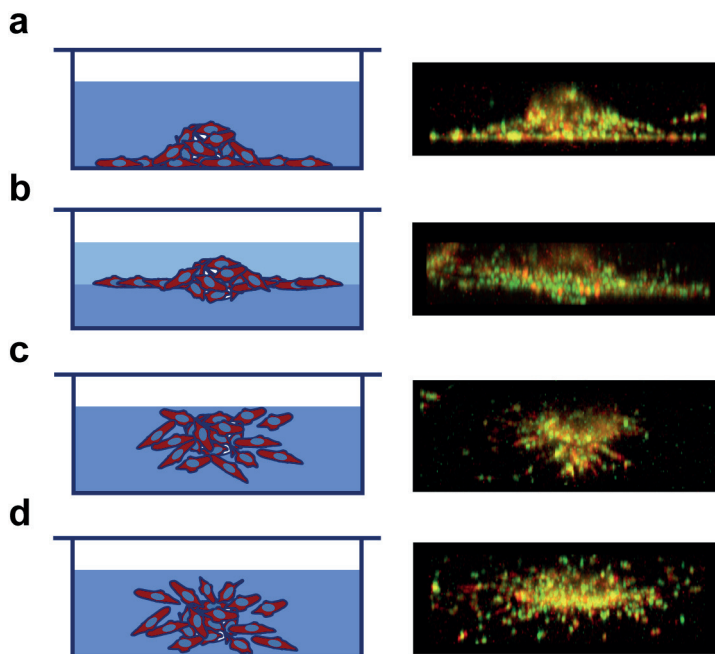


Fig. 5 Positions of spheroids in matrices and subsequent cell migration. Schematic diagrams on the left panel indicate corresponding spheroids position of the fluorescent image on the right panel. The images show an x-z view of LLC cells migrating in collagen I. (a) Spheroids sediment at the bottom in matrix and cells tend to follow the interface between gel and bottom surface. (b) A bottom layer of gel was made in the culture plate before adding matrix with spheroids. Most cells move along the interface between the two layers of gel. (c) To prevent spheroids settling, 96-well plate was inverted for 1-2 min at room temperature and spheroids may stay in matrix or near to top. (d) A representative picture of cell dispersing when spheroids are in a proper position of a homogenous collagen I gel.

DISCUSSION

This microcarrier-based spheroid invasion assay provides a powerful approach to assess cell biological behavior in a 3D format, including motility, invasion, angiogenesis, morphological changes, and cell-cell interaction. This method has been used to study the effect of specific gene on cell migration and invasion [14, 15]. It can also be adapted to investigate endothelial cells sprouting and vessel formation [16-18]. After microscopy the gel with invading cells can be fixed for immunofluorescence staining, or can be degraded to isolate cells for further analysis.

The application of microcarrier beads is a fast and highly reproducible way to make spheroids. It allows adherent cells, especially cells which cannot form aggregates with regular shape, to be embedded in matrix as spheroids for invasion study. The microcarrier beads we used in this assay are made of cross-linked dextran coated with a thin layer of denatured collagen. The coating provides a good culture surface for cells to attach and grow. Considering different cell types, beads can be coated with other attachment factors to fit demanding culture conditions.

The matrix selection may lead to different results of cell invasion. Collagen I is the main component of ECM and forms fibrillary networks to withstand stretching. Matrigel is extracted from Engelbreth-Holm-Swarm murine sarcoma and consists of laminin, collagen IV, heparin sulfate proteoglycans, entactin and a few growth factors, which simulates the ECM complex [19]. Here we used growth factor reduced Matrigel so as to decrease the impact of these factors on cell proliferation and invasion. To examine cell invasiveness both of the matrices mentioned above can be used in this method. Importantly, other types of matrices extracted from animal or human tissues can be used as an alternative as long as the matrix can solidify at 37°C [20]. Moreover, modification of the matrix by adding ECM components enables fine tuning of the conditions in which the cells reside. Our results indicate that the content and concentration of matrix will affect cell performance and therefore results. For appropriate use of this method we recommend to choose or modify the matrix according to the experimental design, and to try different concentrations or compositions if necessary.

In this study we dilute matrix with serum-free medium to generate a determined concentration. On top of the gel culture medium is added to maintain cell growth and prevent gel from drying out. To examine if agents added to the culture medium would influence cell behavior, we compared cell invasion when exposed to 10 or 20% serum. Although a higher serum concentration did not increase the outcome significantly, a positive trend was observed because of enhanced cell proliferation with or without migration. Cell proliferation is inevitable but can be reduced by decreasing the concentration of serum or other growth promoting supplements. Our results indicate that nutrients or treatments in

the medium can penetrate into the gel and act on the cells. So, to test different treatments in this 3D invasion assay, growth factors, inhibitors or drugs can be supplemented either in the medium or directly in the gel.

Another interesting finding is that the position of a spheroid in the matrix has an impact on cell moving paths. When spheroids sediment at the bottom of a culture vessel, most cells move along the interface between culture vessel and matrix; while if spheroids are in the middle of two gel layers as a “sandwich”, most cells move between these two gel layers. These observations demonstrate that cells tend to migrate along the path of the least resistance, and researchers need to pay attention to this issue when using this method or similar 3D settings.

Although the microcarrier-based 3D invasion assay has a broad application, the presence of a carrier limits the use to study tumor cell behavior in a spheroid with an anoxic core. Moreover, to study infiltration of tumor cells into a spheroid of normal cells, or to study infiltration of immune cells into a tumor cell spheroid, the assay needs to be extended. A multilayer spheroid can be created over time for this purpose by adjusting the matrix to inhibit migration away from the bead but allow growth. Notably, the described microcarrier-based method cannot be applied to non-adherent cells.

CONCLUSIONS

This study displays a highly reproducible and less time-consuming 3D invasion assay together with practical quantifications and data analysis. Introducing microcarriers to generation of spheroids contributes to uniformity control, short experimental period and the use of a broad range of cell types. We also show time-lapse imaging of cell movement in 3D, which allows visualization of the whole process and advanced analysis. In conclusion, this microcarrier-based 3D invasion assay is a powerful tool to study cell invasion *in vitro*.

MATERIALS AND METHODS

Reagents

Dulbecco's modified Eagle's medium (DMEM, D0819, Sigma); Trypsin-EDTA (BE-17-161E, Lonza); Dulbecco's Phosphate Buffered Saline (PBS, Ca²⁺ and Mg²⁺ free, D8537, Sigma-Aldrich); Fetal bovine serum (FBS, F7524, Sigma); Collagen type I, rat tail (08-115; Millipore); Matrigel Growth factor reduced (356231, Corning); Agar (A1296, Sigma-Aldrich); Sodium bicarbonate (11810-017, Life technologies).

Imaging system and climate control configuration

As time-lapse imaging may take hours to days, a screening system, e.g. confocal microscope, integrated with a cell incubation setup is indispensable. Here we show our imaging workspace setup as an example (Fig. 6). A sealed Perspex box was built on the microscope to maintain temperature. The box is heated by a heating unit through a ventilation duct. A sensor in the box is connected to the temperature controller normally set to 37 °C. A 5% CO₂/air mixture is supplied through a gas wash bottle for humidification, and the flow goes directly to the cell culture plate. Medium evaporation needs to be tested to optimize air flow before experiment. Since cells move in three dimensions in matrices, the microscope with z stacks scanning is recommended for continuous screening with the climate control system. A standard microscope can be used for manual image acquisition as the focus needs to be adjusted over time.

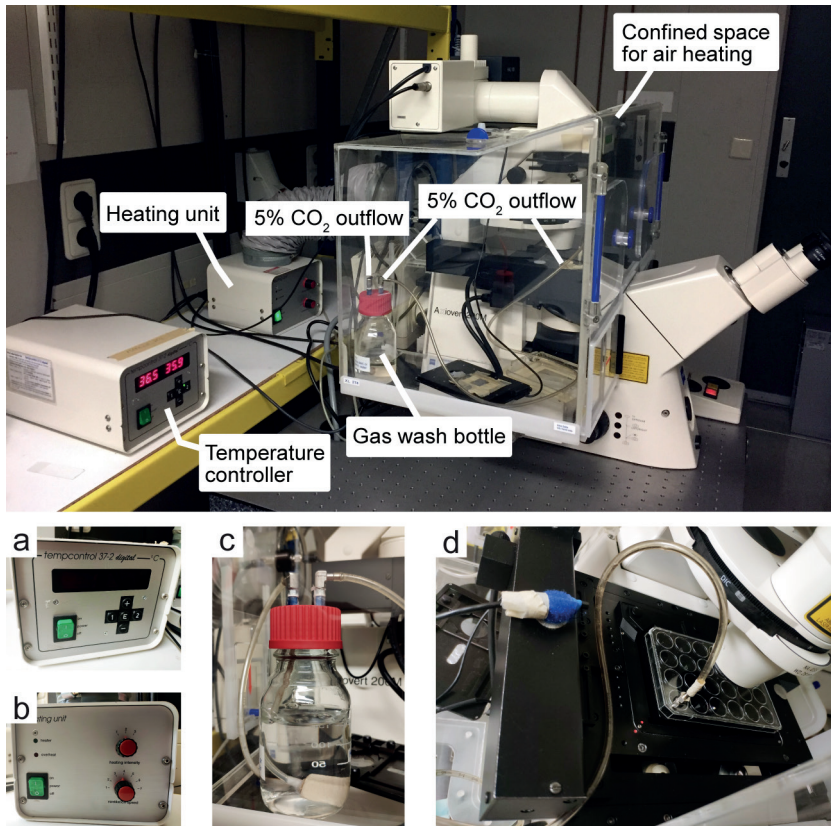


Fig. 6 Climate controlled confocal microscopy configuration for time-lapse imaging. (a) Temperature controller. (b) Heating unit. (c) Gas wash bottle. (d) Motorized stage with an experimental plate on top. A tube with humidified airflow containing 5% CO₂ is connected to the plate.

Preparation of microcarrier beads

Cytodex Microcarrier beads (C3275, Sigma-Aldrich) were hydrated in PBS for at least 3 h at room temperature. After beads settlement, discard the supernatant and add fresh Ca^{2+} and Mg^{2+} free PBS to a stock concentration of 50 ml/g. The beads in PBS are sterilized by autoclaving at 120°C for 20 min and can be stored at 4°C. Upon use, mix bead suspension in stock thoroughly and pipette 1 ml to a 15 ml Falcon tube. Centrifuge the mixture at 400 g for 5 min and aspirate the supernatant carefully. Re-suspend beads in a volume of 10 ml culture medium to make the final suspension.

Cell culture

Human melanoma cell lines (BLM, M14 and Mel57), colorectal cancer cell lines (SW480 and CACO2) and mouse Lewis lung carcinoma (LLC) cells were maintained in Dulbecco's modified Eagle's medium (DMEM) supplemented with 10% fetal bovine serum (FBS) under conditions of 5% CO_2 at 37 °C.

Preparation of cell spheroids with microcarrier beads

Cells were suspended in culture medium at a density of $2\sim5 \times 10^5$ cells/ml. Add 1 ml cell suspension and 1 ml bead suspension to a round bottom tube with snap cap (352059, Corning). Place the tube in a 37°C incubator with 5% CO_2 for 6 hours and gently shake the tube manually every two hours to allow cells to evenly distribute on the beads. Manually shaking cannot be replaced by a shaker as most cells will not adhere under continuous shaking. After 6 hours of incubation, transfer the mixture (2 ml) to a 6-well plate or a 35 mm petri dish and incubate for 1 to 2 days until most beads are fully covered with cells. Gently clap the culture plate to let spheroids detached for further use. The cell number required to obtain a confluent coverage of beads vary for different cell lines, and should be tested beforehand.

Embedding spheroids into matrix gel

Spheroid suspension was transferred to a Falcon tube and left for 5 min allowing spheroids to settle. Aspirate all culture medium carefully and add the same amount (2 ml) of DMEM to re-suspend spheroids. Prepare a certain concentration of matrix with collagen (option A), Matrigel (option B) or agar (option C). The recommended concentration of collagen type I is 1.4-2.3 mg/ml according to the quantity of collagen I in human fresh tissue [21]. For Matrigel, the concentration that forms a solid gel and allows cells to invade properly in 2 to 3 days (e.g. 4-5 mg/ml) should be determined in pilot assays before further experimentation, as it may vary between companies and batches. Here we show the volume of reagents for duplicates preparation in a 24-well format.

(A) Collagen gel formulation for cell invasion

- (i) Keep collagen on ice. Pre-chill pipette tips and Eppendorf tubes used for matrix preparation.
- (ii) Mix 340 μl DMEM and 27 μl 7.5% (w/v) NaHCO_3 in a sterile Eppendorf tube.
- (iii) Add 100 μl spheroid suspension to the Eppendorf tube. Slowly add 533 μl collagen (3mg/ml) and gently pipette up and down to mix well. The final concentration of collagen is 1.6 mg/ml. Dispense 400 μl mixture in each well without air bubbles and incubate the plate at 37°C for at least 30 min until a solid gel formed.
- (iv) Add 500 μl warm (37°C) culture medium carefully along the side wall onto the gel. To investigate treatment effects, agents can be mixed in the culture medium before adding to the gel.

(B) Matrigel formulation for cell invasion

- (i) Keep Matrigel on ice. Pre-chill pipette tips and Eppendorf tubes used for matrix preparation.
- (ii) Add 440 μl DMEM and 100 μl spheroid suspension to a sterile Eppendorf tube.
- (iii) Slowly add 460 μl Matrigel GFR (10.9 mg/ml) and gently pipette up and down to mix well. The final concentration of Matrigel is 5 mg/ml. Dispense 400 μl mixture in each well without air bubbles and incubate the plate at 37°C for at least 30 min until a solid gel formed.
- (iv) Add 500 μl warm (37°C) culture medium carefully along the side wall onto the gel. To investigate treatment effects, agents can be mixed in the culture medium before adding to the gel.

(C) Agar formulation for cell invasion

- (i) Sterilize 0.6% (w/v) agar by autoclaving at 120°C for 20 min and store at 4°C. Before use agar should be completely boiled in a microwave and mixed well. Keep agar in a 42°C water bath to prevent solidification.
- (ii) Mix 375 μl DMEM and 25 μl 7.5% NaHCO_3 in a sterile Eppendorf tube.
- (iii) Add 100 μl spheroids suspension to the Eppendorf tube. Slowly add 500 μl 0.6% agar and gently pipette up and down to mix well. The final concentration of agar is 0.3%. Dispense 400 μl of the mixture in each well without air bubbles and incubate the plate at room temperature for 20-30 min until a solid gel formed.
- (iv) Add 500 μl warm (37°C) culture medium carefully along the side wall onto the gel. To investigate treatment effects, agents can be mixed in the culture medium before adding to the gel.

Imaging cell invasion in matrix

Cell invasion can be monitored by time-lapse microscopy (option A) for several days. It requires a climate control system to keep cells alive during imaging. Here we use a confocal microscope installed with a cell culture box. A sealed Perspex box is built on the microscope to maintain temperature. Assemble the heating unit to warm the air inside the Perspex box and the motorized stage where culture plate is placed. A 5% CO₂/air mixture is supplied through a heated gas wash bottle for humidification, and it goes directly to the cell culture plate or chamber on the motorized stage (Fig. 6). The flow rate needs to be low to prevent evaporation of medium in the plate, and it can be adjusted based on the frequency of air bubbles in the gas wash bottle. In the absence of a climate-controlled configuration, it is also possible to image cell dispersion and invasion manually (option B). Image acquisition in bright field or fluorescence can be done in this setting, and several time points were recorded.

(A) Time-lapse imaging

- (i) Switch heating unit on and set it to 37°C before imaging to ensure the heating is stable.
- (ii) Place the experimental plate or cell chamber on the stage of the confocal microscope and let temperature, CO₂ and humidity stabilize.
- (iii) Turn on and configure the confocal imaging software to appropriate settings (e.g. lasers, channels, scan parameters). Apply the same configuration when repeating experiments.
- (iv) Browse spheroid distribution in matrix with a 10× 0.3NA Plan-Neofluar objective lens. Choose a spheroid which is fully covered with cells and far enough from other spheroids. Adjust the position to center the spheroid of interest in the middle of the image and save this position in the location list. Repeat this step to find other spheroids and save their coordinates.
- (v) Set z stack interval and range. The interval is determined by the pinhole. The range is usually set to ~200 μm and can be adjusted for different cells.
- (vi) Determine the time interval and repetitions which vary depending on cell invasion ability. Usually we set the time interval to 30 min and the duration to 2-3 days.
- (vii) Start imaging and check if the setup runs well during imaging acquisition. In particular check above mentioned environmental settings and whether evaporation of medium occurs.

(B) Imaging cell dispersion manually

- (i) Place the multi-well plate or culture chamber on the stage of a standard

microscope.

- (ii) Turn on the imaging software connected to the microscope and set up for image acquisition in bright-field or fluorescence. The software needs to display x and y coordinates.
- (iii) Make a mark with a pen on the upper left corner of the plate and set this mark to 0 position manually. Browse spheroids distribution in matrix under a 10× objective lens. Choose spheroids which are fully covered with cells and far enough from other spheroids. Adjust the position to center the spheroid of interest in the middle of the image, save this position in the location list and take a picture as T=0. Repeat this for other spheroids of interest. After photographing all the selected spheroids, put the plate back in the incubator.
- (iv) Pictures of the same spheroids can be taken every 12 or 24 hours until cells spread out of frame or at a desired end point of this experiment. At every time point, reset the mark at the 0 position before taking pictures to avoid shifting of position.

Quantification of migratory parameters and data analysis

Several methods can be performed to quantify migratory parameters under different conditions. The maximum migrating distance (option A) or the average of maximum migrating distance (option B) is applied when cells migrate cohesively and very few cells move far away from the cell cluster (Fig. 7a,b). Here we use the AxioVision image analysis module as an example to measure these parameters which can alternatively be done in Fiji [22] or similar software. Some cell lines move individually or follow a path created by front cells, thus show spotted or radiating/sprouting dispersion respectively. In this case a migration index (option C) can be applied to determine cell invasion characteristics. The migration index is defined as the sum of all migrating cells multiplied with the distance from the bead. If time-lapse imaging is conducted, moving trajectories of individual cells can be tracked manually or with tracking software from which migration distances and velocity are calculated (option D).

(A) Measuring maximum migrating distance

- (i) Open file at a time point in AxioVision. Under “Measure” menu select the “Circle” tool.
- (ii) Draw a circle matching the bead to measure size of bead (Fig. 7a, red circle). From the center draw another circle involving all migrating cells (Fig. 7a, white circle).
- (iii) Calculate maximum migrating distance at this time point. Max migrating distance (μm) = radius of migrating front circle – radius of bead circle

(B) Measuring average of maximum migrating distance

- (i) Open file at a time point in AxioVision.
- (ii) Under “Measure” menu select the “Circle” tool. Draw a circle matching the bead to measure size of bead (Fig. 7b, red circle).
- (iii) Under “Measure” menu select the “Curve” tool. Draw a curve along the migrating front to generate a convex polygon (Fig. 7b, yellow curve) to measure the perimeter. Only the perimeter of convex polygon can be used to calculate the radius with this formula [23]. A concave polygon extends the perimeter which causes incorrect result.
- (iv) Calculate average of maximum migrating distance at this time point (Fig. 7b, white circle). Avg. max migrating distance (μm) = (perimeter of the polygon/ 2π) – radius of bead circle

(C) Computing migration index

- (i) Open file with z stack at a selected time point in Fiji.
- (ii) Find the contours of the bead in the spheroid by browsing through the z stack and draw a circle (Circle0) matching the biggest bead diameter. Record this instruction in the macro recorder.
- (iii) Make a z projection of the original file. Set threshold to include all cells. Recreate Circle0 by running the recorded macro. Measure the area of the circle (Area0).
- (iv) Draw Circle1 with the same center as Circle0 and radius 10 μm larger than Circle0. Area1 = area of Circle1 - Area0. Each time draw a circle 10 μm larger than the previous one and measure the area until the circle reaches the edge of image (Fig. 7c). The whole automated image processing macros can be found in Additional File 1.
- (v) Export results to Excel. Calculate the increasing area of each circle. Area(i) = area of Circle(i) – area of Circle($i-1$) where $i = 1, 2, 3, \dots$ max number of circles. A graph can be drawn to display distribution of cells around the bead at this time point, in which x axis represents distance to bead and y axis represents migration area (Fig. 4b).
- (vi) If we assume every cell has the same size, then the area is proportional to cell numbers. The migration index can be calculated using the equation:

$$\text{Migration index} = \sum_{i=1}^n 10 \times i \times \text{Area}(i)$$

where n is the maximum number of circles. This formula is adapted from Jozaki, K. et al [24].

(D) Cell trajectory and velocity

- (i) Open the time-lapse sequence of each selected position in Fiji.
- (ii) Make a z-projection and adjust brightness and color to make cells easily recognized.
- (iii) Use “Manual tracking” plug-in to track individual cells (Fig. 7d). Results will show distance and velocity between every two slices. Export results in Excel and calculate the migration distance and velocity. Other automated tracking methods are available for analysis [25, 26].

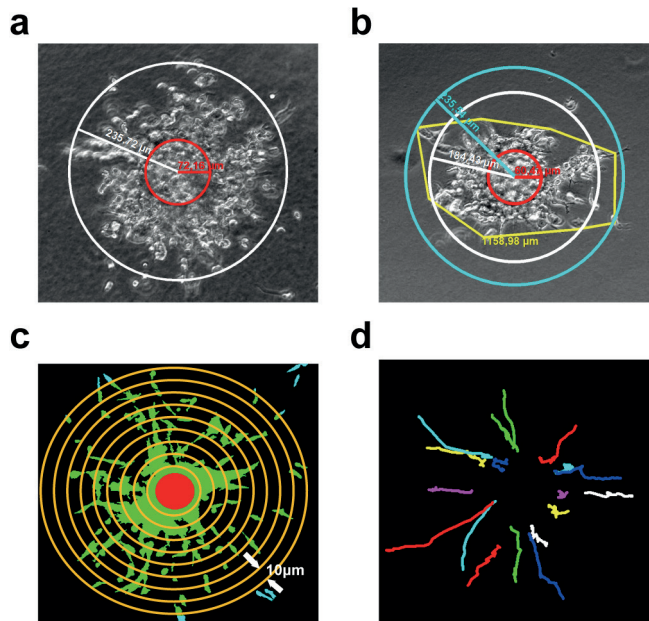


Fig. 7 Quantification of migratory parameters. (a) Maximum migrating distance measured when cells evenly distributed in all directions. White circle, cell migration front. Red circle, size of bead. (b) Average of maximum migrating distance applied when cells showed uneven distribution in a shape of a polygon rather than a sphere. Yellow curve, cell migration front. White circle, calculated average of maximum distance. Light blue circle, maximum of cell migration front. Red circle, size of bead. (c) Schematic diagram to show the principle of computing migration area on the basis of the distance to the core. Cells are selected and filled with green. Light blue represents cells out of range. Red core is where the bead resides. Yellow concentric circles with radius difference of 10 μm are drawn to measure the migration area of increasing distance to beads. In this schematic the yellow circles do not have a radius difference of exact 10 μm but were only drawn to illustrate this quantification method. (d) Cell trajectories in collagen I between 55 to 70 hours, tracked manually. Panels a-b show representative images of M14 cells, and panels c-d show examples of quantification on LLC cell images.

List of abbreviations

ECM: extracellular matrix; 3D: three dimensions; 2D: two dimensions; DMEM: Dulbecco's modified Eagle's medium; PBS: phosphate buffered saline; FBS: fetal bovine serum; GFR: growth factor reduced; LLC: Lewis lung carcinoma; NS: not significant.

ACKNOWLEDGEMENTS

This study is supported by Erasmus MC Mrcare grant (343566) to TtH. HL is financially supported by China scholarship council for her doctorate program.

REFERENCES

1. Chambers A.F., Groom A.C., MacDonald I.C. Dissemination and growth of cancer cells in metastatic sites. *Nat Rev Cancer*. 2002;2(8):563-72.
2. Friedl P., Wolf K. Tumour-cell invasion and migration: diversity and escape mechanisms. *Nat Rev Cancer*. 2003;3(5):362-74.
3. Sahai E. Illuminating the metastatic process. *Nat Rev Cancer*. 2007;7(10):737-49.
4. Christiansen J.J., Rajasekaran A.K. Reassessing epithelial to mesenchymal transition as a prerequisite for carcinoma invasion and metastasis. *Cancer Res*. 2006;66(17):8319-26.
5. Friedl P., Locker J., Sahai E., Segall J.E. Classifying collective cancer cell invasion. *Nat Cell Biol*. 2012;14(8):777-83.
6. Albin A., Benelli R. The chemoinvasion assay: a method to assess tumor and endothelial cell invasion and its modulation. *Nat Protoc*. 2007;2(3):504-11.
7. Liu H., Zhu M., Li Z., Wang Y., Xing R., Lu Y., et al. Depletion of p42.3 gene inhibits proliferation and invasion in melanoma cells. *J Cancer Res Clin Oncol*. 2017;143(4):639-48.
8. Benien P., Swami A. 3D tumor models: history, advances and future perspectives. *Future Oncol*. 2014;10(7):1311-27.
9. Nath S., Devi G.R. Three-dimensional culture systems in cancer research: Focus on tumor spheroid model. *Pharmacol Ther*. 2016;163:94-108.
10. Vinci M., Gowan S., Boxall F., Patterson L., Zimmermann M., Court W., et al. Advances in establishment and analysis of three-dimensional tumor spheroid-based functional assays for target validation and drug evaluation. *BMC Biol*. 2012;10:29.
11. Lee J.M., Mhawech-Fauceglia P., Lee N., Parsanian L.C., Lin Y.G., Gayther S.A., et al. A three-dimensional microenvironment alters protein expression and chemosensitivity of epithelial ovarian cancer cells in vitro. *Lab Invest*. 2013;93(5):528-42.
12. Dolznig H., Rupp C., Puri C., Haslinger C., Schweifer N., Wieser E., et al. Modeling colon adenocarcinomas in vitro a 3D co-culture system induces cancer-relevant pathways upon tumor cell and stromal fibroblast interaction. *Am J Pathol*. 2011;179(1):487-501.
13. Johns R.A., Tichotsky A., Muro M., Spaeth J.P., Le Cras T.D., Rengasamy A. Halothane and isoflurane inhibit endothelium-derived relaxing factor-dependent cyclic guanosine monophosphate accumulation in endothelial cell-vascular smooth muscle co-cultures independent of an effect on guanylyl cyclase activation. *Anesthesiology*. 1995;83(4):823-34.
14. Bakker E.R., Das A.M., Helvensteijn W., Franken P.F., Swagemakers S., van der Valk M.A., et al. Wnt5a promotes human colon cancer cell migration and invasion but does not augment intestinal tumorigenesis in Apc1638N mice. *Carcinogenesis*. 2013;34(11):2629-38.
15. Janmaat V.T., Liu H., da Silva R.A., Wisse P.H.A., Spaander M.C.W., Ten Hagen T.L.M., et al. HOXA9 mediates and marks premalignant compartment size expansion in colonic adenomas. *Carcinogenesis*. 2019.
16. Dietrich F., Lelkes P.I. Fine-tuning of a three-dimensional microcarrier-based angiogenesis assay for the analysis of endothelial-mesenchymal cell co-cultures in fibrin and collagen gels. *Angiogenesis*. 2006;9(3):111-25.
17. Kniazeva E., Putnam A.J. Endothelial cell traction and ECM density influence both capillary morphogenesis and maintenance in 3-D. *Am J Physiol Cell Physiol*. 2009;297(1):C179-87.
18. Juliar B.A., Keating M.T., Kong Y.P., Botvinick E.L., Putnam A.J. Sprouting angiogenesis induces significant mechanical heterogeneities and ECM stiffening across length scales in fibrin hydrogels. *Biomaterials*. 2018;162:99-108.

19. Kleinman H.K., Martin G.R. Matrigel: basement membrane matrix with biological activity. *Semin Cancer Biol.* 2005;15(5):378-86.
20. Kaukonen R., Jacquemet G., Hamidi H., Ivaska J. Cell-derived matrices for studying cell proliferation and directional migration in a complex 3D microenvironment. *Nat Protoc.* 2017;12(11):2376-90.
21. Rojkind M., Giambrone M.A., Biempica L. Collagen types in normal and cirrhotic liver. *Gastroenterology.* 1979;76(4):710-9.
22. Schindelin J., Arganda-Carreras I., Frise E., Kaynig V., Longair M., Pietzsch T., et al. Fiji: an open-source platform for biological-image analysis. *Nat Methods.* 2012;9(7):676-82.
23. Merkus H.G. Particle size measurements: fundamentals, practice, quality: Springer Science & Business Media, Dordrecht, the Netherlands; 2009 7 January 2009.
24. Jozaki K., Marucha P.T., Despins A.W., Kreutzer D.L. An in vitro model of cell migration: evaluation of vascular endothelial cell migration. *Anal Biochem.* 1990;190(1):39-47.
25. Tokunaga T., Hirose O., Kawaguchi S., Toyoshima Y., Teramoto T., Ikebata H., et al. Automated detection and tracking of many cells by using 4D live-cell imaging data. *Bioinformatics.* 2014;30(12):i43-51.
26. Dzyubachyk O., van Cappellen W.A., Essers J., Niessen W.J., Meijering E. Advanced level-set-based cell tracking in time-lapse fluorescence microscopy. *IEEE Trans Med Imaging.* 2010;29(3):852-67.

SUPPLEMENTARY MATERIALS

Supplementary File 1: Homemade macros to quantify migrating cell areas of each distance range in Fiji.

```

Threshold = 10;           // threshold used to segment cells from background
IncreaseRadius = 10;      // increase in diameter in micrometer
x = 223; y = 220; d = 77  //makeOval(x, y, d, d); numbers need to match the location of beads
r = d / 2
run("Clear Results");
roiManager("Reset");

list = getList("window.titles");
for (i=0; i<list.length; i++) {
    if (list[i]=="Results") {
        selectWindow("Results");
        run("Close");
    }
    if (list[i]=="Summary of StackCircles") {
        selectWindow("Summary of StackCircles");
        run("Close");
    }
}

list = getList("image.titles");
for (i=0; i<list.length; i++) {
    if (list[i]=="MaxProjection") {
        selectWindow("MaxProjection");
        run("Close");
    }
    if (list[i]=="StackCircles") {
        selectWindow("StackCircles");
        run("Close");
    }
    if (list[i]=="temp") {
        selectWindow("temp");
        run("Close");
    }
}

run("Duplicate...", "title=temp duplicate channels=2");
run("Median...", "radius=1 stack");
run("Z Project...", "projection=[Max Intensity]");
rename("MaxProjection");
getDimensions(width, height, channels, slices, frames);

run("Duplicate...", "title=ColorCoded");
run("RGB Color");
selectWindow("MaxProjection");
setThreshold(Threshold, 255);
run("Analyze Particles...", "size=100-Infinity add stack");
selectWindow("ColorCoded");
roiManager("OR");
run("Clear Outside");

```

```
setForegroundColor(0, 255, 0);
run("Fill");
roiManager("Reset");
selectWindow("MaxProjection");
setThreshold(Threshold, 255);
selectWindow("ColorCoded");
makeOval(x, y, d, d);
roiManager("Add");
setForegroundColor(255, 0, 0);
run("Fill");

run("Split Channels");

selectWindow("ColorCoded (red)");
roiManager("Select", 0);
OldArea = getResult("Area",0);
run("Set Measurements...", "center");
roiManager("Measure");
CenterOfMass_X = getResult("XM",0);
toUnscaled(CenterOfMass_X);
CenterOfMass_Y = getResult("YM",0);
toUnscaled(CenterOfMass_Y);
selectWindow("Results");
run("Close");
roiManager("Reset");

//Calculate center of circles and max number of circles
if (CenterOfMass_X <= width/2) {
    DistanceToEdge_X = CenterOfMass_X;
}
else {
    DistanceToEdge_X = width - CenterOfMass_X;
}
if (CenterOfMass_Y <= height/2) {
    DistanceToEdge_Y = CenterOfMass_Y;
}
else {
    DistanceToEdge_Y = height - CenterOfMass_Y;
}
if (DistanceToEdge_X <= DistanceToEdge_Y) {
    MaxDistanceToCenter = DistanceToEdge_X;
}
else {
    MaxDistanceToCenter = DistanceToEdge_Y;
}

toScaled(MaxDistanceToCenter);
NrOfCircles = floor((MaxDistanceToCenter-d)/IncreaseRadius)+1;

run("Set Measurements...", "area limit display redirect=None decimal=0");
// Fill Arrays: DistanceToCore, AreaTotal, AreaIncrease -----
selectWindow("ColorCoded (red)");
run("Select None");

for(i=1; i<=NrOfCircles; i++){
    toUnscaled(IncreaseRadius);
    makeOval(CenterOfMass_X-(IncreaseRadius*i)-r,CenterOfMass_Y-(IncreaseRadius*i)-r,
```

```

2*IncreaseRadius*i+d, 2*IncreaseRadius*i+d);
    setThreshold(0, 255);
    run("Measure");
    toScaled(IncreaseRadius);
}
resetThreshold();

DistanceToCore=newArray(NrOfCircles);
AreaTotal=newArray(NrOfCircles);
AreaIncrease=newArray(NrOfCircles);
ThresholdedAreaIncrease=newArray(NrOfCircles);
Core_Area=newArray(NrOfCircles);
Migration_Area=newArray(NrOfCircles);

for(i=1; i<=NrOfCircles; i++) {
    DistanceToCore[i-1] = i * IncreaseRadius;
    AreaTotal[i-1] = getResult("Area",i-1);
    AreaIncrease[i-1] = AreaTotal[i-1] - OldArea;
    OldArea = AreaTotal[i-1];
}
selectWindow("Results");
run("Close");

selectWindow("ColorCoded (green)");
run("Select None");
run("Duplicate...", "title=tempGr");
for(i=1; i<=NrOfCircles; i++){
    toUnscaled(IncreaseRadius);
    makeOval(CenterOfMass_X-(IncreaseRadius*i)-r,CenterOfMass_Y-(IncreaseRadius*i)-r,
2*IncreaseRadius*i+d, 2*IncreaseRadius*i+d);
    setThreshold(Threshold, 255);
    run("Measure");
    run("Clear", "slice");
    toScaled(IncreaseRadius);

    ThresholdedAreaIncrease[i-1] = getResult("Area",i-1);
    Migration_Area[i-1] = ThresholdedAreaIncrease[i-1] ;
}

selectWindow("tempGr");
run("Make Inverse");
run("Cut");
selectWindow("ColorCoded (blue)");
run("Paste");
run("Select None");
selectWindow("tempGr");
run("Close");
selectWindow("MaxProjection");
run("Close");
selectWindow("temp");
run("Close");
selectWindow("Results");
run("Close");

run("Merge Channels...", "c1=[ColorCoded (red)] c2=[ColorCoded (green)] c3=[ColorCoded (blue)] create");
run("RGB Color");
Array.show("Results", DistanceToCore, Migration_Area);

```


Chapter 3

CREPT promotes melanoma progression through accelerated proliferation and enhanced migration by RhoA-mediated actin filaments and focal adhesion formation

Hui Liu, Ann L.B. Seynhaeve, Rutger W.W. Brouwer, Wilfred F.J. van IJcken, Liu Yang, Yinyin Wang, Zhijie Chang, Timo L.M. ten Hagen

Cancers (Basel) 2019.

ABSTRACT

Melanoma is one of the most aggressive cancers, and patients with distant metastases have dire outcomes. We observed previously that melanoma progression is driven by a high migratory potential of melanoma cells, which survive and proliferate under harsh environmental conditions. In this study, we report that CREPT (cell-cycle related and expression-elevated protein in tumor), an oncoprotein highly expressed in other cancers, is overexpressed in melanoma cells but not melanocytes. Overexpression of CREPT stimulates cell proliferation, migration, and invasion in several melanoma cell lines. Further, we show that CREPT enhances melanoma progression through upregulating and activating Ras homolog family member A (RhoA)-induced actin organization and focal adhesion assembly. Our study reveals a novel role of CREPT in promoting melanoma progression. Targeting CREPT may be a promising strategy for melanoma treatment.

Keywords: melanoma; CREPT; proliferation and migration; cytoskeleton organization; RhoA activation

INTRODUCTION

Malignant melanoma, which derives from melanocytes and mostly arises in the skin, is characterized as a highly metastatic tumor. In the past 30 years, the incidence of cutaneous melanoma has grown rapidly [1]. Around 300,000 new cases of melanoma were reported worldwide in 2018, and the incidence of melanoma was ranked fifth of all cancers in the United States [1, 2]. Due to the rapid progression and metastasis, ~5% of patients present distant metastasis at the initial diagnosis [3]. Although immunotherapy or targeted therapy drugs yield notable clinical benefits, increasing five-year overall survival to 35% to 50%, a great proportion of metastatic melanoma patients remain unresponsive to treatments [4-6]. For this reason, finding the cause of melanoma progression remains crucial to further improve therapeutic strategies.

Metastases, in which tumor cells disseminate to a distant site, are the main cause of cancer deaths [7]. Several steps can be identified during the metastatic process, which demands certain cell characteristics. Tumor cells dissociating from primary sites must have the ability to migrate and invade through the basement membrane and extracellular matrix (ECM). To pass through tissues, tumor cells change their morphology and stiffness to fit in and interact with surrounding ECM structures [8]. These morphological changes, like cell polarization and formation of membrane extensions, are inseparable with filamentous actin and related cell-matrix attachments [9-11]. Integrins, which are transmembrane receptors and couple the cell to ECM components, regulate focal contact assembly and cell migration in melanoma [12]. Rho GTPase signaling contributes to cell movement by influencing cytoskeleton reorganization [13, 14]. After the process of intravasation and extravasation, metastatic tumor cells travel to a secondary site, adapt to the local microenvironment for survival, proliferate, and develop a vasculature to establish a new tumor [15, 16]. Melanoma cells are also able to sustain the survival of endothelial cells under restrictive conditions [17]. The strong angiogenic potential contributes to fast metastasis of melanoma.

Regulation of nuclear pre-mRNA domain-containing (RPRD) proteins are identified as novel RNA polymerase II (RNAPII)-interacting proteins, which are evolutionarily conserved and ubiquitously expressed in human tissues. All three RPRDs (including RPRD1A, RPRD1B, and RPRD2) contain C-terminal domain (CTD) interaction domains. RPRD1A and RPRD1B associate with RNAPII phosphatase directly and interact with CTD heptapeptide repeats to recruit RNAPII for dephosphorylation of phosphor-S5 [18, 19]. Recently, an enhanced expression of CREPT, also known as RPRD1B or C20orf77, is reported in many human tumors, including gastric cancer, endometrial cancer, and colorectal cancer [20]. CREPT promotes cell proliferation and tumorigenesis by regulating the cell cycle process by enhancing transcription of Cyclin D1, Cyclin

B1, Cyclin-dependent kinase 4 and 6 (CDK4 and CDK6) [20-22]. CREPT also shows an oncogenic potential as a transcription co-activator of the β -catenin-TCF4 (transcription factor 4) complex to promote the transcriptional activity of the Wnt signaling pathway [23]. Besides, it is reported that a new CREPT/c-myc/CDC25A pathway may result in cell growth and migration promotion [24]. While the function of CREPT has been characterized to some degree in several cancers, the role in cell migration and invasion is less known, and the contribution of CREPT in melanoma tumorigenesis has not been studied.

Here, we show the differential expression of CREPT in melanoma cells and melanocytes, and evaluate the oncogenic potential by assessing the association with cell proliferation, migration, and invasion. Moreover, we find that CREPT influences cell migration by regulating RhoA-related actin filaments' polymerization and focal adhesion formation. Our results demonstrate that CREPT functions as an oncoprotein in melanoma and modulates cell migration and invasion.

RESULTS

Differential Expression of CREPT in Melanoma Cells and Melanocytes

To investigate whether CREPT plays a role in melanoma, the expression in different cell lines was examined at both the mRNA and protein level. PCR, qPCR, and western

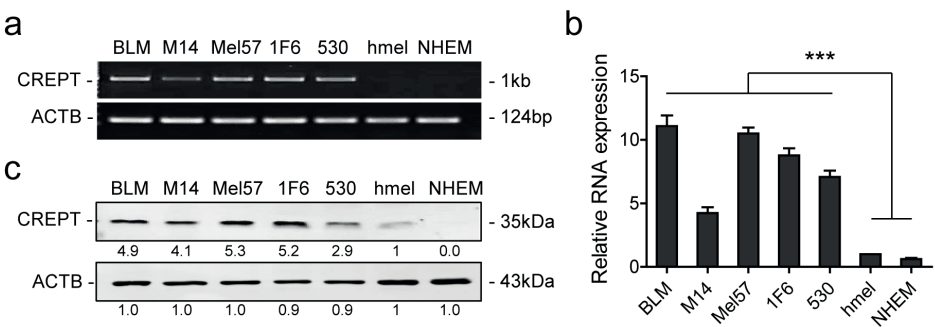


Figure 1. CREPT is highly expressed in melanoma cells compared to melanocytes. (a) Representative pictures of RT-PCR to show CREPT expression in all cell lines. (b) Quantitative PCR is displayed as mean \pm SEM and statistical analysis was conducted with hmel as the control group. (c) Representative pictures of western blotting showing endogenous CREPT protein expression in all cell lines. Beta-actin (ACTB) is used as a loading control. Numbers under the bands show the mean of the intensity ratios standardized to hmel. *** $p < 0.001$. All experiments were repeated at least three times.

blotting results show high expression of CREPT in all five melanoma cell lines (BLM, M14, Mel57, 1F6, 530) and low or absent expression in two melanocyte lines (hmel and NHEM) (Figure 1). These results suggest that CREPT is elevated in melanoma but is low in normal melanocytes.

Depleted or Enforced Expression of CREPT Influences Melanoma Cell Proliferative Capacity

To reveal the function of CREPT in melanoma, BLM cells were stably transfected with CREPT coding sequence plasmid and empty vector (shown as “CREPT” and “Control”, respectively, in Figures 2–7) for enhanced expression, and with plasmids inserted with short hairpin RNA (shRNA) against CREPT and scrambled shRNA (shown as “shCREPT” and “shNC”, respectively, in Figures 2–7) for depleted expression (Figure S1). We performed SRB assays to evaluate cell proliferation rates. The results show that depletion of CREPT led to a decreased growth rate, and reciprocally, overexpression of CREPT promoted cell proliferation significantly (Figure 2a,b). To verify CREPT functions in other melanoma cells, we also selected M14 cells for CREPT overexpression and MEL57 cells for CREPT depletion because M14 had a relatively low endogenous CREPT level and MEL57 had a high level (Figure 1 and S1). SRB assays show similar trends of CREPT-regulated cell growth rates to BLM cells (Figure S2a). To address the role of CREPT in the malignant feature of melanoma, we examined the colony formation ability of CREPT-modified BLM cells. The results show that colonies of CREPT-depleted cells were reduced to 54.0 ± 4.4 per well as compared to 112.5 ± 16.2 per well for non-depleted cells ($p < 0.05$) while CREPT-overexpressed cells formed more colonies than control cells (162.3 ± 4.9 vs. 116.8 ± 9.9 per well, $p < 0.01$) (Figure 2c–f). The tumor growth was significantly increased with CREPT overexpression (vs. control, $p < 0.01$), and mice injected with CREPT depleted cells did not grow visible tumor within 40 days (Figure 3). These results suggest that proliferative and tumorigenic potentials of melanoma cells are, at least in part, dependent on CREPT expression.

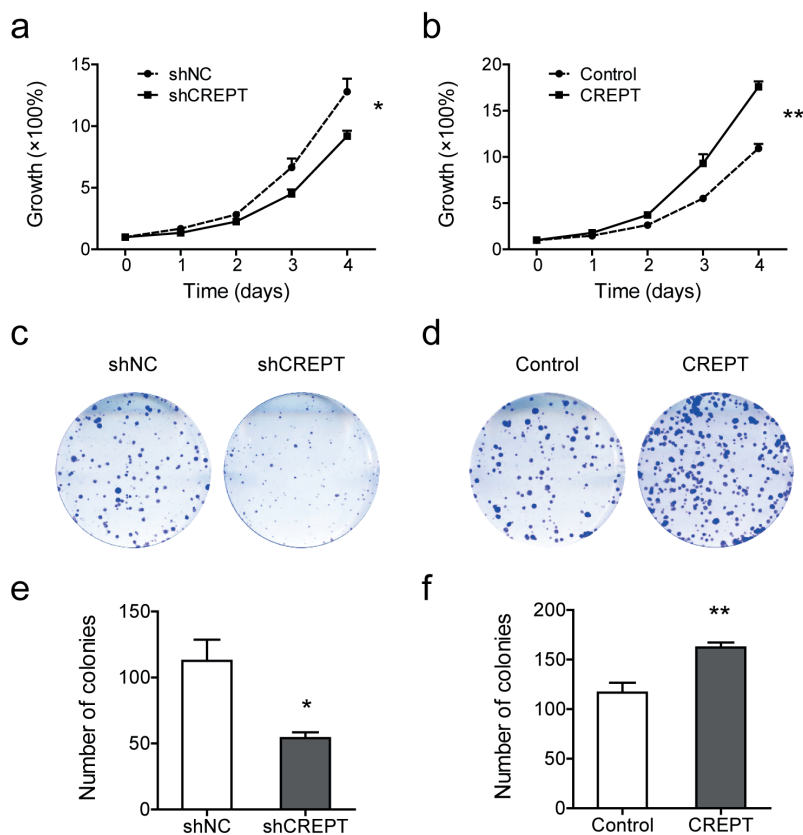


Figure 2. Depletion or overexpression of CREPT affects BLM cell proliferation. Knockdown of CREPT (shCREPT) is compared with control (shNC), and overexpression of CREPT (CREPT) is compared with control (Control). (a,b) In vitro cell growth rates of BLM cells with different CREPT expressions are shown as mean \pm SEM of three independent experiments. (c,d) Representative pictures of the colony formation status in cell lines with distinct CREPT expression. (e,f) Colony numbers were measured in Fiji and data are shown as mean \pm SEM of four independent experiments. * $p < 0.05$, ** $p < 0.01$.

CREPT Promotes Melanoma Cell Migration and Invasion in Vitro

To address the effect of CREPT on cell migration, migratory profiles of melanoma cells were evaluated by a ring-barrier migration assay. Cell movement was monitored in reduced-serum media (DMEM supplemented with 1% FBS) to diminish the impact of cell proliferation. We followed cell trajectories for 24 h and measured total and directional distances. Total migration indicates the capacity of cell motility, and effective migration shows net displacement, implying persistent directionality of cell migration. BLM cells

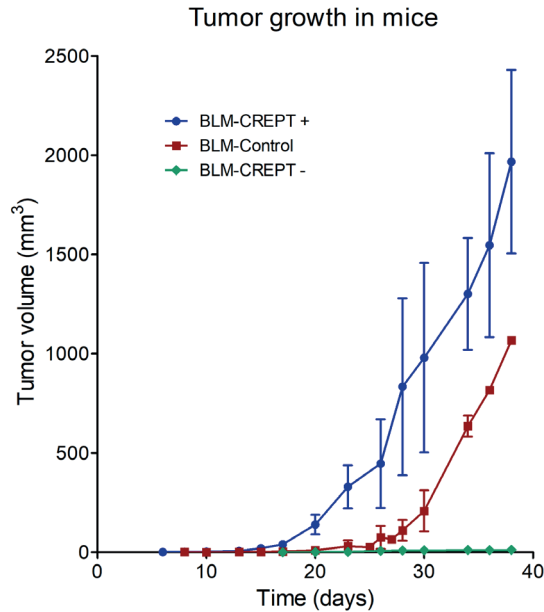


Figure 3. Effect of CREPT expression on tumor growth. Since two control cells (control to overexpression and control to depletion) had no significant on tumor growth, we combined these two groups into one, showed in red line. The BLM with CREPT overexpression was showed in blue line, and CREPT depletion in green. Data represent mean \pm SD of 7 mice per group.

with CREPT depletion (BLM-shCREPT) show significantly reduced total migration distances and net displacement (Figure 4a,c) while overexpression of CREPT increased the total migration and effective migration ($p < 0.01$) (Figure 4b,d). Similar results were observed in MEL57 and M14 cells (Figure S2b). These results demonstrate that CREPT facilitates melanoma cell motility and migration.

The migration potential in two dimensions was tested with cells attached to a surface, where cells can only have contact with the extracellular matrix (ECM) on the surface side. To investigate the effect of CREPT on three-dimensional migration or invasion capacity, we used microcarrier beads as supporting cores to grow spheroids and monitor cell invasion by embedding spheroids into a 3D matrix. This assay enables cell-ECM interaction on all sides of the cell during movement, resembling a more realistic microenvironment. In 5 days, BLM-shCREPT cells displayed a decreased invasive distance ($148.7 \pm 4.1 \mu\text{m}$) in comparison to BLM-shNC cells ($212.7 \pm 5.3 \mu\text{m}$, $p < 0.01$) (Figure 5a,c). On the contrary, overexpression of CREPT led to an faster invasion into the matrix than control

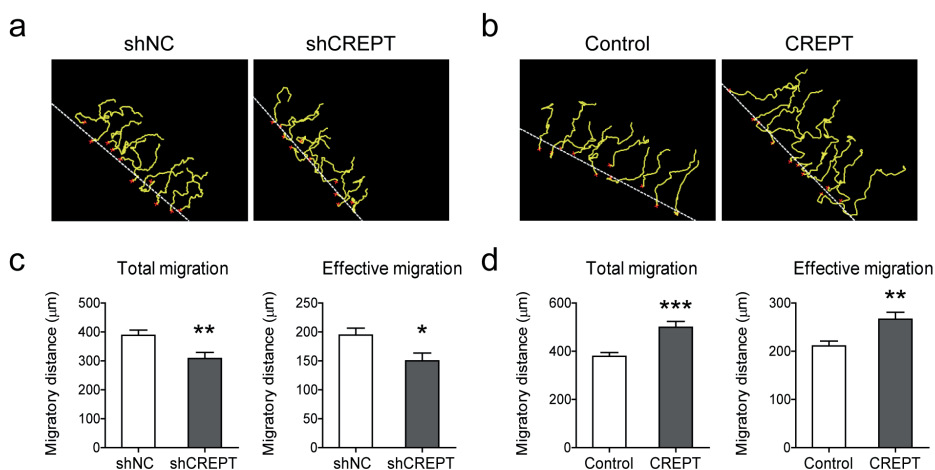


Figure 4. Effect of CREPT expression on BLM cell migration. Knockdown of CREPT (shCREPT) is compared with control (shNC), and overexpression of CREPT (CREPT) is compared with control (Control). (a,b) Representative pictures of cell trajectories in 24 h. Dotted white lines indicate the migration front at $t = 0$, red crosses indicate cells selected for tracking, and yellow lines represent single cell trajectories representing the total migration. (c,d) Migratory parameters were quantified and calculated of 30 cells in each individual experiment. Total migration (μm) is the total distance every cell moves in 24 h. Effective migration (μm) is the net displacement from 0 to 24 h. Data represent mean \pm SEM of three independent experiments. * $p < 0.05$, ** $p < 0.01$, *** $p < 0.001$.

BLM cells ($255.0 \pm 7.7 \mu\text{m}$ vs. $198.1 \pm 7.1 \mu\text{m}$, $p < 0.001$) (Figure 5b,c). The results were confirmed with MEL57 and M14 cells (Figure S2c). These data illustrate that CREPT stimulates the invasive process of melanoma cells in the 3D collagen matrix.

Global Gene Expression Profiling Based on CREPT Expression Modification

To understand the molecular mechanisms of CREPT-induced changes in cell behavior, we performed whole transcriptome sequencing using BLM-shCREPT cells and BLM-shNC cells. In total, 366 downregulated and 524 upregulated transcripts were obtained when comparing BLM-shCREPT to BLM-shNC samples (Figure 6a). Gene molecular and cellular function analysis indicated that these genes were enriched in functions “cellular movement”, “cellular assembly and organization”, and “cellular growth and proliferation” (Figure 6b). Further, to visualize gene changes in categories, we clustered significantly altered genes and showed the results in heat maps. In correlation with our experimental observations on CREPT-regulated cell proliferative and migratory capacity, we first checked GO:0030334 “regulation of cell migration” and GO:0042127 “regulation of cell

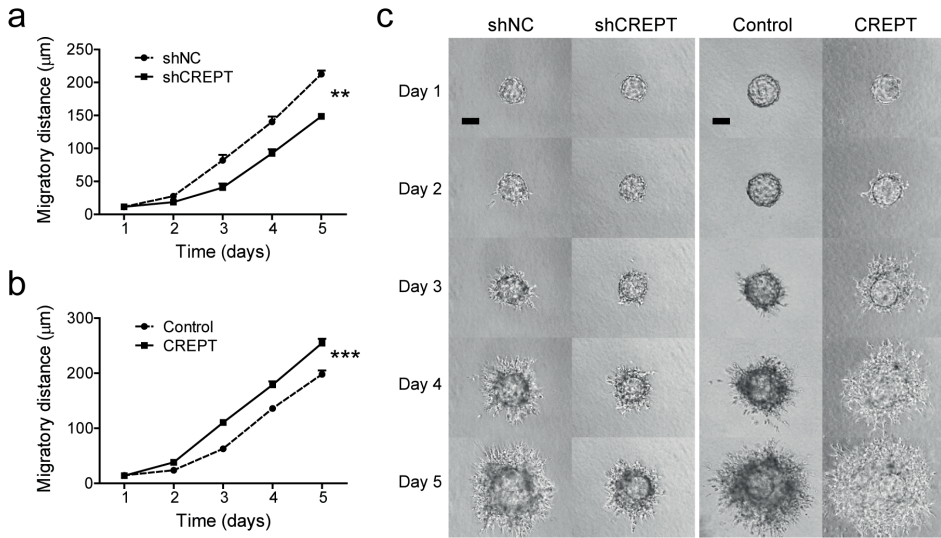


Figure 5. The invasive capacity of BLM cells is affected by modified CREPT expression. Microcarrier beads covered with cells were embedded in collagen gel and cell dispersion into the matrix was photographed every day for evaluation. In total, 10 to 15 beads per group were included in each independent experiment, and dispersion distances were quantified and analyzed as shown in panels (a,b). Data is depicted as mean \pm SEM of three independent experiments. ** $p < 0.01$, *** $p < 0.001$. (c) Representative pictures of cell dispersion over time for different cell lines. Scale bars, 100 μ m.

population proliferation”, which represent the process modulating the frequency, rate, or extent of cell migration and cell proliferation, respectively. Genes involved in positive regulation of cell migration and proliferation were mostly downregulated (23/32, 72% in migration; 23/35, 66% in proliferation) in BLM-shCREPT samples while genes involved in negative regulation of cell migration and proliferation were mainly upregulated (13/17, 76% in migration; 28/35, 80% in proliferation) (Figure 6c,d). The results support the biology profiling that CREPT improved melanoma cell proliferation and migration. Apart from the functions we observed in the experiments, the gene expression profiling also showed a link between CREPT expression and actin cytoskeleton organization, which is essential for cell migration. To maintain the actin skeleton structure, globular actins firstly polymerize to filaments. Actin filaments together with myosin II and other cytoskeletal proteins assemble to form stress fibers working as contractile structures. These actin bundles terminate at the cell surface, where focal adhesion assemblies anchor the cell to the extracellular matrix [25]. Therefore, we zoomed in on the expression profile of genes involved in focal adhesion, actin polymerization, and stress fiber assembly. The RNA-Seq data show that the major cluster of genes in BLM-shCREPT samples are down-

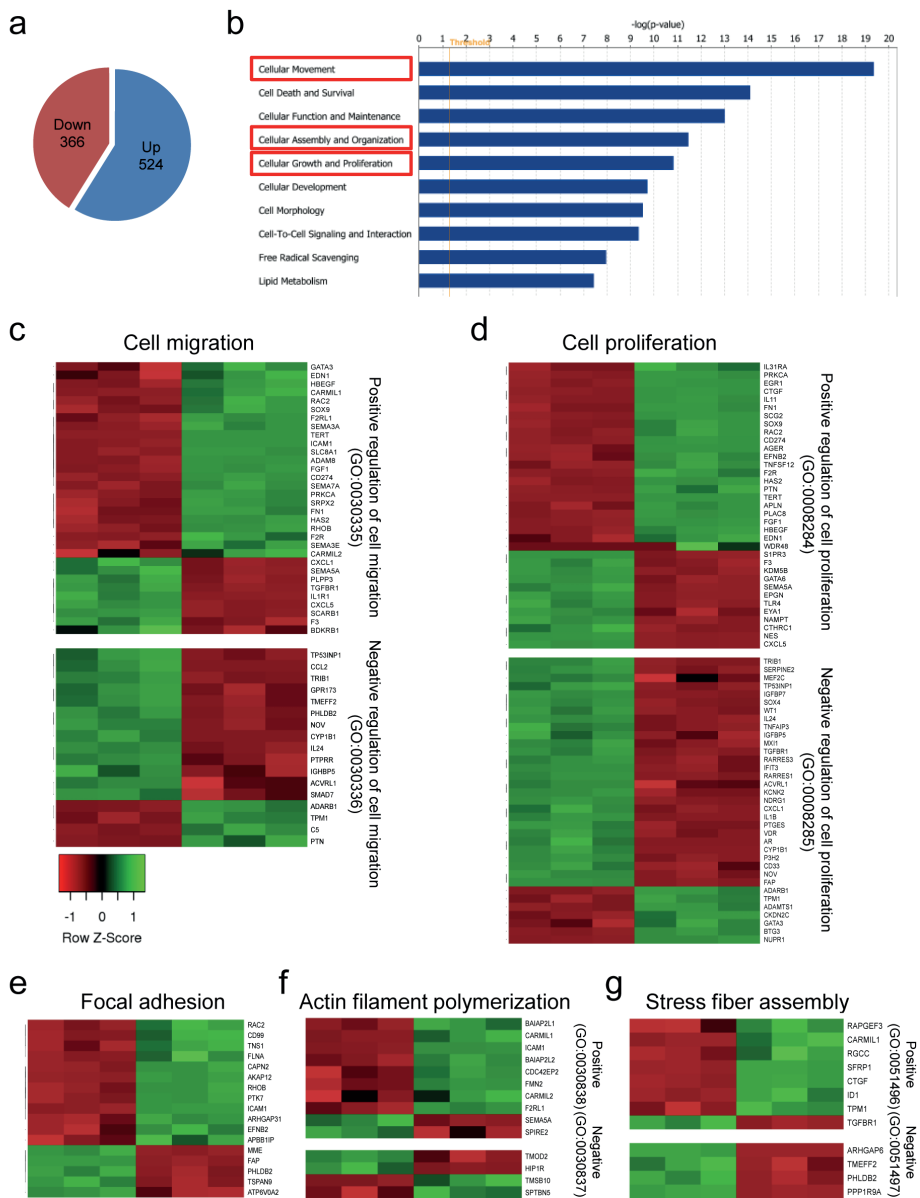


Figure 6. Global gene changes in melanoma cells with differential CREPT expression in BLM cells. (a) The pie chart shows the global up- and downregulated transcript numbers. (b) The top 10 most correlated molecular and cellular functions. The x-axis displays the $-\log$ of significance. (c–g) Heat maps of gene ontology (GO) classification in which genes are significantly changed according to the depletion of CREPT. Samples are displayed in the order of BLM-shCREPT ($n=3$, left) and BLM-shNC ($n=3$, right). Heat maps were made based on z-scores, which indicate the data dispersion from the mean. (c) Altered genes in the GO term “regulation of cell migration”. The majority of the downregulated genes involved in positive regulation of cell

migration and most upregulated genes in the negative effect were observed in CREPT-depleted samples. Similar observations were made in the “regulation of cell proliferation” (d), GO:0005925 “focal adhesion” (e), “actin filament polymerization” (f), and “stress fiber assembly” (g).

regulated in “focal adhesion” (12/17, 71%), “positive regulation of actin polymerization” (8/10, 80%), and “positive regulation of stress fiber assembly” (7/8, 88%) (Figure 6e–g). Taken together, the gene profiling confirms the experimental results that CREPT promotes cell proliferation and migration, and gives directions for further examination of molecular mechanisms.

CREPT Regulates Actin Filament Polymerization and Focal Adhesion Formation

According to global gene expression profiling, we identified the effect of CREPT on the actin cytoskeleton and focal adhesion-related biological processes. To visualize actin filaments and focal adhesions at the cellular level, immunofluorescence staining was performed against F-actin and vinculin (Figure 7a). The quantified data show significantly shorter lengths of filaments and fewer focal adhesion numbers in BLM-shCREPT cells than those in BLM-shNC cells (Figure 7b,e). On the contrary, BLM-CREPT cells demonstrated more filaments and focal adhesions than control cells ($p < 0.001$) (Figure 7c,f). In addition to focal adhesion numbers, we also quantified the mean size of focal adhesions but found no significant changes in size based on CREPT differential expression (Figure 7g). Measurements of the mean fluorescence intensity of focal adhesions indicated the vinculin expression level as a component of the focal adhesion complex. We detected a decrease of vinculin in low CREPT-expressing cells and an increase of vinculin in high CREPT-expressing cells (Figure 7d). These results illustrate that CREPT promotes actin filament polymerization and focal adhesion formation in melanoma cells.

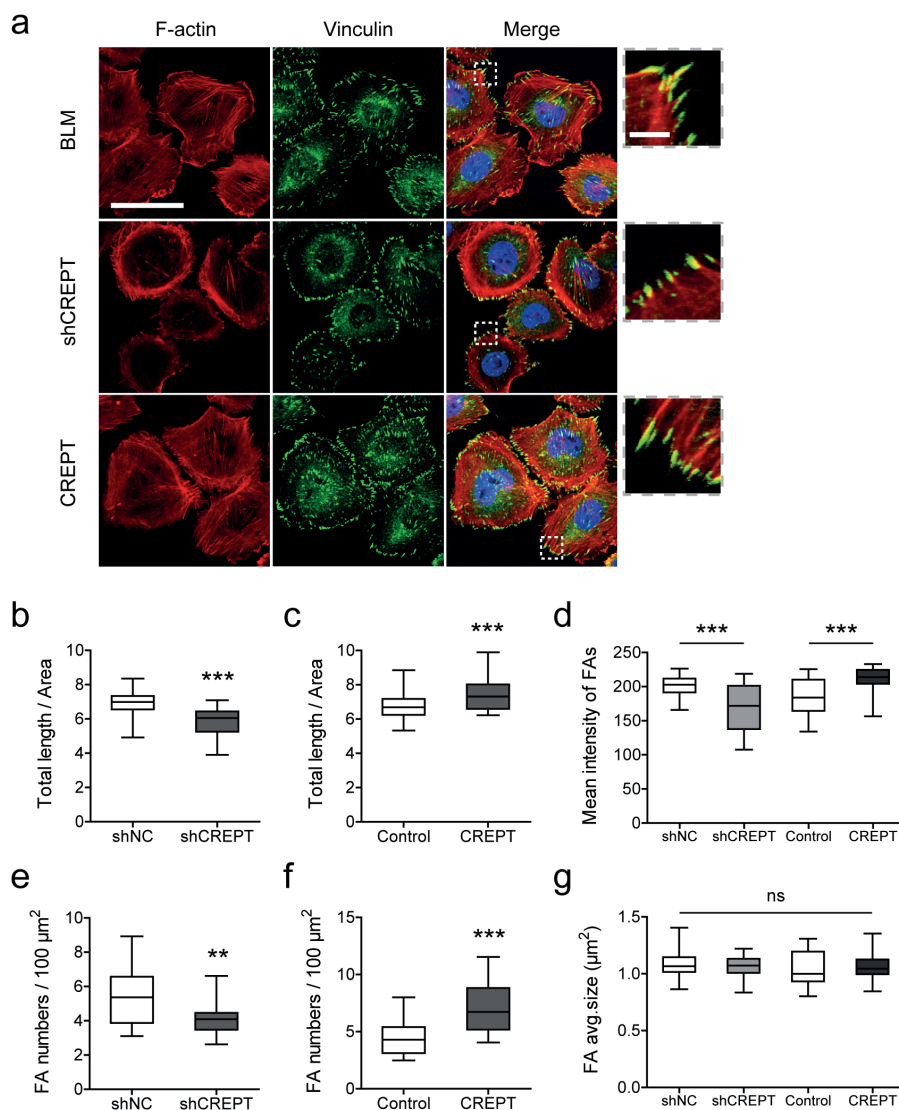


Figure 7. Fluorescent staining to visualize F-actin and focal adhesions in BLM cells. (a) Representative pictures of non-transfected BLM, BLM with low CREPT levels (BLM-shCREPT), and BLM with high CREPT levels (BLM-CREPT). Images in dotted squares are magnified to see focal adhesions at the end of actin filaments. Scale bar in large images, 50 μm ; scale bar in zoomed in panels, 5 μm . After image processing and quantification, the total length of actin filaments and focal adhesion numbers in each cell were measured. To eliminate bias against different cell sizes, data were standardized by the area unit and are shown in boxplots. (b,c) The total length (μm) of actin filaments per area (μm^2). (d) Mean fluorescence intensity of focal adhesions in individual cells. (e,f) Focal adhesion numbers per 100- μm^2 area. (g) Average size of focal adhesions in individual cells. Data in panels (b–g) represent 40 cells/measurements in three independent experiments. ** $p < 0.01$, *** $p < 0.001$; ns, not significant.

CREPT Influences Focal Adhesion Signaling-Related Molecules

To interpret the difference in actin filament polymerization and focal adhesion formation, gene expression was examined on the protein level by western blotting. CREPT protein was detected to show an efficacy of depletion and overexpression. For BLM-CREPT cells, exogenous CREPT protein was labelled with an HA (hemagglutinin)-tag, which made the protein size approximately 36 to 37 kDa, showing a band above endogenous CREPT in western blotting. We observed that expression of actin polymerization-related genes (RhoA, mDia1) and focal adhesion-related genes (FilaminA, FAK, Talin-1, Paxillin, Tensin 2) correlates with the expression of CREPT (Figure 8a, S3.1 and S3.2). We verified with the small GTPase activation assay that activation of RhoA is regulated by CREPT (Figure 8b). These results demonstrate that CREPT activates the RhoA/mDia1 axis and increases the expression of focal adhesion-related proteins.

The Role of RhoA on Actin Filaments and Cell Migration

To decipher whether the influence of CREPT on cell migration and formation of actin filaments/focal adhesions correlated with RhoA activation, we inactivated Rho proteins in BLM cells using C3 transferase. The results show that C3 transferase inhibited Rho activity to 50% at a dosage of 1 to 2 $\mu\text{g/mL}$ (Figure 9a). As the high dosage did not increase the efficiency, we treated cells with 1 $\mu\text{g/mL}$ C3 transferase to observe actin filament formation and evaluate cell migration ability. The immunofluorescence staining results show a significant decrease of the total length and focal adhesion numbers of actin filaments in Rho-inhibited cells (Figure 9b,c). Intriguingly, cell migratory capacity in 2D was significantly inhibited by Rho inactivation (Figure 9d). These results link the CREPT-regulated phenotype with RhoA activation, and demonstrate that CREPT influences cell migration, and actin filaments/focal adhesion formation, through RhoA activation.

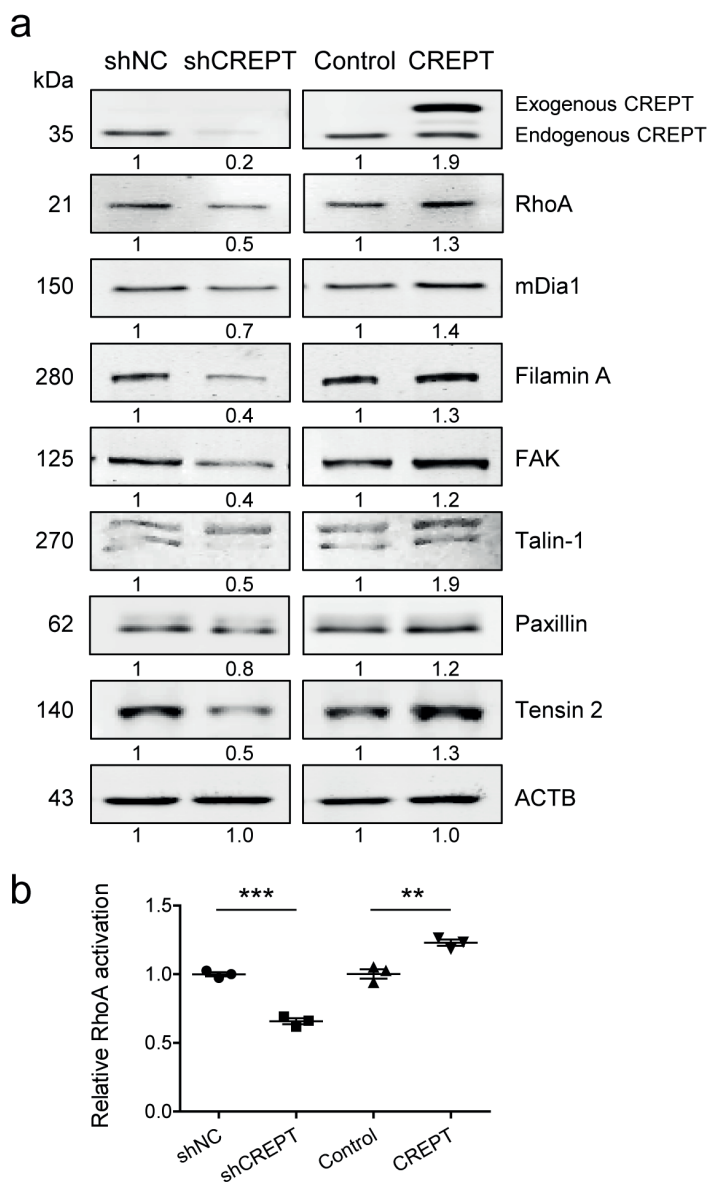


Figure 8. CREPT expression influences actin filament/focal adhesion formation-related signaling molecules in BLM cells. (a) Western blotting was performed to evaluate expression of RhoA, Diaphanous related Formin 1 (mDia1), FilaminA, focal adhesion kinase (FAK), Talin-1, Paxillin, Tensin 2. Beta-actin (ACTB) was used as the loading control. Representative results are shown followed by mean protein expression values from four independent experiments. (b) Activated RhoA levels were quantified with small GTPase activation assay, and relative values are shown as mean \pm SEM of three independent experiments. ** $p < 0.01$, *** $p < 0.001$.

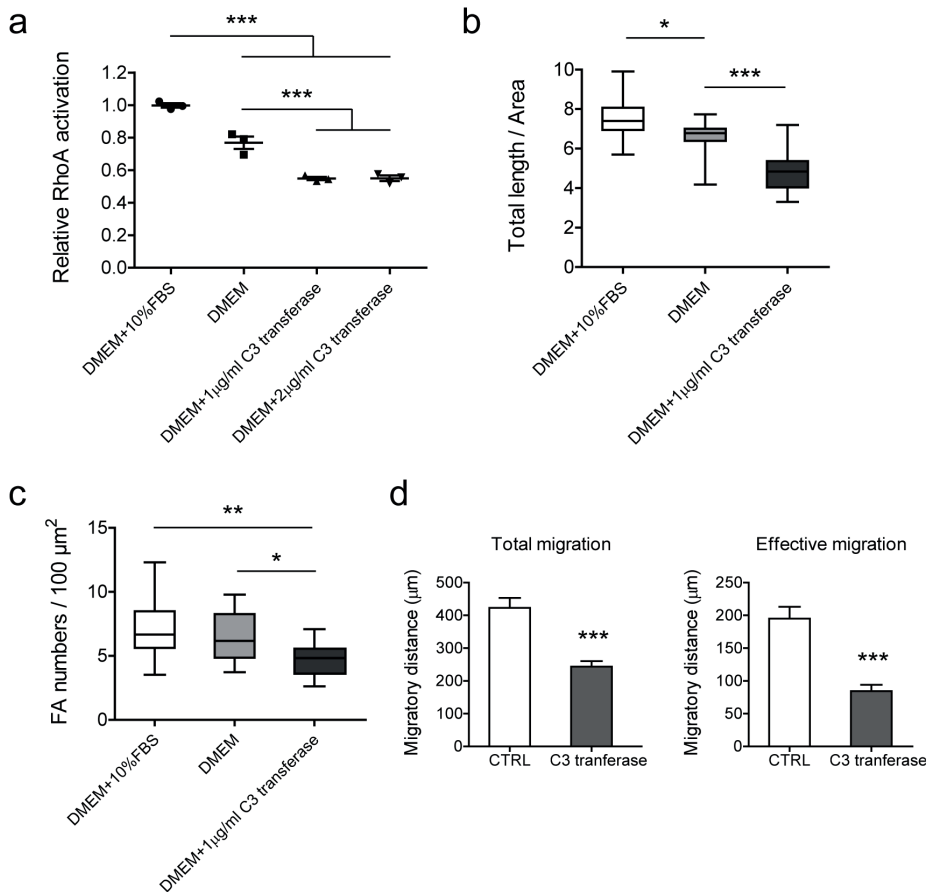


Figure 9. The effect of Rho inhibition on actin filaments, focal adhesion, and cell migration in BLM cells. (a) Cell-permeable C3 transferase was used in serum-free medium to inhibit Rho activation. BLM cells were treated with different conditions for 2 h and lysates were collected for RhoA activation assay. Standardized activation levels are shown as mean \pm SEM of three independent experiments. Immunofluorescence staining was performed to evaluate changes in actin filaments (b) and focal adhesions (c). Data of 16 cells were measured and statistically analyzed from three independent experiments. (b) Total length (μm) of actin filaments of per cell area (μm^2). (c) Focal adhesion numbers of per cell area ($100 \mu\text{m}^2$). (d) Cell migration was determined by ring-barrier migration assay. BLM cells were treated with serum-free DMEM as a control and $1 \mu\text{g}/\text{mL}$ C3 transferase in DMEM for Rho inhibition. After the 2-h treatment, medium was refreshed with DMEM + 1% FBS and time-lapse imaging was performed for 24 h. Data represent mean \pm SEM of three independent experiments. * $p < 0.05$, ** $p < 0.01$, *** $p < 0.001$.

DISCUSSION

Cell migration and metastases formation are crucial for malignant progression, which leads to increased mortality in cancer patients. Recent studies revealed the oncogenic potential of CREPT expression in multiple cancer types, including correlation with poor prognosis, induction of cell proliferation *in vitro*, and tumorigenesis *in vivo* [26-28]. Knockdown of RPRD1B increased cell sensitivity to treatment in endometrial adenocarcinoma, which suggests a therapeutic potential for targeting CREPT [21]. However, the role of CREPT in regulating cell migration and invasion is rarely discussed. As melanoma is known for high aggressiveness and strong potential of metastasis, in this study, we examined the contribution of CREPT on the migration and motility in melanoma cells. PCR and western blotting data show high transcription and protein level of CREPT in melanoma cells, and low or absent expression in human melanocytes. Melanocytes were immortalized for *in vitro* culture and served as the non-tumor control here. The findings demonstrate a differential expression of CREPT in melanoma and non-tumor cells, indicating that CREPT may function as an oncogene and may contribute to melanoma progression.

Enhanced cell growth is a typical feature of cancer. A previous study showed that CREPT promotes cell growth by regulating cell cycle-related cyclins and kinases [20]. It was also reported that CREPT regulates colorectal cancer cell proliferation and tumorigenesis through Wnt/ β -catenin signaling [29]. In addition to improving proliferation, CREPT also reduces cell apoptosis by regulating the ROS/p53 pathway, and thus increases tumor growth [30]. Consistent with the published data, our results indicate that a high level of CREPT facilitates cell division and tumorigenesis in melanoma. Another feature of cancer is metastasis. Increasing cell motility provides more possibilities for tumor metastasis. A study in gastric cancers revealed that CREPT increases cell migration by regulating E-cadherin, vimentin, N-cadherin, and matrix metalloproteinase 1 (MMP-1) expressions [30]. To assess the effect of CREPT on cell motility, we examined cell migration in 2D conditions and invasive capacity in 3D matrices, which mimicked an *in vivo* environment. Since maintaining living cells inevitably causes cell division during migration assays, we tracked single cell movement to reveal cell motility. 2D and 3D migration results indicate that CREPT induces melanoma cell motility, migration, and invasion. The low expression level of CREPT in melanocytes provides an interesting possibility to study whether forced expression of CREPT in these cells would inflict a malignant transformation, which is currently under investigation in our group. Taken together, our findings show evidence at the cellular level that CREPT promotes tumorigenesis-related biological processes, suggesting a non-negligible role of CREPT in the progression of melanoma.

Migrating cells have a polarized morphology with protrusions like lamellipodia and filopodia, which are the leading part in the direction of movement. These protrusions are driven by actin polymerization and filament assembly [31]. Focal adhesions connect actin cytoskeleton and extracellular matrix at the cell membrane, allowing actin networks to pull the cell forward [32]. The transcriptome sequencing analysis indicates that genes involved in the processes of “focal adhesion”, “actin polymerization”, and “stress fiber assembly” are regulated by CREPT. Further, immunofluorescence staining shows a CREPT-related enhancement of actin filaments and focal adhesion formation, which gives a subcellular interpretation of CREPT-regulated migration. Assembly and disassembly of focal adhesions dynamically occur during cell migration but are regulated by different mechanisms. Integrins aggregate and recruit adaptor proteins, like talin, tensin, and paxillin, to form adhesions connecting ECM structures and actin filaments. On the other hand, the disassembly process is triggered by microtubule extensions to focal adhesions [33]. In our study, the result of the dynamic equilibrium of focal adhesion formation. Focal adhesion protein levels and size were reported to be closely related to cell migration [34] while in this study, we did not observe a significant change in the mean size of focal adhesions with respect to CREPT differential expression. This result may be explained by the biphasic relationship between focal adhesion size and cell migration speed. It is reported that the mean size of focal adhesions is highly predictive of cell migration speed, however, the correlation is non-linear. Increased migration speed is accompanied by an increase in focal adhesion size until it plateaus, after which growing focal adhesions are associated with reduced migration speed. [35]. This phenomenon is also related to adhesion maturation and turnover. How and to what extent CREPT influences the focal adhesion dynamic process is still under investigation in our group.

Small GTPase protein RhoA is involved in the focal adhesion signaling pathway (KEGG:hsa04510) and regulates actin cytoskeleton organization. RhoA can activate Rho effector mDia1, which binds directly to the fast-growing barbed end of actin filaments and facilitates actin nucleation and elongation [36, 37]. In this study, we observed that CREPT upregulates RhoA activation and mDia1 expression. The results indicate a CREPT-RhoA-mDia1 signaling axis, which leads to actin organization regulation. One limitation is that we show an indirect interaction of CREPT and RhoA. How CREPT activates RhoA remains unknown, which would be an interesting question to study. To verify the role of RhoA in CREPT-induced cellular processes, we inhibited RhoA activation and consequently, actin filament/focal adhesion formation was reduced, and cell migration restrained. According to these findings, we conclude that CREPT promotes melanoma cell migration and actin filament/focal adhesion formation through RhoA activation.

CONCLUSIONS

This study demonstrated the oncogenic role of CREPT in melanoma by promoting cell proliferation, migration, and invasion. This phenomenon is dependent on the upregulation and activation of RhoA-induced actin organization and focal adhesion assembly. Our findings contribute to a better understanding of melanoma progression, and provide a potential therapeutic target for melanoma treatment.

MATERIALS AND METHODS

Antibodies and Plasmids

Anti-RhoA (2117), anti-mDia1 (5486), anti-FilaminA (4762), anti-FAK (3285), anti-Talin-1 (4021), anti-Paxillin (12065), and anti-Tensin 2 (11990) monoclonal antibodies were purchased from Cell Signaling Technology Europe B.V. (Leiden, Rotterdam, Netherlands). Anti-ACTB antibodies (A2066 and A5441) were from Sigma-Aldrich Chemie N.V. (Zwijndrecht, South Holland, Netherlands). Anti-CREPT monoclonal antibody and plasmids (pcDNA3.1-HA-CREPT, pLL3.7-shRNA-CREPT) were kindly provided by Zhijie Chang (Tsinghua University, Beijing, China) [38].

Cell Lines and Culture Conditions

Human melanoma cell lines BLM, M14, Mel57, 1F6, and 530 were maintained in Dulbecco's modified eagle's medium (DMEM) supplemented with 10% fetal bovine serum (FBS). Normal human epidermal neonatal melanocytes (NHEMs) were cultured with Melanocyte Growth Medium-4 BulletKit (Lonza Benelux BV, Breda, Netherlands). All cell lines above were routinely maintained in 5% CO₂ at 37 °C. Immortalized human melanocytes (hmels) were grown in RPMI medium supplemented with 10% FBS, tetradecanoyl phorbol acetate (TPA, 200 nM), cholera toxin (200 pM), human stem cell factor (SCF, 10 ng/mL), and endothelin 1 (10 nM), and cultured under conditions of 10% CO₂ at 37 °C.

Reverse Transcription Polymerase Chain Reaction (RT-PCR) and Quantitative PCR

Total RNA was extracted with TRIzol reagent (Invitrogen, Carlsbad, CA, USA). Reverse transcription was performed with 1 µg of total RNA using the Superscript III First-Strand Synthesis System (Invitrogen). In total, 50 ng of cDNA were used for each reaction. The sequences of PCR primers were as follows: CREPT forward: 5'-TAT AGG TAC CAT GTC CTC CTT CTC TGA G-3';

CREPT reverse: 5'-TAT ACT CGA GCT AGT CAG TTG AAA ACA GGT C-3';
 ACTB forward: 5'- GTC ATT CCA AAT ATG AGA TGC GT-3';
 ACTB reverse: 5'- AAT GCT ATC ACC TCC CCT GT-3'. Quantitative PCR was performed in duplicate, using the iCycler iQ5 platform (Bio-Rad Laboratories, Munich, Germany) with specific TaqMan Gene Expression assays (Applied Biosystems, Foster City, CA, USA). Gene expression levels are presented as relative ratio.

Western Blotting

Cells were washed with ice-cold phosphate-buffered saline (PBS) and lysed in lysis buffer (50 mM Tris-HCl pH 7.4, 150 mM NaCl, 1 mM ethylenediaminetetraacetic acid (EDTA), 1% NP-40, protease inhibitor cocktail and phosphatase inhibitor cocktail) for 30 min on ice. Lysates were cleared by centrifugation at $12,000 \times g$ for 10 min at 4 °C. Samples were electrophoresed and transferred to polyvinylidene difluoride (PVDF) membranes. Blocking was conducted in Odyssey blocking buffer (LI-COR Biosciences, Lincoln, NE, USA) for 1 h at room temperature, followed by overnight incubation of diluted primary antibodies. Membranes were further incubated with IRDye-labeled secondary antibodies (LI-COR) for 1 h at room temperature and scanned using Odyssey Infrared Imaging System (LI-COR).

Cell Transfection

The transfection was performed with DharmaFECT kb DNA transfection reagent (Horizon Discovery Group, Waterbeach, United Kingdom) according to the manufacturer's instructions. Melanoma cells were transfected with pcDNA3.1-HA-CREPT for CREPT overexpression and pcDNA3.1-HA as the control. Stable clones were selected using 600 µg/mL G418 (Thermo Fisher Scientific, Waltham, MA, USA) and maintained in culture medium with 300 µg/mL G418. CREPT-depleted cells were generated by transfection with plasmids (pLL3.7-shRNA-CREPT: pLKO.1-puro = 10:1) and control cells were transfected with plasmids (pLL3.7-shRNA-control: pLKO.1-puro = 10:1). Stable cells were selected based on fluorescence and maintained in culture medium with 1 µg/mL puromycin (Thermo Fisher Scientific, Waltham, MA, USA). Western blotting was performed to detect the transfection efficiency. BLM cells with stable transfection were used in the following experiments.

Cell Proliferation Assay

Transfected cells were seeded in a 96-well plate at a density of 2000 cells/well and allowed to attach for 6 h. After attachment, cells were fixed with 10% trichloroacetic acid at 0, 24, 48, 72, and 96 h, followed by staining with sulphophodamine B (SRB) as described [39].

The absorbance was measured at 510 nm using a microplate reader (Victor 1420, Wallac, Turku, Finland). All proliferation data were normalized to the 0-h time point and showed as the percentage growth rate.

Colony Formation Assay

A total of 500 cells/well were seeded in a 6-well plate with culture medium. After 10 to 14 days, cells were fixed with methanol for 15 min and stained with 0.1% crystal violet for 20 min. Plates were washed and air-dried. Three independent experiments were performed in 6-well plates. Colonies counting was performed by ImageJ with a minimum size of a 10-pixel area.

Tumor Growth In Mice

NMRI nude mice were obtained from Envigo (Huntingdon, United Kingdom). Upon eight weeks old, mice were subcutaneously inoculated 1×10^6 cells with serum-free DMEM on the right flank. The tumor was measured with three dimensions: length (L), width (W) and depth (D). Tumor volumes were calculated with the formula $\pi/6 \times L \times W \times D$. Mice were sacrificed with one of the endpoints: tumor volume over 1800 mm³; tumor with large ulceration or necrosis; other regular human endpoints.

Ring-Barrier Migration Assay

Cell migration was observed using the ring-barrier migration assay as previously described [40]. Briefly, 3×10^5 cells were seeded on fibronectin (10 µg/mL, Sigma-Aldrich, St. Louis, MO, USA)-coated coverslips in an Attofluor Cell Chamber (Invitrogen, Carlsbad, CA, USA) and migration was monitored for 24 h in DMEM medium supplemented with 1% FBS. Time-lapse imaging was conducted on an Axiovert 100 M inverted microscope (Carl Zeiss B.V., Sliedrecht, Netherlands). Parameters of cell migration were obtained from the acquired sequence using AxioVision SE64 Rel.4.9.1 software (Carl Zeiss, Oberkochen, Germany). Three independent experiments were performed in triplicates, and from each replicate, 10 cells' trajectories were obtained.

3D Invasion Assay

Cytodex-3 microcarrier beads (Sigma-Aldrich, St. Louis, MO, USA) were mixed with 5×10^5 cells in a falcon tube and incubated at 37 °C for 6 h with gentle mixing to ensure complete coverage of the beads. Next, the suspension was transferred to a 25-cm culture flask and incubated overnight to remove unattached cells. The cell coated beads were embedded in 1.6 mg/mL collagen gel in a 24-well plate. Post-polymerization at 37 °C for 30 min, the gel was covered with 500 µL of culture medium. Cell invasion was followed

for up to 5 days with a 10× (NA 0.30) objective lens on an Axiovert 100 M microscope (Carl Zeiss, Oberkochen, Germany). Image acquisition and analysis were conducted with AxioVision software (Carl Zeiss, Oberkochen, Germany). For each cell line, images of 10 to 15 beads were captured to measure the dispersion distance and the assay was performed three times independently.

Gene Expression Profiling

RNAs isolated from cell lines were processed with the Illumina TruSeq Stranded mRNA Library Prep Kit (Illumina, San Diego, CA, USA). The resulting indexed DNA libraries were pooled and sequenced according to the Illumina TruSeq Rapi v2 protocol on an Illumina HiSeq2500 sequencer using 50 base-pair reads. Adapter sequences were trimmed off, and resulting sequences were mapped against the GRCh38 human reference sequence using HiSat2 (version 2.1.0). Transcripts were quantified using htseq-count (version 0.9.1). Differential gene expression was performed based on the cutoff criteria of a 1.5-fold change and p -value < 0.01 . Gene ontology and pathway analysis were performed with Ingenuity Pathway Analysis (IPA, Qiagen, Hilden, Germany) and DAVID bioinformatics resources 6.8 [41]. Heat maps were created by Heatmapper [42] with variance stabilizing transformed values from DESeq2 package.

Fluorescent Staining

Cells were cultured on fibronectin (10 µg/mL)-coated 12-mm glass coverslips in 24-well plates. After incubation overnight, cells were fixed with 4% paraformaldehyde in PBS for 15 min, and permeabilized with PBS/0.1% Triton X-100 for 5 min. After being blocked with 1% BSA for 1 h at room temperature, cells were incubated with Rhodamine Phalloidin (Cytoskeleton Inc, Denver, CO, USA) and Anti-Vinculin Alexa Fluor 488 (Invitrogen, Carlsbad, CA, USA) for 1 h at room temperature. Nuclei were stained with 4',6-diamidino-2-phenylindole (DAPI, Invitrogen, Carlsbad, CA, USA). Fluorescent images were acquired using a Zeiss LSM 510 META microscope with a 63× lens (NA 1.40, Carl Zeiss, Oberkochen, Germany). F-actin quantification was performed using LPIXEL ImageJ Plugins (LPIXEL Inc, Tokyo, Japan), and focal contacts were quantified in Fiji as described [43, 44].

Small GTPase Activation Assay

The RhoA activation level of each cell line was evaluated using the RhoA G-LISA Activation Assay kit (Cytoskeleton Inc, Denver, CO, USA) according to the manufacturer's instructions.

Inactivation of Rho

BLM cells were grown to 30% to 50% confluence in 25 cm² flasks under normal culture conditions. Culture medium was aspirated, and cells were treated with 1 µg/mL C3 transferase (Cytoskeleton Inc, Denver, CO, USA) diluted in serum-free DMEM. After incubating for 2 h at 37 °C, the inactivation efficiency was measured using the small GTPase activation assay. Treated cells were fixed for immunofluorescence staining or collected for migration assay as mentioned above.

Statistical Analysis

Statistical analysis was performed using GraphPad Prism version 5.01 (GraphPad Software, San Diego, CA, USA). Multiple groups were compared using one-way ANOVA followed with Dunnett's multiple comparison test. For the comparison of two groups, student's t-test was performed for normally distributed data sets; otherwise, the Mann-Whitney test was executed. Time-varying covariates comparisons were evaluated by two-way ANOVA. A significant difference was considered when $p < 0.05$.

ACKNOWLEDGEMENTS

This study was funded by Erasmus MC Mrace grant (343566), and the grant from the National Natural Science Foundation of China (81830092). H.L. was financially supported by China scholarship council for the doctorate program.

REFERENCES

1. Siegel R.L., Miller K.D., Jemal A. Cancer statistics, 2019. *CA Cancer J Clin.* 2019;69(1):7-34.
2. Bray F., Ferlay J., Soerjomataram I., Siegel R.L., Torre L.A., Jemal A. Global cancer statistics 2018: GLOBOCAN estimates of incidence and mortality worldwide for 36 cancers in 185 countries. *CA Cancer J Clin.* 2018;68(6):394-424.
3. Weide B., Elsasser M., Buttner P., Pflugfelder A., Leiter U., Eigentler T.K., et al. Serum markers lactate dehydrogenase and S100B predict independently disease outcome in melanoma patients with distant metastasis. *Br J Cancer.* 2012;107(3):422-8.
4. Robert C., Grob J.J., Stroyakovskiy D., Karaszewska B., Hauschild A., Levchenko E., et al. Five-Year Outcomes with Dabrafenib plus Trametinib in Metastatic Melanoma. *N Engl J Med.* 2019;381(7):626-36.
5. Larkin J., Chiarion-Sileni V., Gonzalez R., Grob J.J., Rutkowski P., Lao C.D., et al. Five-Year Survival with Combined Nivolumab and Ipilimumab in Advanced Melanoma. *N Engl J Med.* 2019;381(16):1535-46.
6. Robert C., Ribas A., Schachter J., Arance A., Grob J.J., Mortier L., et al. Pembrolizumab versus ipilimumab in advanced melanoma (KEYNOTE-006): post-hoc 5-year results from an open-label, multicentre, randomised, controlled, phase 3 study. *Lancet Oncol.* 2019;20(9):1239-51.
7. Chaffer C.L., Weinberg R.A. A perspective on cancer cell metastasis. *Science.* 2011;331(6024):1559-64.
8. Lauffenburger D.A., Horwitz A.F. Cell migration: a physically integrated molecular process. *Cell.* 1996;84(3):359-69.
9. Adams J.C. Cell-matrix contact structures. *Cell Mol Life Sci.* 2001;58(3):371-92.
10. Burridge K., Chrzanowska-Wodnicka M. Focal adhesions, contractility, and signaling. *Annu Rev Cell Dev Biol.* 1996;12:463-518.
11. Cramer L.P. Organization and polarity of actin filament networks in cells: implications for the mechanism of myosin-based cell motility. *Biochem Soc Symp.* 1999;65:173-205.
12. Siret C., Terciolo C., Dobric A., Habib M.C., Germain S., Bonnier R., et al. Interplay between cadherins and alpha 2 beta 1 integrin differentially regulates melanoma cell invasion. *Br J Cancer.* 2015;113(10):1445-53.
13. Wen S.J., Zhang W., Ni N.N., Wu Q., Wang X.P., Lin Y.K., et al. Expression of Rho GTPases family in melanoma cells and its influence on cytoskeleton and migration. *Oncotarget.* 2017;8(18):30112-22.
14. Klein R.M., Aplin A.E. Rnd3 Regulation of the Actin Cytoskeleton Promotes Melanoma Migration and Invasive Outgrowth in Three Dimensions. *Cancer Res.* 2009;69(6):2224-33.
15. Haass N.K., Smalley K.S., Li L., Herlyn M. Adhesion, migration and communication in melanocytes and melanoma. *Pigment Cell Res.* 2005;18(3):150-9.
16. Chambers A.F., Groom A.C., MacDonald I.C. Dissemination and growth of cancer cells in metastatic sites. *Nat Rev Cancer.* 2002;2(8):563-72.
17. Das A.M., Pescatori M., Vermeulen C.E., Rens J.A., Seynhaeve A.L., Koning G.A., et al. Melanomas prevent endothelial cell death under restrictive culture conditions by signaling through AKT and p38 MAPK/ ERK-1/2 cascades. *Oncoimmunology.* 2016;5(10):e1219826.
18. Ni Z., Olsen J.B., Guo X., Zhong G., Ruan E.D., Marcon E., et al. Control of the RNA polymerase II phosphorylation state in promoter regions by CTD interaction domain-containing proteins RPRD1A and RPRD1B. *Transcription.* 2011;2(5):237-42.
19. Ni Z., Xu C., Guo X., Hunter G.O., Kuznetsova O.V., Tempel W., et al. RPRD1A and RPRD1B are human RNA polymerase II C-terminal domain scaffolds for Ser5 dephosphorylation. *Nat Struct Mol Biol.* 2014;21(8):686-95.

20. Lu D.D., Wu Y.Y., Wang Y.Y., Ren F.L., Wang D.J., Su F.Q., et al. CREPT Accelerates Tumorigenesis by Regulating the Transcription of Cell-Cycle-Related Genes. *Cancer Cell*. 2012;21(1):92-104.
21. Wang Y., Qiu H., Hu W., Li S., Yu J. RPRD1B promotes tumor growth by accelerating the cell cycle in endometrial cancer. *Oncol Rep*. 2014;31(3):1389-95.
22. Ding L., Yang L., He Y., Zhu B., Ren F., Fan X., et al. CREPT/RPRD1B associates with Aurora B to regulate Cyclin B1 expression for accelerating the G2/M transition in gastric cancer. *Cell Death Dis*. 2018;9(12):1172.
23. Zhang Y., Liu C., Duan X., Ren F., Li S., Jin Z., et al. CREPT/RPRD1B, a Recently Identified Novel Protein Highly Expressed in Tumors, Enhances the β -Catenin-TCF4 Transcriptional Activity in Response to Wnt Signaling. *J Biol Chem*. 2014;289(33):22589-99.
24. Liu T., Li W.M., Wang W.P., Sun Y., Ni Y.F., Xing H., et al. Inhibiting CREPT reduces the proliferation and migration of non-small cell lung cancer cells by down-regulating cell cycle related protein. *Am J Transl Res*. 2016;8(5):2097-113.
25. Tojkander S., Gateva G., Lappalainen P. Actin stress fibers--assembly, dynamics and biological roles. *J Cell Sci*. 2012;125(Pt 8):1855-64.
26. Li W.M., Zheng G.X., Xia J.H., Yang G., Sun J.Y., Wang X.J., et al. Cell cycle-related and expression-elevated protein in tumor overexpression is associated with proliferation behaviors and poor prognosis in non-small-cell lung cancer. *Cancer Sci*. 2018;109(4):1012-23.
27. Zheng G.X., Li W.M., Zuo B.L., Guo Z.Y., Xi W.J., Wei M., et al. High expression of CREPT promotes tumor growth and is correlated with poor prognosis in colorectal cancer. *Biochem Biophys Res Commun*. 2016;480(3):436-42.
28. She Y., Liang J., Chen L., Qiu Y., Liu N., Zhao X., et al. CREPT expression correlates with poor prognosis in patients with retroperitoneal leiomyosarcoma. *Int J Clin Exp Pathol*. 2014;7(10):6596-605.
29. Zhang Y.Q., Wang S.Y., Kang W., Liu C.X., Dong Y.J., Ren F.L., et al. CREPT facilitates colorectal cancer growth through inducing Wnt/beta-catenin pathway by enhancing p300-mediated beta-catenin acetylation. *Oncogene*. 2018;37(26):3485-500.
30. Sun M., Si G., Sun H.S., Si F.C. Inhibition of CREPT restrains gastric cancer growth by regulation of cycle arrest, migration and apoptosis via ROS-regulated p53 pathway. *Biochem Biophys Res Commun*. 2018;496(4):1183-90.
31. Pollard T.D., Borisov G.G. Cellular motility driven by assembly and disassembly of actin filaments. *Cell*. 2003;112(4):453-65.
32. Ciobanaru C., Faivre B., Le Clainche C. Actin dynamics associated with focal adhesions. *Int J Cell Biol*. 2012;2012:941292.
33. Ezratty E.J., Partridge M.A., Gundersen G.G. Microtubule-induced focal adhesion disassembly is mediated by dynamin and focal adhesion kinase. *Nat Cell Biol*. 2005;7(6):581-U15.
34. Hoock S.C., Ritter A., Steinhäuser K., Roth S., Behrends C., Oswald F., et al. RITA modulates cell migration and invasion by affecting focal adhesion dynamics. *Mol Oncol*. 2019;13(10):2121-41.
35. Kim D.H., Wirtz D. Focal adhesion size uniquely predicts cell migration. *FASEB J*. 2013;27(4):1351-61.
36. Evangelista M., Zigmond S., Boone C. Formins: signaling effectors for assembly and polarization of actin filaments. *J Cell Sci*. 2003;116(13):2603-11.
37. Rose R., Weyand M., Lammers M., Ishizaki T., Ahmadian M.R., Wittinghofer A. Structural and mechanistic insights into the interaction between Rho and mammalian Dia. *Nature*. 2005;435(7041):513-8.
38. Ren F., Wang R., Zhang Y., Liu C., Wang Y., Hu J., et al. Characterization of a monoclonal antibody against CREPT, a novel protein highly expressed in tumors. *Monoclon Antib Immunodiagn Immunother*. 2014;33(6):401-8.

39. Vichai V., Kirtikara K. Sulforhodamine B colorimetric assay for cytotoxicity screening. *Nat Protoc.* 2006;1(3):1112-6.
40. Das A.M., Eggermont A.M., ten Hagen T.L. A ring barrier-based migration assay to assess cell migration in vitro. *Nat Protoc.* 2015;10(6):904-15.
41. Huang D.W., Sherman B.T., Lempicki R.A. Systematic and integrative analysis of large gene lists using DAVID bioinformatics resources. *Nat Protoc.* 2009;4(1):44-57.
42. Babicki S., Arndt D., Marcu A., Liang Y., Grant J.R., Maciejewski A., et al. Heatmapper: web-enabled heat mapping for all. *Nucleic Acids Res.* 2016;44(W1):W147-53.
43. Schindelin J., Arganda-Carreras I., Frise E., Kaynig V., Longair M., Pietzsch T., et al. Fiji: an open-source platform for biological-image analysis. *Nat Methods.* 2012;9(7):676-82.
44. Horzum U., Ozdil B., Pesen-Okvur D. Step-by-step quantitative analysis of focal adhesions. *MethodsX.* 2014;1:56-9.

SUPPLEMENTARY MATERIALS

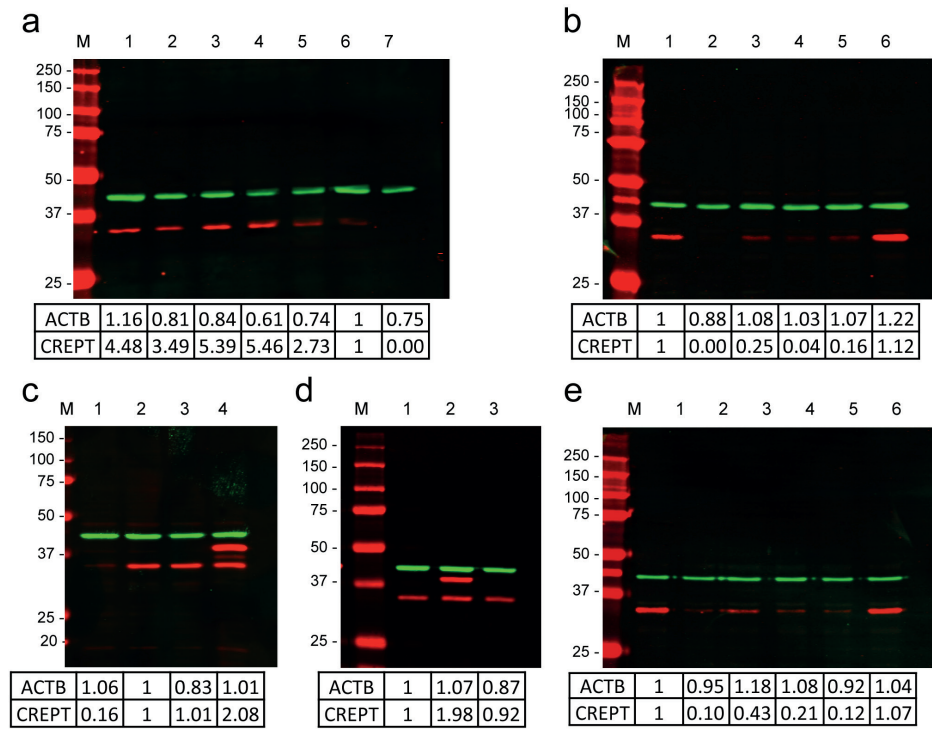


Figure S1: CREPT expression examined by western blotting. : ACTB; : CREPT. (a) CREPT in melanoma cells and melanocytes. M: marker; 1: BLM; 2: M14; 3: MEL57; 4: 1F6; 5: 530; 6: hmel; 7: NHem. (b) BLM cells were transfected with shRNAs to knockdown CREPT expression. M: marker; 1: scrambled shRNA; 2: shRNA-1; 3: shRNA-2; 4: shRNA-3; 5: shRNA-4; 6: BLM. (c) CREPT knockdown and overexpression in BLM cells used in the main text. M: marker; 1: shRNA-1; 2: scrambled shRNA; 3: empty vector; 4: vector + CREPT. (d) CREPT was overexpressed in M14 cells. M: marker; 1: empty vector; 2: vector + CREPT; 3: M14. (e) MEL57 cells were transfected with shRNAs to knockdown CREPT expression. M: marker; 1: scrambled RNA; 2: shRNA-1; 3: shRNA-2; 4: shRNA-3; 5: shRNA-4; 6: MEL57.

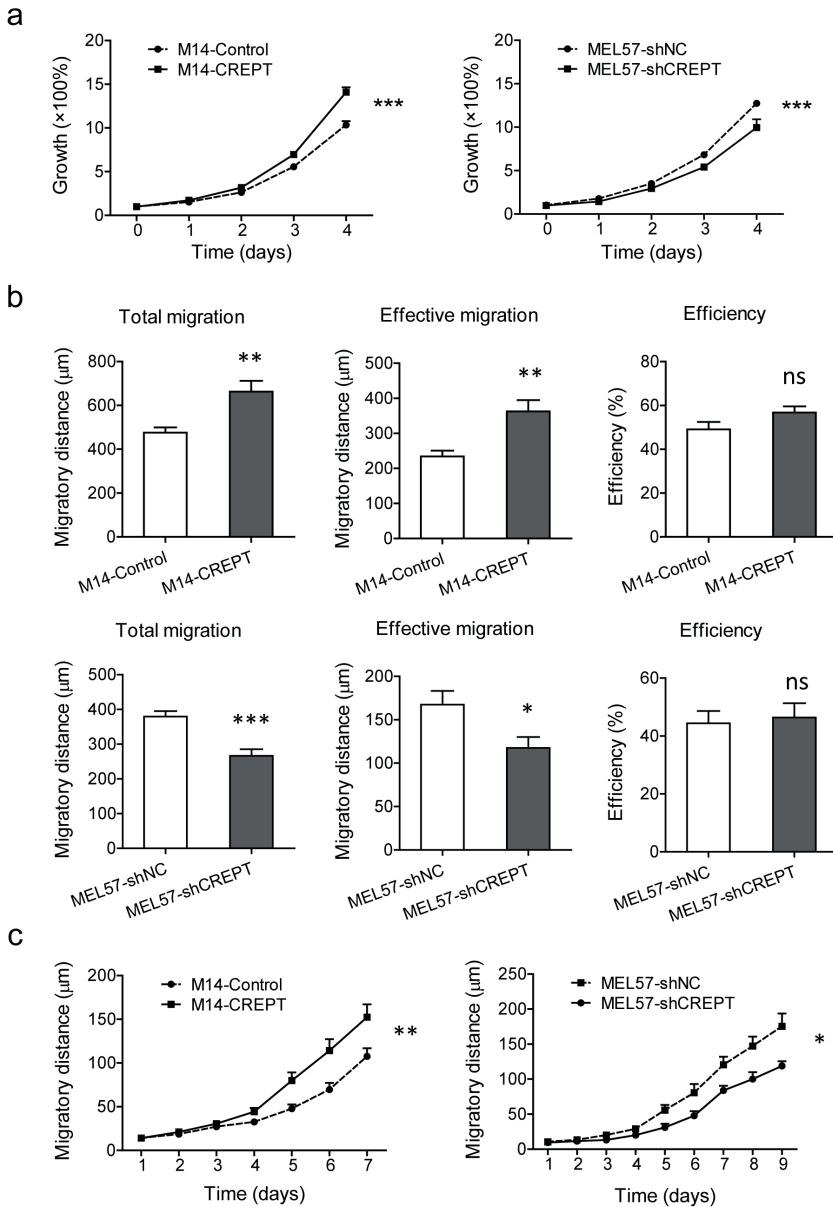


Figure S2: CREPT affects M14 and MEL57 proliferation, migration and invasion. CREPT was overexpressed in M14 cells and knocked down in MEL57 cells. (a) Cell growth rate was examined by SRB assay and standardized to the first time point. (b) Migratory parameters were obtained from ring-barrier migration assay by tracking at least thirty cells. (c) Cell invasive capacity was evaluated through microcarrier based spheroid 3D invasion assay. Cell dispersion distances were measured over time. Data represent mean \pm SEM of three independent experiments * $p < 0.05$, ** $p < 0.01$, *** $p < 0.001$. ns: not significant.

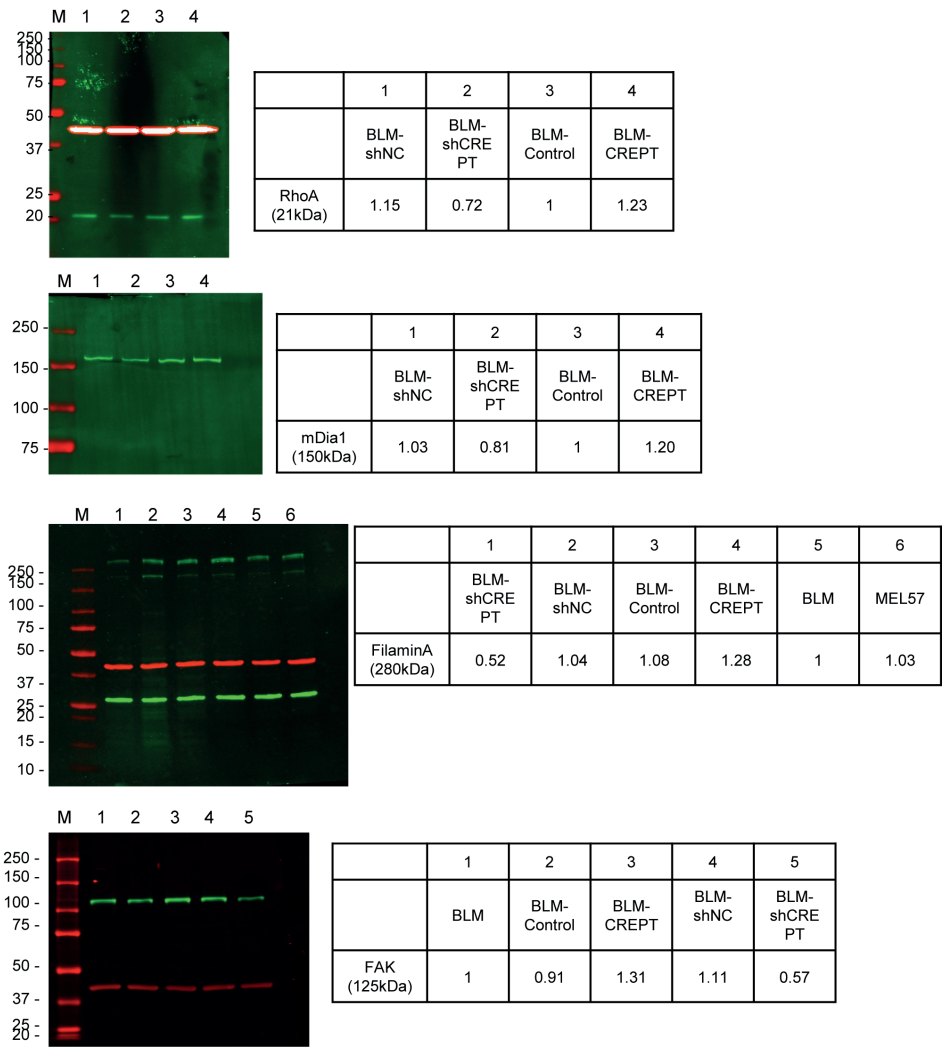


Figure S3.1: Protein expression of RhoA, mDia1, FilaminA and FAK by western blotting in CREPT modified BLM cells. Red bands show ACTB as loading control. Intensity ratios of each band is displayed in tables next to the images. The ratios were calculated on the basis of the sample with the ratio of 1.

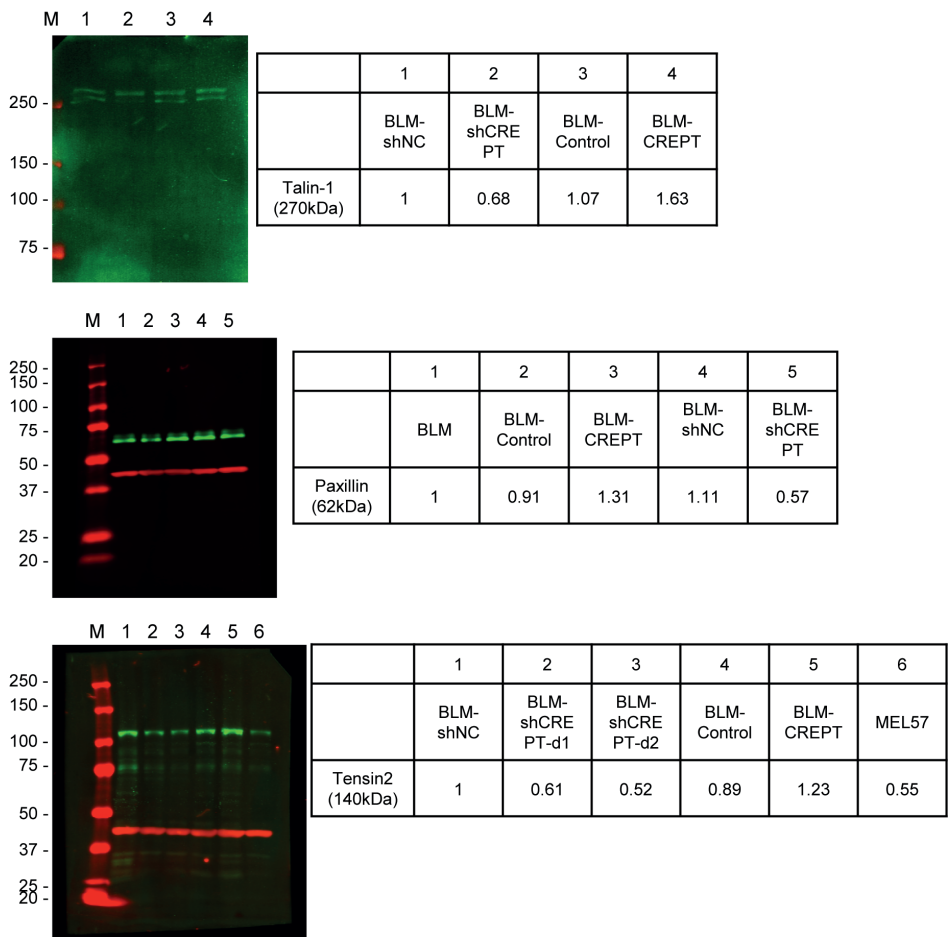


Figure S3.2: Protein expression of Talin-1, Paxillin and Tensin2 by western blotting in CREPT modified BLM cells. Red bands show ACTB as loading control. Intensity ratios of each band is displayed in tables next to the images. The ratios were calculated on the basis of the sample with the ratio of 1.

Chapter 4

Melanoma promotes pericyte survival under restrictive conditions and in vitro migration

Hui Liu, Raymond D. Schellevis, Ann L.B. Seynhaeve, Timo L.M. ten
Hagen

Chapter 5

HOXA9 mediates and marks premalignant compartment size expansion in colonic adenomas

Vincent T. Janmaat, Hui Liu, Rodrigo A. Silva, Pieter H.A. Wisse, Manon C.W. Spaander, Timo L.M. Ten Hagen, Ron Smits, Marco J. Bruno, Gwenny M. Fuhler, Maikel P. Peppelenbosch

Carcinogenesis 2019.

ABSTRACT

The transformation of normal colonic epithelium to colorectal cancer (CRC) involves a relatively ordered progression, and understanding the molecular alterations involved may aid rational design of strategies aimed at preventing or counteracting disease. Homeobox A9 (HOXA9) is an oncogene in leukemia and has been implicated in CRC pathology, although its role in disease etiology remains obscure at best. We observe that HOXA9 expression is increased in colonic adenomas compared with location-matched healthy colon epithelium. Its forced expression results in dramatic genetic and signaling changes, with increased expression of growth factors IGF1 and FLT3, super-activity of the AKT survival pathway and a concomitant increase in compartment size. Furthermore, a reduced mRNA expression of the epithelial to mesenchymal transition marker N-cadherin as well as reduced activity of the actin cytoskeletal mediator PAK was seen, which is in apparent agreement with an observed reduced migratory response in HOXA9-overexpressing cells. Thus, HOXA9 appears closely linked with adenoma growth while impairing migration and metastasis and hence is both a marker and driver of premalignant polyp growth. Colonic polyps grow but remain premalignant for up to decades. Here, we show that HOXA9 drives growth in premalignant polyps, but simultaneously prevents further transformation.

INTRODUCTION

Colorectal cancer (CRC) is the second most common cancer in men and the third in women (1). Its incidence has slightly risen in The Netherlands over the past decades while prognosis improved (2). In Europe, high CRC prevalence has resulted in the initiation of many national CRC screening programs (3). These programs are continuously evaluated and improved (4, 5). In Europe, incidence rates are declining, probably due to changes in life style and more intensive screening. However, CRC is still the second leading cause of cancer death in Europe (6). Obviously, better understanding of the molecular pathways that mediate progression from normal colonic epithelium to invasive carcinoma would aid efforts aimed at improving prevention and treatment of CRC.

Better definition of molecular markers that relate to the natural history of early CRC would prove exceedingly useful. About 30 years ago, Vogelstein et al. described the importance of premalignant lesions and their role in the adenoma–carcinoma sequence (7). The prevalence of these premalignant lesions is considered to be 25% at the age of 50 years and increases up to 50% at the age of 70 (8–11). The mechanisms driving premalignant lesions growth remain poorly understood. Also, it is not practical currently to distinguish truly benign premalignant lesions from those at risk to undergo micro-metastasis. Identifying the involved molecular determinants defines a major question in contemporary preclinical cancer research.

Molecular pathways that underlie carcinogenesis are often aberrations of normal cellular physiology. Carcinogenesis can be seen as an aberrant form of organogenesis (12–14). Homeobox genes, which include the HOX gene clusters, regulate important pathways with relation to both embryogenesis and carcinogenesis (15). The evolutionary well-conserved mammalian HOX genes encode for transcription factors regulating the formation of tissues, structures and organs along the longitudinal body axis during embryology (15–17). Thus far, 39 HOX genes have been identified in humans, which are organized in four clusters (A to D) on separate chromosomes (7, 17, 12, and 2, respectively). During embryogenesis, the different HOX clusters are expressed with temporal and spatial colinearity (18). The nested pattern of HOX genes along the length of the human body's axis is most clearly observed in segmented structures like the vertebrae, branchial arches and limbs (19–21). However, position-specific expression of HOX genes is also present in discreet organs, including the human gut (22, 23). However, the specific functionality of expression of single HOX genes in gastrointestinal pathophysiology remains to be established.

As HOX genes are important regulators of tissue growth and differentiation, it is conceivable that they also play a role in malignant transformation. This has led to an increasing interest in HOX expression patterns in different forms of cancer (24–30). Interestingly,

when screening for the expression of HOX family members in gastrointestinal pathophysiology, we observed markedly high expression of HOXA9 in esophageal adenomas when compared with normal esophagus (unpublished data). HOXA9 overexpression as a result of the NUP98-HOXA9 translocation-derived fusion gene is seen in patients with the premalignant myelodysplastic syndrome (MDS) as well as overt myeloid leukemia (31). In MDS, in particular patients with refractory anemia with excess of blasts in transformation (REAB-t) show HOXA9 fusion genes (32). In line with the fact that the NUP98/HOXA9 fusion transcript has been shown to induce hematopoietic hyperproliferation (33), this suggests that it drives the transformation process of MDS to acute myeloid leukemia (AML). HOXA9 overexpression was also shown to be the strongest factor associated with poor prognosis in AML (34). In addition to hematopoietic malignancies, HOXA9 has a pro-oncogenic effect in epithelial ovarian cancer, osteosarcoma, breast and oral squamous cell cancer (35–37). Moreover, an upregulation of HOXA9 has been described in CRC (38–41). However, it is as yet unclear whether this upregulation of HOXA9 is already present in premalignant colonic tissues. Furthermore, to what extent aberrant HOXA9 expression may drive oncogenic hallmarks is unknown. The above-mentioned considerations prompted us to compare HOXA9 expression between adenoma tissue and location-matched healthy colon epithelium and to investigate the role of HOXA9 in oncological transformation of colonic epithelial cells. We observe that HOXA9 is overexpressed in colonic adenomas and drives compartment expansion but concomitantly counteracts metastasis. Thus, HOXA9 expression emerges as a molecular determinant for pre-micrometastatic colonic adenomas and may be a marker for benign polyp growth in the colon.

MATERIALS AND METHODS

Sample collection and preparation

Participants were recruited at the Havenziekenhuis (Rotterdam, The Netherlands) in the context of the nationwide screening for CRC. Asymptomatic patients, aged between 55 and 75 years, with a positive immunologic fecal occult blood test (iFOBT) were referred to this hospital for colonoscopy. If during colonoscopy a premalignant lesion was found, biopsies were taken; one from the center of the premalignant lesion and another from healthy mucosa located in the vicinity of the lesion. Biopsies were immediately stored in RNAlater™ (Qiagen, Germany) at 4°C and stored at –80°C within 24 h until RNA was extracted. After the biopsy was taken, the remainder of the colonic polyp was resected and examined by a pathologist. Only biopsies from lesions classified as tubular adenoma with low-grade dysplasia were included for further examination. Thus, only early stages in the adenoma–carcinoma sequence were studied (7). The biopsies were collected as part

of the 'biobank for premalignant colonic lesions' and material collection was approved by the medical ethical committee of both the Erasmus Medical Center (Rotterdam, The Netherlands; MEC-2015-199) and the Havenziekenhuis. Written informed consent was obtained from all participants.

Transduction

A GeneArt bacterial plasmid (Thermo Fisher Scientific, Waltham, MA) containing the HOXA9 gene and a kanamycin-resistance gene were used for the construction of the lentiviral vector. Firstly, the HOXA9 gene was cloned into the pEN_TmiRc3 plasmid, which was a kind gift from Iain Fraser (California Institute of Technology, CA). Subsequently, the HOXA9 insert was transferred into a pSLIK-Hygro plasmid, also received from Iain Fraser (plasmid #25737; Addgene, USA), using a Gateway reaction. The same procedure was followed to create a control plasmid, lacking the HOXA9 insert. All created plasmids were sequenced by LGC Genomics (LGC Genomics GmbH, Germany) and were confirmed to be sequence correct. The pSLIK-Hygro plasmid was transiently transfected in HEK293T cells together with three packaging plasmids (VSV-G, MD and REV). After 2 days, the medium was harvested and viral particles were collected by ultracentrifugation. Caco-2 cells were transduced with the concentrated virus, after 1 day the transduced cells were selected by adding hygromycin B (Thermo Fisher Scientific, The Netherlands) (400 µg/mL) for a period of 1 week. Expression of HOXA9 was confirmed after stimulation doxycycline hyclate by qRT-PCR (Supplementary Figure 1).

Cell culture

The monthly short tandem repeat identity-verified (verification commercially performed by the molecular pathology department of the Erasmus MC) and American Type Culture Collection (ATCC, Manassas, VA)-obtained mycoplasma-free (monthly commercially checked by GATC Biotech, Konstanz, Germany) human CRC cell line Caco-2 was cultured at 37°C in a 5% CO₂ incubator using Dulbecco's modified Eagle's medium (DMEM; Lonza, Basel, Switzerland) containing 10% fetal calf serum (FCS; Sigma-Aldrich) and 1% Penicillin/Streptomycin (antibiotics) (P/S; Gibco, USA). The cells were routinely confirmed to be mycoplasma-free using the LookOut Mycoplasma PCR Detection Kit (Sigma-Aldrich). Before performing experiments, HOXA9 expression in transduced Caco-2 cells was induced by culturing in the presence of 0.5 ng/ml doxycycline hyclate (Sigma-Aldrich) and 200 µg/ml hygromycin B for up to 3 days.

RNA isolation, cDNA synthesis and PCR array/qRT-PCR

Total RNA was extracted with the NucleoSpin® RNA kit (Machery-Nagel, Germany).

For cDNA preparation, the reverse transcription system from TAKARA (TAKARA BIO INC) was used according to the manufactures manual. A cDNA concentration of 10 ng/ μ l for patient material and 30 ng/ μ l for Caco-2 cells was used for quantitative polymerase chain reaction (qPCR). The commercially available RT2 ProfilerTM PCR Array (PAHS-033ZC-2, Qiagen, Germany) was used. This array focuses on genes important in human cancer. Gene expression in HOXA9-overexpressing cells were expressed when compared with control cells by $\Delta\Delta$ CT method, using ACTB, B2M, GAPDH, HPRT1, and RPLPO represented on the plate as housekeeping controls. In addition, potential interesting candidates as derived from the array as well as HOXA9 targets identified in literature but not present in the array were tested separately (for primers and conditions, see Supplementary Table 1) in three independent experiments. Quantitative PCR was performed with SYBR Green (Applied Biosystems, USA) in an IQ5 PCR machine (Bio-Rad, Hercules, CA). To establish a loading control, TPT1, UBC, and GAPDH were used as reference genes (42). The $\Delta\Delta$ CT method was used to calculate expression values.

(Phospho)protein profiling

Caco-2 control and HOXA9-transduced cell lines were seeded in a Petri dish (60 cm) at 500 000 cells/dish and treated with 0.5 ng/ml doxycycline hyclate. After 72 h, proteins were extracted in 500 μ l Laemmli Buffer [SDS 4%, glycerol 20%, Tris-Cl (pH 6.8) 120 mM, bromophenol blue 0.02% (wt/vol) and DTT 0.1 M] and the protein concentrations were determined using a commercial kit (RC DC Protein Assay-Bio Rad). Western blotting was performed as described (43, 44). In short, 40 μ g protein was resolved by SDS-PAGE and blotted onto Immobilon FL PVDF membranes (Millipore, Bedford, MA). Membranes were blocked in Odyssey Blocking Buffer (PBS) and incubated overnight at 4°C with appropriate primary antibody (Supplementary Table 2), followed by the appropriate Alexa-linked secondary antibodies, at 1:5000 dilution, in Odyssey Blocking Buffer for 1 h. The fluorescent bands were detected using fluorescent Odyssey Imaging System and densitometric analysis was performed with ImageJ (45). All blots were reprobed for actin to control for equal loading and normalized results are represented as ratios of protein of interest over actin levels per lane. Three independent experiments were performed, run together on one blot, and heat maps of the phospho-protein profile (46) in the six samples were constructed with CIMminer (Genomics and Bioinformatics Group, Laboratory of Molecular Pharmacology, Center for Cancer Research, National Cancer Institute) (47).

Cell count and 3-(4,5-dimethylthiazol-2-yl)-2,5-diphenyltetrazolium bromide assay

For these experiments, 4×10^5 cells of the HOXA9-transduced and control-transduced cell lines were seeded and cultured for 6 days in separate T75 Cellstar culture flasks. After

6 days of culturing, the number of cells in both flasks was measured using a Cellometer™ Auto T4 cell counter (Nexcelom Bioscience LLC, USA). After 6 days of stimulation, the total number of HOXA9-overexpressing cells in the T75 flask was calculated relative to the number of cells in the control cell line. This experiment was repeated four times. MTT assays were performed as described previously (48). Transduced Caco-2 cells were seeded in a 96 well plate, each well containing 1 000 cells. After 24, 48, 72 and 96 h, cell metabolic activity and viable cells were detected by firstly adding 10 μ l 5mg/ml MTT to 100 μ l DMEM, followed by 3 h incubation at 37°C and replacing the DMEM by dimethyl sulfoxide (DMSO; Sigma–Aldrich). Intensity of color was measured in a Model 680 XR microplate reader (Bio-Rad, USA). This experiment was repeated eight times.

3D Spheroid-based cell expansion assay

Cytodex-3 microcarrier beads (Sigma–Aldrich) were mixed with 5×10^5 Caco-2 HOXA9 overexpression and control cell suspensions, at a density of 40 cells per bead and incubated at 37°C for 6 h with gentle mixing. The suspension was transferred to 25 cm² flasks and incubated for 48 h. Coated beads were embedded in 1.6 mg/ml collagen gel (collagen: modified Eagle's medium: 7.5% wt/vol NaHCO₃ in the ratio 11:8:1), put in plates, incubated at 37°C for 2 h to polymerize and covered with 500 μ l DMEM, 10% FBS, 1% p/s and 5 ng/ml doxycycline. Spheroid growth was measured by quantifying the cell layer extending from the surface of the bead. Ten coated beads were photographed every 24 h with a 10 \times objective. All measurements were performed using AxioVision 4.5 software and assays were performed three times independently. Data were statistically analyzed by two-way ANOVA.

Migration assay

Migration assays were performed as described (49). Briefly, a barrier is inserted in a culture chamber and this prevents cells from entering a defined area occupied by the barrier. Cells were seeded around this barrier to form a monolayer, the barrier is removed, and migration into the defined cell-free area is measured.

cBioportal query

We performed a query on 15 April 2018 on <http://www.cbioportal.org> (50, 51). We selected all eight studies from the category 'bowel' including a total of 3 473 cases. This included four published studies (52–55), and 'colorectal adenocarcinoma (TGCA, Provisional)', 'Colorectal adenocarcinoma (TCGA, PanCancer Atlas)', 'Rectum adenocarcinoma (TGCA, PanCancer Atlas)' and 'Targeted sequencing of 1134 samples from metastatic colorectal cancer samples (MSK, Cancer Cell 2018)'.

Statistics

Relative expression of potential target genes was calculated comparing the transduced cell line overexpressing HOXA9 to the control cell line. The one-sample t-test was used to test for statistical significance. The Komogorov–Smirnov test, the D’Agostino and Pearson omnibus normality test and the Shapiro–Wilk normality test were used for each target gene to see if the results came from a Gaussian distribution. If this assumption was violated, the relative expression of the target gene was displayed using the median and the interquartile range. In those cases, the Wilcoxon Signed-Rank Test was used to test for the difference in expression. The Student’s t-test was used to test for statistical significance in phospho-protein profile. To test for significance of the observed difference in cell number after 6 days of stimulation, the paired t-test was used (Graphpad Prism 5; GraphPad Software, Inc., USA). A two-way analysis of variance (ANOVA) was used to test for significant difference at each time point in the MTT assay. *P* values < 0.05 were considered to be statistically significant. Given that the biological significance of a given fold-change probably depends on the gene and on the experimental context, no fixed fold change cut-off was employed in this study.

RESULTS

HOXA9 is overexpressed in colonic adenomas

HOX genes have been linked to cancer development and especially HOXA9 is interesting in this respect as it functions as an oncogene in various hematological malignancies (56). It has been reported that HOXA9 contributes to self-renewal and overpopulation of cancer stem cells in CRC (57). Thus, we decided to investigate whether HOXA9 mRNA expression is deregulated in colonic premalignant tissue. To this end, we collected 27 biopsies from colonic adenomas and location-matched healthy tissue and determined HOXA9 expression by qPCR. A direct comparison between the paired adenoma and healthy tissues demonstrates significantly increased HOXA9 mRNA expression levels in the adenoma samples [fold change (FC) 1.95; $P < 1.0 \times 10^{-4}$; Figure 1]. Of note, five patients did not adhere to this trend of upregulated HOXA9 in their adenomatous tissue; however, no differences in clinical parameters (age, gender, ethnicity or type of polyp) could be detected and no follow-up data were available to assess long-term consequences of differences in HOXA9 between patient groups. We concluded that pre-malignant colonic polyps are characterized by an abundance of HOXA9 expression when compared with healthy colonic tissue.

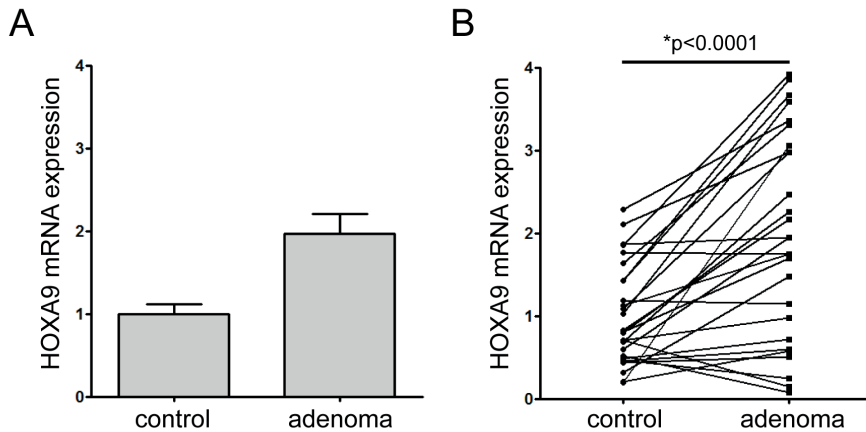


Figure 1. mRNA expression of HOXA9 in colonic adenoma tissue and matched healthy control tissue. Paired tissue samples were taken and analyzed for HOXA9 expression by RT-qPCR. In the left panel (A) mean expression levels with standard error of the mean (SEM) are depicted. In the right panel (B) the pairs are linked and the result of a paired sample t-test is shown ($P < 0.0001$).

HOXA9 overexpression substantially alters the oncogenic mRNA profile

Having shown that HOXA9 upregulation is an early event during colonic carcinogenesis, we next investigated the molecular consequences of this upregulation by overexpressing HOXA9 in the CRC model cell lines. Transduction of such cells with an inducible HOXA9 lentiviral vector results in a ≈ 30 –70 fold increase in HOXA9 mRNA expression upon doxycycline induction, when compared with cells transduced with a control plasmid (Supplementary Figure 1). Next, the effect of HOXA9 overexpression on potential target genes was examined. To identify potentially interesting HOXA9 targets, we employed the Cancer Pathway Finder RT² Profiler PCR Array (Figure 2A). Intriguingly, analysis of the differentially expressed genes showed that the most drastically downregulated gene was CCL2, which encodes for the chemokine MCP-1, and is a well-known mediator of tumor metastasis. Indeed, high levels of CCL2 are associated with poor outcome in CRC patients due to high incidence of metastasis (58, 59). Thus, this result implies that HOXA9 expression might be specific to pre-metastatic lesions.

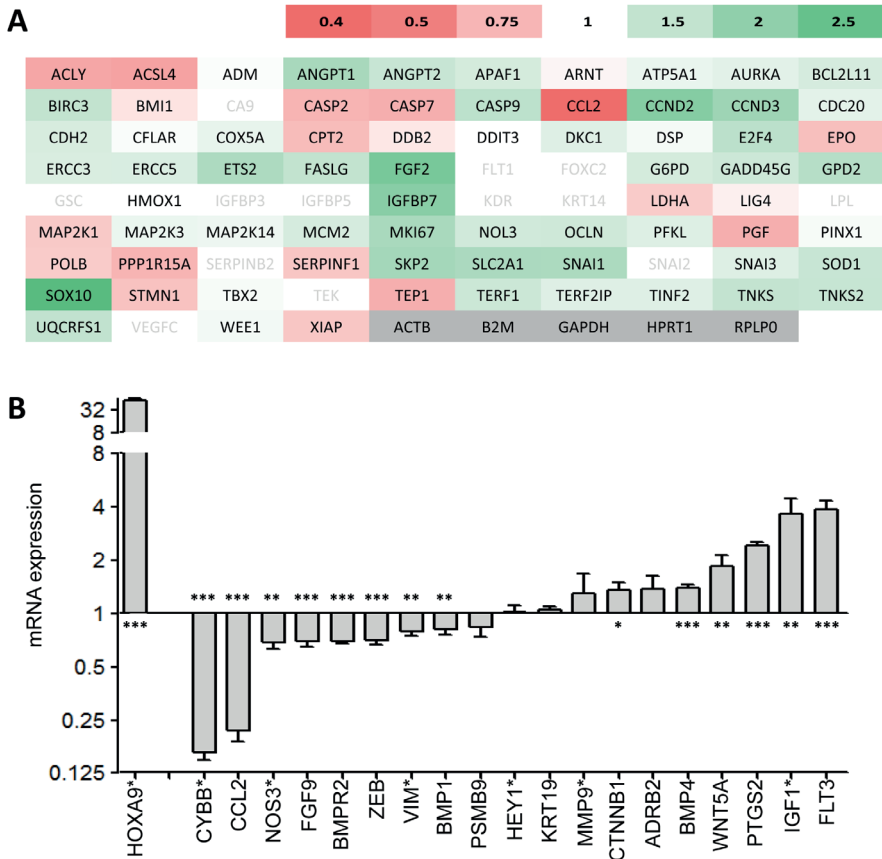


Figure 2. Effect of HOXA9 overexpression on target genes. (A) The RT2 ProfilerTM PCR Array was used to detect differential expression profiles between HOXA9-overexpressing cells and control cells. Depicted are the mRNA levels quantified in a single experiment. mRNAs in red are downregulated upon HOXA9 overexpression compared with a control transduced Caco-2 cell line, conversely, mRNAs in green are upregulated. See scale bar in the right upper corner for the magnitude of the fold changes. (B) The overexpression of HOXA9 is depicted in this panel. RT-qPCR was performed on 25 mRNA targets identified to be modulated by HOXA9 in literature (Supplementary Supplementary Table 2). Of these, six were not detectable by qPCR, the expression of the remainder of mRNAs (19) are shown as a fold change compared with control cells. Expression data of mRNAs that did not meet the assumption of Gaussian distribution, according to both the Komogorov–Smirnov test, the D’Agostino and Pearson omnibus normality test and the Shapiro–Wilk normality test were indicated with an * next to their name on the x-axis. Expression data of mRNAs that did not meet assumption of Gaussian distribution are presented as medians \pm IQR. * $P < 0.05$; ** $P < 0.01$; *** $P < 0.001$. For the genes that did meet the assumption of Gaussian distribution, results presented as means \pm SEM.

Other downregulated genes included the metabolism genes *ACLY* and *ACSL4* and the apoptosis genes *CASP2* and *CASP7*. Among the most prominently upregulated genes were the cell cycle genes *CCND2*, *CCND3*, *SKP2* and *MKI67* and the growth factor *FGF2*, suggesting that *HOXA9* overexpression provokes a proliferative phenotype. Another highly upregulated gene is the insulin growth factor binding protein 7 (*IGFBP7*). This gene is part of the category of IGF1 signaling modulating genes, and while often considered tumor suppressive, has also been shown to be upregulated in some cancers, and may have growth-stimulatory effects in CRC (60–62). *HOXA9* overexpression led to overexpression of the HMG-box gene *SOX10*. This gene is best known for its role in neural crest differentiation during embryogenesis, but its ectopic expression in tumors has also been shown to confer tumor aggressiveness in some tumor types (63–66), although a tumor-suppressive role has also been reported (67). In conjunction, these results are best interpreted as indicating that *HOXA9* expression may stimulate adenoma growth and is responsible for compartment expansion but concomitantly would be associated with non-metaplastic behavior.

Taken together, this exploratory analysis suggests a decreased migratory phenotype, with reduced apoptosis, and increased proliferation markers. Next, we expanded on these findings by designing qPCR primers for a range of target genes not included in the array, but with specific connection to *HOXA9* as identified in literature search including all tissues and model systems (Supplementary Table 1) (68–72). In addition, we also verified the main interesting finding of the Cancer Pathway Finder array, *CCL2* expression using alternative primers. The statistically significantly regulated genes with the highest upregulation were *FLT3* (mean FC = 3.8), *IGF1* (mean FC = 2.8), *PTGS2* (mean FC = 2.4) and *WNT5a* (mean FC = 1.8). *FLT3*, *IGF1* and *WNT5a* are all associated with compartment expansion (Figure 2B). *FLT3* is a tyrosine kinase receptor, *IGF* is a growth factor which stimulates phosphorylation-dependent kinase cascades via the *IGF*-receptor and *WNT5a* activates intracellular signaling through ligation to the *Ror2*/*Frizzled* receptors. Overexpression of *PTGS2* (better known as *COX2*) has been associated with adenomatous changes and its inhibition is well-established to counteract colorectal polyp formation (73, 74). The genes with the highest relative downregulation were *CYBB* (mean FC = 0.2), encoding for the NADPH oxidase complex protein *NOX2* and *CCL2* (mean FC = 0.2). Interestingly, a switch in expression from *NOX1* to *NOX2* induced a migratory invasive phenotype in CRC cells (75), which, together with the decreased *CCL2* expression, suggests that *HOXA9* overexpression decreases CRC migratory behavior. Genes associated with epithelial to mesenchymal transition (EMT) (*BMP1*, *BMPR2*, *KRT19*, *VI* *M* and *ZEB*) measured in this study showed little to no difference in expression as a result of *HOXA9* overexpression. Overall, a picture emerges that *HOXA9* is associated with polyp formation but also counteracts malignant progression.

Changes in cellular phosphoprofile support a role for HOXA9 in polyp growth but not malignant expansion

As HOXA9 overexpression modulates genetic transcription patterns towards an early proliferative phenotype, we next sought to determine to what extent HOXA9-induced changes are translated to altered signal transduction patterns. We performed extensive (phospho) protein profiling to quantify the expression and activation status of several important signal transduction molecules (Supplementary Table 2). Analysis of constitutive expression of signaling molecules did not reveal significantly discriminative patterns between HOXA9 overexpressing and mock-transduced cell pools (Supplementary Figure 2A and B). However, a distinct phosphoprofile upon HOXA9 overexpression was seen, as evidenced by the clustering of control and overexpression samples (Figure 3).

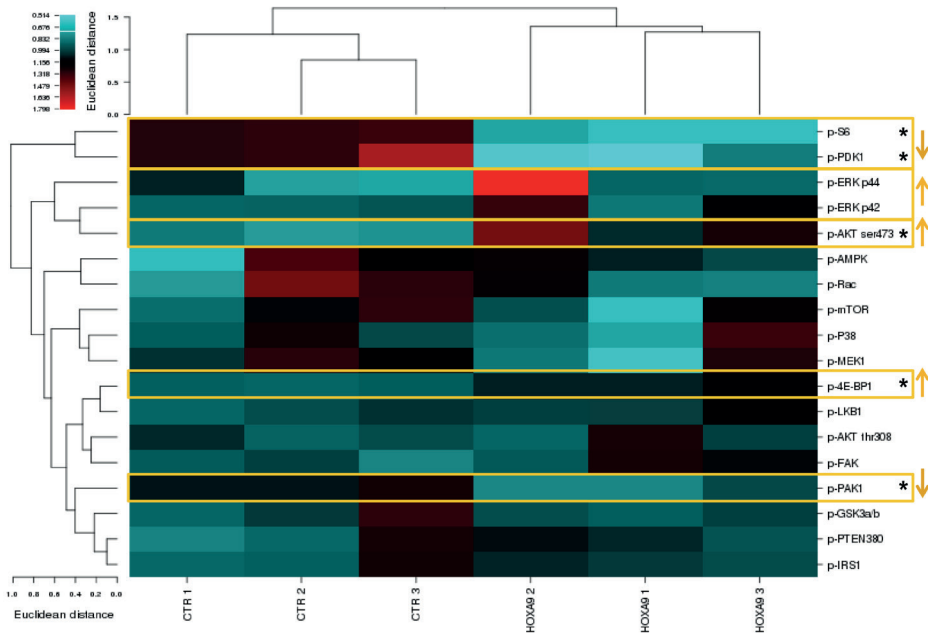


Figure 3. HOXA9 influences cellular phosphoprofile. Heat maps of the phospho-protein profile constructed with CIMminer. Increased phosphorylation is depicted in red, conversely decreased phosphorylation is depicted in blue. See scale bar in the top left corner for magnitude of the phosphorylation. Euclidian distance between the samples is depicted on top. For the phosphorylation status of the various signaling proteins, Euclidian distance is depicted to the left. Statistical significance was indicated on the right side of the figure with an asterisk * $P < 0.05$; ** $P < 0.01$; *** $P < 0.001$. Orange boxes and arrows are placed over molecules or molecule pairs to clarify the direction of regulation visually.

The most discriminate findings were a clustering of downregulated p-S6 ($FC = 0.50$, $P < 1.0 \cdot 10^{-4}$) and p-PDK1 ($FC = 0.45$, $P = 5.9 \cdot 10^{-3}$) upon HOXA9 overexpression (see Figure 4 for individual analyses). Canonical signaling dictates that activity of PDK1 results in phosphorylation of the Thr308 residue of AKT, a survival protein, whereas phosphorylation of this protein on its Ser473 residue is dependent on the mammalian target of rapamycin (mTOR) when in association with Rictor in the so-called mTORC2 complex (Figure 5A). Fully activated AKT in turn is known to activate the mTOR/Raptor complex (mTORC1), which results in phosphorylation both the ribosomal S6 kinase and the translation factor 4E-BP regulating cell size and protein synthesis, respectively (76). However, our results indicate an uncoupling with canonical mTOR signaling in cells overexpressing HOXA9: (i) the decreased PDK activity was not accompanied by reduced AKT-thr308 phosphorylation, but corresponded closely to decreased S6 phosphorylation. (ii) Although there was a trend towards lower mTOR phosphorylation, this was not significant, suggesting that the phosphorylation of S6 upon HOXA9 is not a direct effect of reduced mTOR signaling. (iii) 4E-BP phosphorylation was significantly increased ($FC = 1.21$, $P = 2.0 \cdot 10^{-3}$), rather than decreased HOXA9-overexpressing cells. Uncoupling between mTOR and its downstream targets is not unprecedented, as a direct activation of S6 via PDK1 has also been described (77, 78), and 4E-BP1 signaling can be independent of mTOR activity in CRC (79). However, this begs the question as to what activates 4E-BP, if not mTOR. Based on our data set, it is tempting to speculate that AKT activity ($FC = 1.6$, $P = 2.12 \cdot 10^{-2}$) may bypass mTOR in the phosphorylation of 4E-BP (Figure 5B). Adding a further layer of complexity, it was previously shown that knockdown of Rictor promotes AKT phosphorylation, and it is conceivable that HOXA9 modulates part of the mTORC2 complex rather than mTOR per se (80).

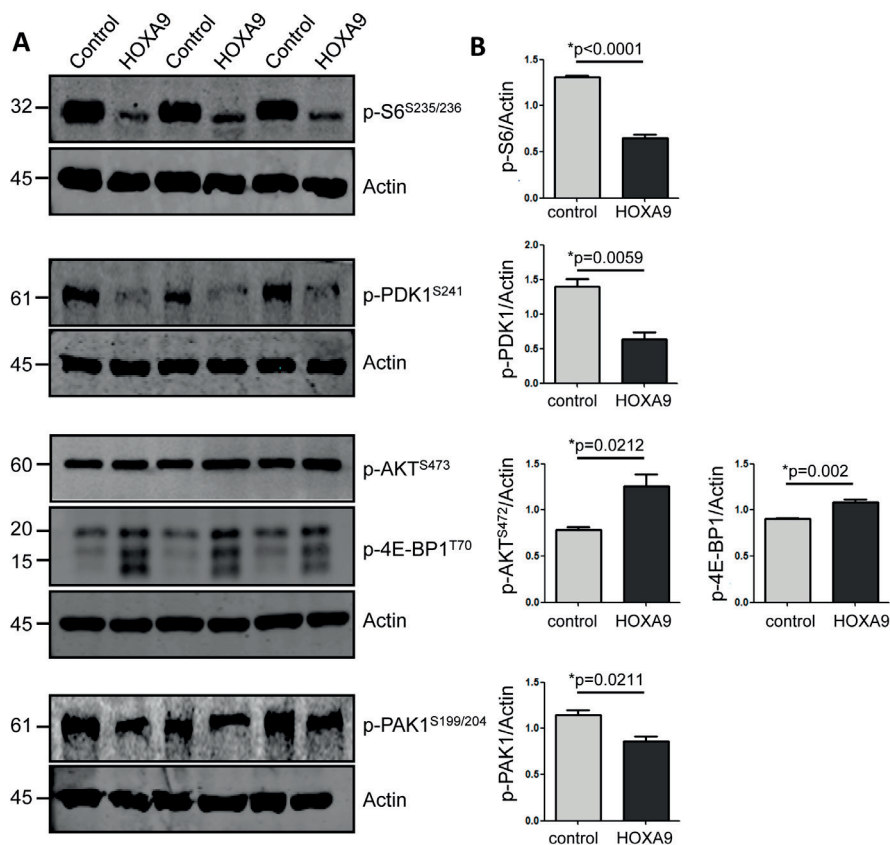


Figure 4. HOXA9 induces differential protein expression. (A) Western blots of the five proteins for which the phosphorylation status was significantly altered by HOXA9, their names are depicted on the right, the size of the band is indicated on the left. The HOXA9 status of the samples is depicted on top. (B) The results of densitometric analysis of the fluorescence bands are depicted and expressed in normalized densitometry values (AU, arbitrary units). Blots were reprobed for actin for loading control. Additionally, their corresponding *P* values are depicted above the panels.

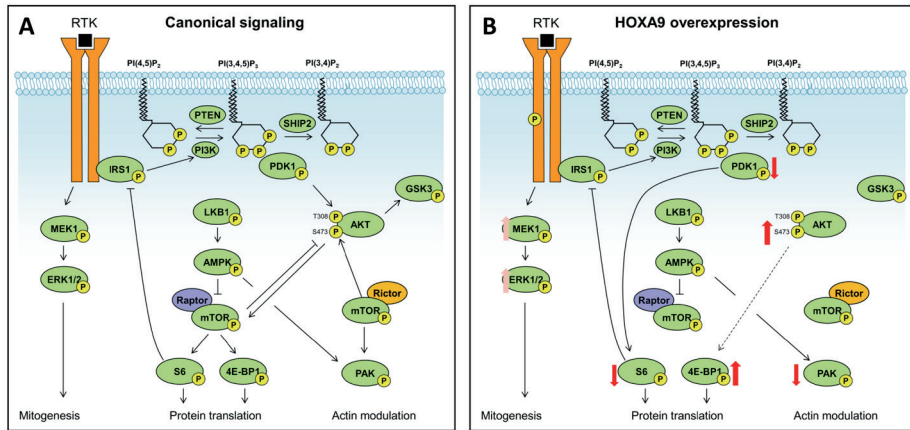


Figure 5. HOXA9 influences mitogenesis, protein translation and actin modulation. (A) Canonical signaling pathways of phosphoproteins. (B) Altered signaling upon HOXA9 overexpression. Red arrows indicate statistically significant directional regulation and pink arrows depict a trend in regulation.

HOXA9 overexpression stimulates adenoma growth

Taken together, our mRNA and protein analyses of forced HOXA9 expression indicate that this gene provokes increased growth-factor (IGF1, FLT3, WNT5a) action and enhances survival (pAKT) signaling and protein synthesis (phosphorylation of p-4E-BP1) which relieves its suppressive action on the translation-initiation factor eIF4E, resulting in increased translational activity (83). We next sought to validate whether these molecular consequences of HOXA9 overexpression translate into cellular phenotypic changes. Therefore, we compared the cell pool growth of both the HOXA9 overexpressing and control cell lines. Starting with equal cell numbers, 70% more cells were seen after 6 days of culture in cell cultures of HOXA9-overexpressing cells when compared with controls ($P < 4.0 \cdot 10^{-3}$; Figure 6A), suggesting that HOXA9 confers a growth advantage to cells. To confirm this, the cell pool size was measured daily for four consecutive days. Figure 6B shows that HOXA9-overexpressing cells have a significantly increased growth rate compared with control cell cultures (day 2, $P < 0.05$; day 3, $P < 1.0 \cdot 10^{-3}$ and day 4, $P < 1.0 \cdot 10^{-3}$; Figure 6B). We further confirmed these data by culturing cells in a 3D spheroid-based model, which again indicated that HOXA9-overexpressing cells grow faster in 3D when compared with control cells ($P = 0.0272$; Figure 6, C1 for quantified results and C2 for illustrations of cells on the beads). Hence, increased HOXA9 expression may be directly related to the compartment size expansion that characterizes the adenomatous epithelium.

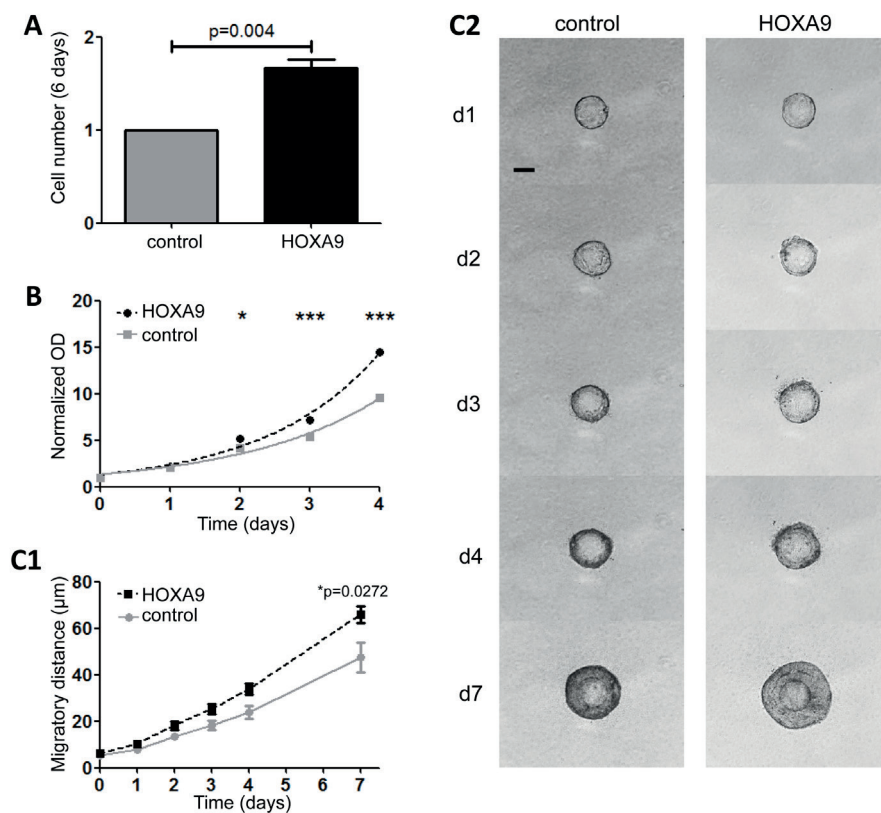


Figure 6. HOXA9 overexpression results in increased growth of the cell pool. (A) Cell count after 6 days stimulation with doxycycline. Amount of control cells after 6 days is the reference value. (B) MTT assay measuring viable cells in HOXA9 and control transduced Caco-2 cells. Results are represented as mean \pm SEM of three independent experiments. $*P < 0.05$, $***P < 0.001$ compared with control by Student's T-test. (C1) 3D-migration assay, quantified results of one representative experiment (out of three) with data of ten coated beads. (C2) Photographs of control and HOXA9-overexpressing cells on beads in gelatin at days 1, 2, 3, 4, and 7. 'd' = day. Data were statistically analyzed by two-way ANOVA. Scale bar: 100 μm .

HOXA9 overexpression inhibits cellular migration suggesting that its expression is specific for the adenoma stage in CRC progression

The reduced expression of chemokines (CCL2) and cytoskeletal modulators (pPAK) suggests that motility of cells might be affected upon overexpression of HOXA9 (84, 85). Therefore, we investigated migratory ability of these cells using 2D ring-barrier assays which, unlike conventional scratch assays, are not influenced by proliferative capacity of

cell cultures but use time-lapse microscopy to track individual cell movement. Results show that HOXA9 overexpression leads to a significant reduction in individual cell migration, compromising the total and effective migration after 3 days, as well as in the efficiency and speed of cellular migration (Figure 7).

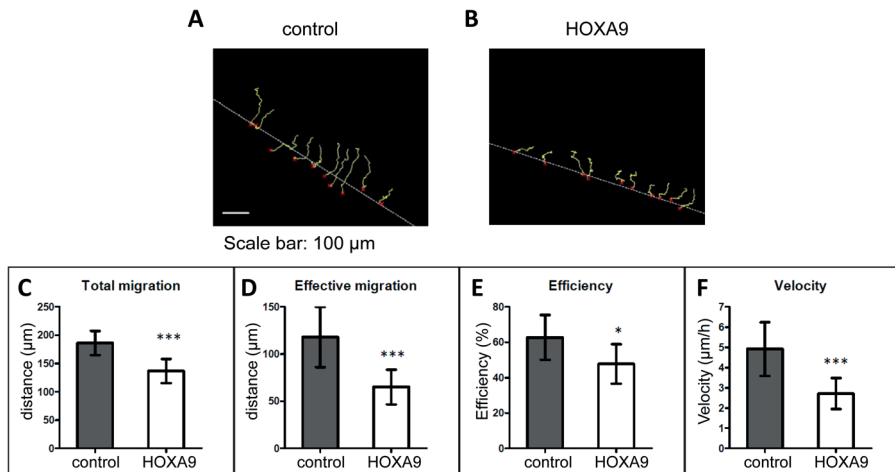


Figure 7. HOXA9 overexpression inhibits cellular migration. Individual cells were tracked in time laps microscopy of cellular migration for control cells (A) and HOXA9-overexpressing cells (B). A minimum of 10 cells were traced for each condition per experiment, and total migration (C), effective migration (D), efficiency (E) and velocity (F) of migration were calculated. Results are represented as mean \pm standard error of the mean (SEM) of three independent experiments.

Tubular adenoma is the precursor to full blown CRC but is considered to have no metastatic potential. The present study shows that HOXA9 is highly expressed in colonic tubular adenomas and this expression can drive compartment expansion in a preclinical model. However, forced expression of HOXA9 also counteracts CCL2 and metastasis. In conjunction, these findings suggest that HOXA9 is a defining molecular marker of specifically the tubular adenoma stage in CRC development. This would fit a recent report that showed that in full blown CRC, tumors are characterized by increased HOXA9 expression but that such expression does not correlate with clinical outcome (41). Here, we show that this increase is particularly manifest at the adenoma stage, but our mechanistic studies also reveal that for successful metastasis, HOXA9 expression is inhibitory. Thus, increased HOXA9 expression has a specific pro-oncogenic functionality only at early stage of the CRC process and can be considered a marker of these early stages.

DISCUSSION

CRC remains a major health problem. Better definition of molecular markers that relate to the natural history of early CRC would prove exceedingly useful. In this study, we compared HOXA9 expression between adenoma tissue and location-matched healthy colon epithelium and we subsequently decided to investigate the role of HOXA9 in oncological transformation of colonic epithelial cells. We observe that HOXA9 is overexpressed in colonic adenomas and drives compartment expansion but concomitantly counteracts metastasis. Thus, HOXA9 expression emerges as a molecular determinant for pre-micrometastatic colonic adenomas and may support benign polyp growth in the colon.

Potential mechanisms mediating increased HOXA9 expression in adenoma

Based on the data from the publically available cBioPortal (Supplementary Figure 3), gene amplification appears not to be involved in the increase of HOXA9 levels in CRC (50) (not shown). Given that gene amplifications are rare in colonic adenomas, this is in line with our findings. Also chromosomal translocation, which can drive altered HOXA9 expression in hematological malignancies, does not appear an important factor in this respect (not shown). Furthermore, HOXA9 was not found to be differentially methylated in CRC (86). Bhatlekar *et al.* found that HOXA4 and HOXA9 are up-regulated in CRC stem cells (57). Their data indicate that HOXA9 aids self-renewal and overpopulation of stem cells in CRC. Multiple reports have described HOXA9 as a pro-oncogenic factor in other solid tumors (87). Hence, increased HOXA9 expression may well be driven by selection of clones that have a competitive advantage because of relatively high HOXA9 expression and the resulting outcompeting of cells not having such high expression. In line with this train of thought is that β -catenin signaling, activated upon WNT5A ligation to its receptor, is required for HoxA9-mediated transformation in the hematopoietic system (88). Additionally, colonic adenomas are almost universally characterized by high levels of β -catenin signaling (89). However, further experimentation is obviously necessary to substantiate this notion.

CONCLUSION

In conclusion, HOXA9 is overexpressed in colonic adenomas. It inhibits cellular migration which appears to be mediated by effects on PAK activity. Strikingly, the pro-oncogenic phenotype of HOXA9 alteration in hematologic malignancies was also found in this study as HOXA9 stimulates cell growth. This phenotype appears to be mediated through increased IGF1, FLT3, PTGS2 and p-AKT and p-4E-BP1. This is the first mechanistic study into the effect of HOXA9 in a premalignant lesion.

List of abbreviations

CRC colorectal cancer
DMEM Dulbecco's modified Eagle's medium
qPCR quantitative polymerase chain reaction

ACKNOWLEDGEMENTS

We would like to acknowledge M.H.W. van Dullemen for experimentation. M.P.P. is grateful to the Dutch Society for the Replacement of Animal Testing" (dsRAT) for the financial support of his work. The authors would like to thank the FAPESP (2016/08888-9, 2016/01139-0) for financial support for RdS.

REFERENCES

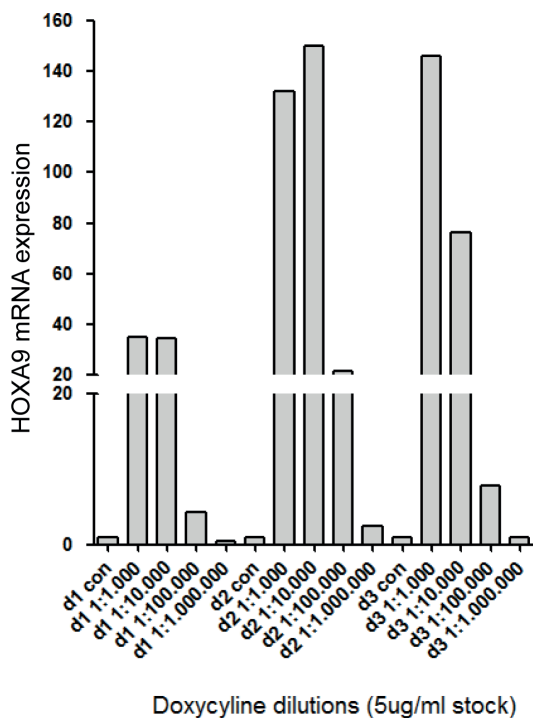
1. Ferlay, J. et al. (2010) Estimates of worldwide burden of cancer in 2008: GLOBOCAN 2008. *Int. J. Cancer*, 127, 2893–2917.
2. Brouwer, N.P.M. et al. (2018) An overview of 25 years of incidence, treatment and outcome of colorectal cancer patients. *Int. J. Cancer*, 143, 2758–2766.
3. Elferink, M.A.G. et al. (2018) [National population screening for colorectal carcinoma in the Netherlands: results of the first years since the implementation in 2014]. *Ned. Tijdschr. Geneesk.*, 162, D2283.
4. Toes-Zoutendijk, E. et al. ; Dutch National Colorectal Cancer Screening Working Group. (2017) Real-time monitoring of results during first year of Dutch Colorectal Cancer Screening Program and optimization by altering fecal immunochemical test cut-off levels. *Gastroenterology*, 152, 767–775.e2.
5. Greuter, M.J.E. et al. (2017) Screening for colorectal cancer with fecal immunochemical testing with and without postpolypectomy surveillance colonoscopy: a cost-effectiveness analysis. *Ann. Intern. Med.*, 167, 544–554.
6. Edwards, B.K. et al. (2010) Annual report to the nation on the status of cancer, 1975–2006, featuring colorectal cancer trends and impact of interventions (risk factors, screening, and treatment) to reduce future rates. *Cancer*, 116, 544–573.
7. Vogelstein, B. et al. (1988) Genetic alterations during colorectal-tumor development. *N. Engl. J. Med.*, 319, 525–532.
8. Williams, A.R. et al. (1982) Polyps and cancer of the large bowel: a necropsy study in Liverpool. *Gut*, 23, 835–842.
9. Rex, D.K. (1995) Colonoscopy: a review of its yield for cancers and adenomas by indication. *Am. J. Gastroenterol.*, 90, 353–365.
10. Rex, D.K. et al. (1993) Colonic neoplasia in asymptomatic persons with negative fecal occult blood tests: influence of age, gender, and family history. *Am. J. Gastroenterol.*, 88, 825–831.
11. Wang, F.W. et al. (2014) Prevalence and risk factors of asymptomatic colorectal polyps in taiwan. *Gastroenterol. Res. Pract.*, 2014, 985205.
12. Abate-Shen, C. (2002) Deregulated homeobox gene expression in cancer: cause or consequence? *Nat. Rev. Cancer*, 2, 777–785.
13. Reya, T. et al. (2005) Wnt signalling in stem cells and cancer. *Nature*, 434, 843–850.
14. Taipale, J. et al. (2001) The Hedgehog and Wnt signalling pathways in cancer. *Nature*, 411, 349–354.
15. McGinnis, W. et al. (1992) Homeobox genes and axial patterning. *Cell*, 68, 283–302.
16. Pearson, J.C. et al. (2005) Modulating Hox gene functions during animal body patterning. *Nat. Rev. Genet.*, 6, 893–904.
17. Hueber, S.D. et al. (2013) Analysis of central Hox protein types across bilaterian clades: on the diversification of central Hox proteins from an Antennapedia/Hox7-like protein. *Dev. Biol.*, 383, 175–185.
18. Lewis, E.B. (1978) A gene complex controlling segmentation in *Drosophila*. *Nature*, 276, 565–570.
19. Hunt, P. et al. (1991) The branchial Hox code and its implications for gene regulation, patterning of the nervous system and head evolution. *Dev. Suppl.*, Suppl 2, 63–77.
20. Pollock, R.A. et al. (1992) Altering the boundaries of Hox3.1 expression: evidence for antipodal gene regulation. *Cell*, 71, 911–923.
21. Yokouchi, Y. et al. (1991) Homeobox gene expression correlated with the bifurcation process of limb cartilage development. *Nature*, 353, 443–445.
22. Yahagi, N. et al. (2004) Position-specific expression of Hox genes along the gastrointestinal tract. *Congenit. Anom. (Kyoto)*, 44, 18–26.

23. Beck, F. (2002) Homeobox genes in gut development. *Gut*, 51, 450–454.
24. Abe, M. et al. (2006) Disordered expression of HOX genes in human non-small cell lung cancer. *Oncol. Rep.*, 15, 797–802.
25. Cantile, M. et al. (2003) In vivo expression of the whole HOX gene network in human breast cancer. *Eur. J. Cancer*, 39, 257–264.
26. Miller, G.J. et al. (2003) Aberrant HOXC expression accompanies the malignant phenotype in human prostate. *Cancer Res.*, 63, 5879–5888.
27. Liu, Y.J. et al. (2015) Overexpression of HOXC11 homeobox gene in clear cell renal cell carcinoma induces cellular proliferation and is associated with poor prognosis. *Tumour Biol.*, 36, 2821–2829.
28. Cantile, M. et al. (2012) Increased HOX C13 expression in metastatic melanoma progression. *J. Transl. Med.*, 10, 91.
29. Cantile, M. et al. (2013) Aberrant expression of posterior HOX genes in well differentiated histotypes of thyroid cancers. *Int. J. Mol. Sci.*, 14, 21727–21740.
30. Cheng, W. et al. (2005) Lineage infidelity of epithelial ovarian cancers is controlled by HOX genes that specify regional identity in the reproductive tract. *Nat. Med.*, 11, 531–537.
31. Nakamura, T. et al. (1996) Fusion of the nucleoporin gene NUP98 to HOXA9 by the chromosome translocation t(7;11)(p15;p15) in human myeloid leukaemia. *Nat. Genet.*, 12, 154–158.
32. Heinrichs, S. et al. (2005) CD34+ cell selection is required to assess HOXA9 expression levels in patients with myelodysplastic syndrome. *Br. J. Haematol.*, 130, 83–86.
33. Baril, C. et al. (2017) Human NUP98-HOXA9 promotes hyperplastic growth of hematopoietic tissues in *Drosophila*. *Dev. Biol.*, 421, 16–26.
34. Golub, T.R. et al. (1999) Molecular classification of cancer: class discovery and class prediction by gene expression monitoring. *Science*, 286, 531–537.
35. Zhang, Z.F. et al. (2017) MicroRNA-182 downregulates Wnt/ β -catenin signaling, inhibits proliferation, and promotes apoptosis in human osteosarcoma cells by targeting HOXA9. *Oncotarget*, 8, 101345–101361.
36. Park, S.M. et al. (2017) A long-range interactive DNA methylation marker panel for the promoters of HOXA9 and HOXA10 predicts survival in breast cancer patients. *Clin. Epigenetics*, 9, 73.
37. Wang, K. et al. (2017) MiR-139-5p inhibits the tumorigenesis and progression of oral squamous carcinoma cells by targeting HOXA9. *J. Cell. Mol. Med.*, 21, 3730–3740.
38. Kanai, M. et al. (2010) Aberrant expressions of HOX genes in colorectal and hepatocellular carcinomas. *Oncol. Rep.*, 23, 843–851.
39. Ko, S.Y. et al. (2012) HOXA9 promotes ovarian cancer growth by stimulating cancer-associated fibroblasts. *J. Clin. Invest.*, 122, 3603–3617.
40. Segditsas, S. et al. (2008) Putative direct and indirect Wnt targets identified through consistent gene expression changes in APC-mutant intestinal adenomas from humans and mice. *Hum. Mol. Genet.*, 17, 3864–3875.
41. Watanabe, Y. et al. (2018) Upregulated HOXA9 expression is associated with lymph node metastasis in colorectal cancer. *Oncol. Lett.*, 15, 2756–2762.
42. van Baal, J.W. et al. (2005) A comparative analysis by SAGE of gene expression profiles of Barrett's esophagus, normal squamous esophagus, and gastric cardia. *Gastroenterology*, 129, 1274–1281.
43. Somasundaram, R. et al. (2017) Analysis of SHIP1 expression and activity in Crohn's disease patients. *PLoS One*, 12, e0182308.
44. de Sousa, R.R. et al. (2007) Phosphoprotein levels, MAPK activities and NFkappaB expression are affected by fisetin. *J. Enzyme Inhib. Med. Chem.*, 22, 439–444.
45. Schindelin, J. et al. (2015) The ImageJ ecosystem: An open platform for biomedical image analysis.

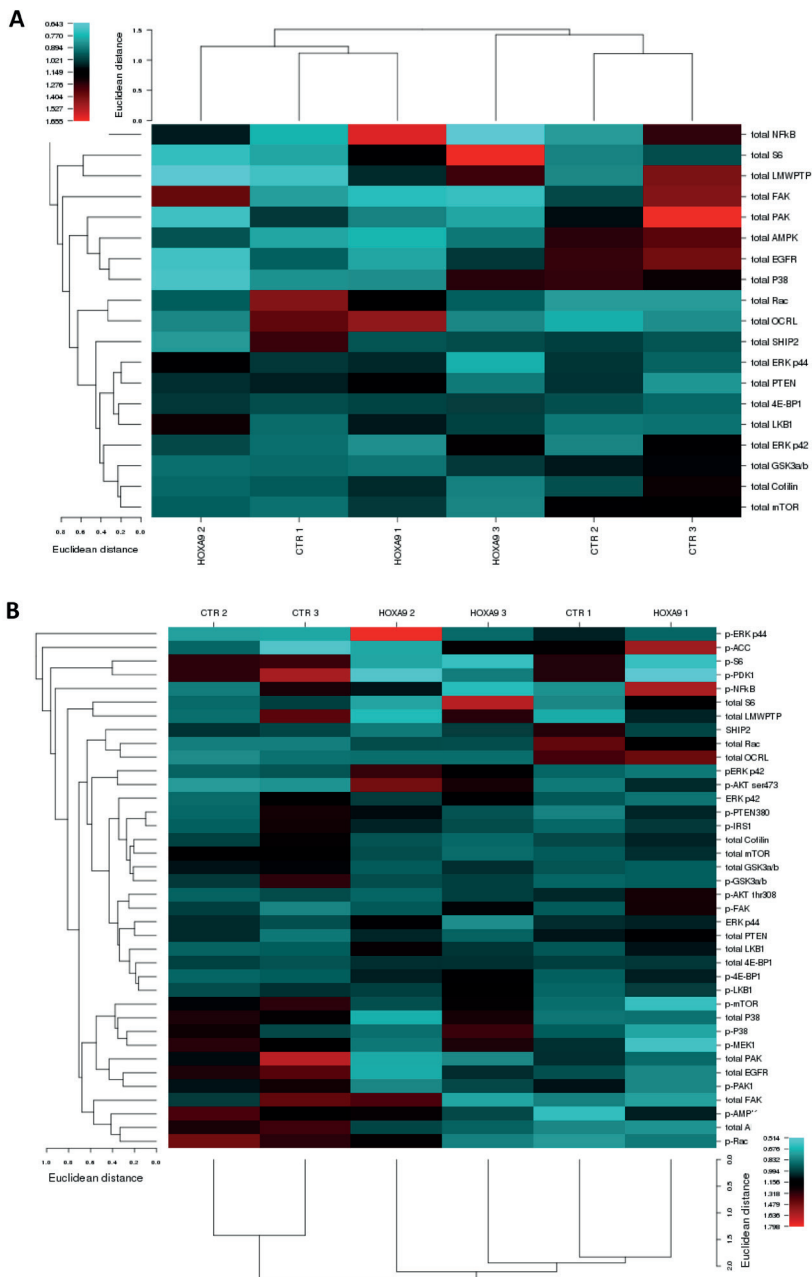
- Mol. Reprod. Dev., 82, 518–529.
46. van Baal, J.W. et al. (2006) Comparison of kinome profiles of Barrett's esophagus with normal squamous esophagus and normal gastric cardia. *Cancer Res.*, 66, 11605–11612.
 47. Myers, T.G. et al. (1997) A protein expression database for the molecular pharmacology of cancer. *Electrophoresis*, 18, 647–653.
 48. Queiroz, K.C. et al. (2012) Virolein induces death of resistant leukaemia cells via kinome reprogramming, endoplasmic reticulum stress and Golgi apparatus collapse. *PLoS One*, 7, e45362.
 49. Das, A.M. et al. (2015) A ring barrier-based migration assay to assess cell migration in vitro. *Nat. Protoc.*, 10, 904–915.
 50. Gao, J. et al. (2013) Integrative analysis of complex cancer genomics and clinical profiles using the cBioPortal. *Sci. Signal.*, 6, p11.
 51. Cerami, E. et al. (2012) The cBio cancer genomics portal: an open platform for exploring multidimensional cancer genomics data. *Cancer Discov.*, 2, 401–404.
 52. Giannakis, M. et al. (2016) Genomic Correlates of Immune-Cell Infiltrates in Colorectal Carcinoma. *Cell Rep.*, 15, 857–865.
 53. Seshagiri, S. et al. (2012) Recurrent R-spondin fusions in colon cancer. *Nature*, 488, 660–664.
 54. Cancer Genome Atlas N (2012) Comprehensive molecular characterization of human colon and rectal cancer. *Nature*, 487(7407), 330–7.
 55. Brannon, A.R. et al. (2014) Comparative sequencing analysis reveals high genomic concordance between matched primary and metastatic colorectal cancer lesions. *Genome Biol.*, 15, 454.
 56. Collins, C.T. et al. (2016) Role of HOXA9 in leukemia: dysregulation, cofactors and essential targets. *Oncogene*, 35, 1090–1098.
 57. Bhatlekar, S. et al. (2018) Overexpression of HOXA4 and HOXA9 genes promotes self-renewal and contributes to colon cancer stem cell overpopulation. *J. Cell. Physiol.*, 233, 727–735.
 58. Borsig, L. et al. (2014) Inflammatory chemokines and metastasis—tracing the accessory. *Oncogene*, 33, 3217–3224.
 59. Chun, E. et al. (2015) CCL2 promotes colorectal carcinogenesis by enhancing polymorphonuclear myeloid-derived suppressor cell population and function. *Cell Rep.*, 12, 244–257.
 60. Ruan, W. et al. (2007) IGFBP7 plays a potential tumor suppressor role in colorectal carcinogenesis. *Cancer Biol. Ther.*, 6, 354–359.
 61. Rupp, C. et al. (2015) IGFBP7, a novel tumor stroma marker, with growth-promoting effects in colon cancer through a paracrine tumor-stroma interaction. *Oncogene*, 34, 815–825.
 62. Georges, R.B. et al. (2011) The insulin-like growth factor binding proteins 3 and 7 are associated with colorectal cancer and liver metastasis. *Cancer Biol. Ther.*, 12, 69–79.
 63. Benassi, M.S. et al. (2015) Tissue and serum IGFBP7 protein as biomarker in high-grade soft tissue sarcoma. *Am. J. Cancer Res.*, 5, 3446–3454.
 64. Bolomsky, A. et al. (2015) Insulin like growth factor binding protein 7 (IGFBP7) expression is linked to poor prognosis but may protect from bone disease in multiple myeloma. *J. Hematol. Oncol.*, 8, 10.
 65. Mito, J.K. et al. (2018) SOX10/keratin dual-color immunohistochemistry: An effective first-line test for the workup of epithelioid malignant neoplasms in FNA and small biopsy specimens. *Cancer Cytopathol.*, 126, 179–189.
 66. Graf, S.A. et al. (2014) SOX10 promotes melanoma cell invasion by regulating melanoma inhibitory activity. *J. Invest. Dermatol.*, 134, 2212–2220.
 67. Bei, L. et al. (2005) HOXA9 activates transcription of the gene encoding gp91Phox during myeloid differentiation. *J. Biol. Chem.*, 280, 12359–12370.
 68. Ghannam, G. et al. (2004) The oncogene Nup98-HOXA9 induces gene transcription in myeloid cells.

- J. Biol. Chem., 279, 866–875.
69. Jiang, X. et al. (2012) Blockade of miR-150 maturation by MLL-fusion/MYC/LIN-28 is required for MLL-associated leukemia. *Cancer Cell*, 22, 524–535.
 70. Rössig, L. et al. (2005) Histone deacetylase activity is essential for the expression of HoxA9 and for endothelial commitment of progenitor cells. *J. Exp. Med.*, 201, 1825–1835.
 71. Shah, C.A. et al. (2013) The leukemia-associated MLL-ELL oncoprotein induces fibroblast growth factor 2 (Fgf2)-dependent cytokine hypersensitivity in myeloid progenitor cells. *J. Biol. Chem.*, 288, 32490–32505.
 72. Steger, J. et al. (2015) Insulin-like growth factor 1 is a direct HOXA9 target important for hematopoietic transformation. *Leukemia*, 29, 901–908.
 73. Gupta, S.D. et al. (2016) Expression of COX-2 and p53 in juvenile polyposis coli and its correlation with adenomatous changes. *J. Cancer Res. Ther.*, 12, 359–363.
 74. Baghaei, R. et al. (2015) An investigation of the rate of cyclooxygenase-2 expression on the surface of adenomatous and colorectal adenocarcinoma polyps. *Adv. Biomed. Res.*, 4, 200.
 75. Banskota, S. et al. (2015) NOX1 to NOX2 switch deactivates AMPK and induces invasive phenotype in colon cancer cells through overexpression of MMP-7. *Mol. Cancer*, 14, 123.
 76. Okkenhaug, K. et al. (2016) Targeting PI3K in Cancer: Impact on Tumor Cells, Their Protective Stroma, Angiogenesis, and Immunotherapy. *Cancer Discov.*, 6, 1090–1105.
 77. Vanhaesebroeck, B. et al. (2012) PI3K signalling: the path to discovery and understanding. *Nat. Rev. Mol. Cell Biol.*, 13, 195–203.
 78. Alessi, D.R. et al. (1998) 3-Phosphoinositide-dependent protein kinase 1 (PDK1) phosphorylates and activates the p70 S6 kinase in vivo and in vitro. *Curr. Biol.*, 8, 69–81.
 79. Zhang, Y. et al. (2012) mTOR-independent 4E-BP1 phosphorylation is associated with cancer resistance to mTOR kinase inhibitors. *Cell Cycle*, 11, 594–603.
 80. Fuhler, G.M. et al. (2009) Distinct roles of the mTOR components Rictor and Raptor in MO7e megakaryocytic cells. *Eur. J. Haematol.*, 83, 235–245.
 81. Symons, M. et al. (2009) Rac and Rho driving tumor invasion: who's at the wheel? *Genome Biol.*, 10, 213.
 82. Alves, M.M. et al. (2015) PAK2 is an effector of TSC1/2 signaling independent of mTOR and a potential therapeutic target for Tuberous Sclerosis Complex. *Sci. Rep.*, 5, 14534.
 83. Gingras, A.C. et al. (2001) Regulation of translation initiation by FRAP/mTOR. *Genes Dev.*, 15, 807–826.
 84. Whale A, Hashim FN, Fram S, Jones GE, Wells CM. (2011) Signalling to cancer cell invasion through PAK family kinases. *Front Biosci (Landmark Ed)*, 16, 849–64.
 85. Foxall, E. et al. (2016) Significance of kinase activity in the dynamic invadosome. *Eur. J. Cell Biol.*, 95, 483–492.
 86. Ahlquist, T. et al. (2008) Gene methylation profiles of normal mucosa, and benign and malignant colorectal tumors identify early onset markers. *Mol. Cancer*, 7, 94.
 87. Ma, Y.Y. et al. (2017) High level of homeobox A9 and PBX homeobox 3 expression in gastric cancer correlates with poor prognosis. *Oncol. Lett.*, 14, 5883–5889.
 88. Wang, Y. et al. (2010) The Wnt/beta-catenin pathway is required for the development of leukemia stem cells in AML. *Science*, 327, 1650–1653.
 89. Segditsas, S. et al. (2006) Colorectal cancer and genetic alterations in the Wnt pathway. *Oncogene*, 25, 7531–7537.

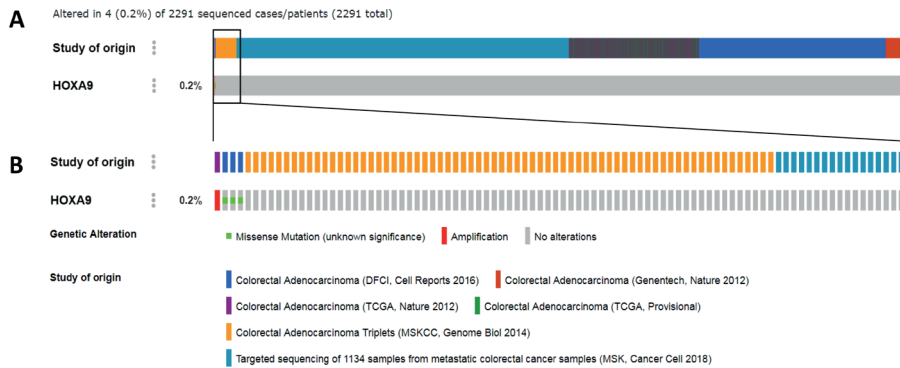
SUPPLEMENTARY MATERIALS



Supplementary Figure 1. Forced HOXA9 overexpression in Caco-2 cells. HOXA9 mRNA expression in Caco-2 cell lines after stimulation with decreasing concentrations of doxycycline. Con: controle cells, untreated with doxycycline. D: day. Maximal HOXA9 expression was observed after two days of docyclycline treatment, in order for HOXA9 to mediate its full effects, all functional experiments were performed after 3 days of doxycycline treatment.



Supplementary Figure 2. Heat maps of the protein profile constructed with CIMminer. Increased protein levels or phosphorylation of proteins is depicted in red, conversely decreased phosphorylation is depicted in blue. See scale bar in the top left corner for magnitude of the phosphorylation. Euclidian distance between the samples is depicted on top. For the phosphorylation status of the various signaling proteins Euclidian distance is depicted to the left. A) Total protein levels. B) All total and phosphoprotein levels.



Supplementary Figure 3. Visual representation of the cBioportal analysis of potential HOXA9 mutations, amplifications, and chromosomal translocations. A) All cases visualized with their study of origin, indicated in the legend. B) The magnification shows the individual cases with alterations, indicated in the legend.

Supplementary Table 1. All primers used in this study.

Name gene	Human sequence forward primer	Human sequence reverse primer	Not expressed in Caco-2
ADRB2	GAGCACAAAGCCCTCAAGAC	TCCTGGATCACATGCACAAT	
BMP1	TTCTCCTCCCCTGAATACCC	GGGACGTGAAGTTCAGGATG	
BMP4	TGAGCCTTTCCAGCAAGTTT	GCATTGGT'TACCAGGAATC	
BMPR2	CTACCATGGACCATCCTGCT	CCAAGGTCT'TGCTGATACGG	
BMX	ACGAGCTGAATGAACGAGAGG	TTTCTTGTCCCGCACGAGATT	X
CCL2	GCCTCCAGCATGAAAGTCTC	AGGTGACTGGGGCATTTGAT	
CDH5	AGAGCTCCACTCACGCTCAG	CATCT'TCCAGGAGGAACAG	X
CTNNB1	CTGAGGAGCAGCTT'CAGTCC	CGCTGGATT'TTCAAAAACAGT	
CYBB	TCGAAATCTGCTGTCTTCC	AATCATCCATGCCACCATTT	
FGF10	CATGTGCGGAGCTACAATCAC	CAGGATGCTGTACGGGCAG	X
FGF9	ATGGCTCCCTTAGGTGAAGTT	CCCAGGTGGTCACTTAACAAAAC	
FLT3	TGTGAGCAAAAGGGTCTTGA	TTGGGCATCATCTTTTCTG	
GAPDH (reference gene)	AAGTGAAGGTCTGGAGTCAA	AATGAAGGGGTCA'TTGATGG	
HEY1	TGGATCACCTGAAAAATGCTG	CGAAATCCCAAACTCCGATA	
HOXA9	AATGCTGAGAATGAGAGCGG	GTATAGGGGCACCGCT'TTTT	
IGF1	GCTGGTGGATGCTCTTCAGT	ACTCATCCACGATGCCTGTC	
KRT19	CCGGACTACAGCCACTACT	GTCGATCTGCAGGACAATCC	
MMP9	TGTACCGCTATGGTTACACTCG	GGCAGGGACAGTTGCTTCT	
NAT6	AGCTAGGACGGGAACATC	GGGTCTAGTGTAGGGGTCAGC	X
NOS3	TGATGGCGAAGCGAGTGAAG	ACTCATCCATACACAGGACCC	
PSMB9	ACCAACCGGGGACTTACC	ACTCGGGAATCAGAAACCCAT	
PTGS2	CCGGGTACAATCGCACTTAT	GGGCTCAGCCATACAG	

Name gene	Human sequence forward primer	Human sequence reverse primer	Not expressed in Caco-2
SMAD4	GCCTTCCCACATCCCCCTC	TTGATCCTTTTGGAAACAGTGAA	X
TPT1 (reference gene)	TTCAAGCGGAGGCATTTTCC	GATCGCGGACGGGTGTGT	
UBC (reference gene)	TGCCCTTGACATTCTCGATGGT	GATTTGGGTCGGGGTTCTTT	
VIM	CTTCAGAGAGAGGAAGCCGA	ATTCCACTTTGCGTTCAAGG	
WNT3A	AGCTACCCGATCTGGTGGTC	CAAACTCGATGTCCTCGCTAC	X
WNT5A	GCCAGTATCAATTCCGACATCG	TCACCGCGTATGTGAAGGC	
ZEB1	GATGATGAATGCGAGTCAGATGC	ACAGCAGTGTCTGTGTGTGT	

Supplementary Table 2. All antibodies used in this study.

Antibody	Dilution	Company	Catalog number
Primary antibodies			
Rabbit-anti-LKB1	1:1000	Cell Signaling Technology	3047
Rabbit-anti-phospho-LKB1 - Ser428	1:1000	Cell Signaling Technology	3482
Rabbit-anti-AMPKa	1:1000	Cell Signaling Technology	2532
Rabbit-anti-phospho-AMPKa - Thr172	1:1000	Cell Signaling Technology	2535
Rabbit-anti-S6K	1:1000	SAB - Signalway Antibody	21225
Rabbit-anti-phospho-S6K - Ser235/236	1:1000	Cell Signaling Technology	4856
Rabbit-anti-PTEN	1:1000	Cell Signaling Technology	9552
Rabbit-anti-phospho-PTEN - Ser380	1:1000	Cell Signaling Technology	9551
Rabbit-anti-mTOR	1:500	Cell Signaling Technology	2972
Rabbit-anti-phospho-mTOR - Ser2448	1:500	Cell Signaling Technology	2971
Mouse-anti-ERK	1:1000	Cell Signaling Technology	4696
Rabbit-anti-phospho-ERK - Thr202/Tyr204	1:1000	Cell Signaling Technology	4370
Rabbit-anti-4E-BP1	1:15000	Cell Signaling Technology	9644
Rabbit-anti-phospho-4E-BP1 - Thr37/46	1:1000	Cell Signaling Technology	2855
Rabbit-anti-GSK3 a/b	1:1000	EPITOMICS	1561-1
Rabbit-anti-phospho-GSK3	1:1000	Upstate (Merck)	05-413
Mouse-anti-p38	1:1000	Cell Signaling Technology	9228
Rabbit-anti-phospho-p38 - Thr180/Tyr182	1:1000	Cell Signaling Technology	4511
Rabbit-anti-RAC1/2/3	1:500	Cell Signaling Technology	2467
Rabbit-anti-phospho-RAC1 - Ser71	1:500	Cell Signaling Technology	2461
Rabbit-anti-PAK1/2/3	1:1000	SAB - Signalway Antibody	21169-1

Antibody	Dilution	Company	Catalog number
Rabbit-anti-phospho-PAK1 - Ser199/204	1:1000	Cell Signaling Technology	2605
Rabbit-anti-FAK	1:1000	SAB - Signalway Antibody	11123-2
Rabbit-anti-phospho-FAK - Tyr925	1:1000	SAB - Signalway Antibody	21076-1
Rabbit-anti-AKT	1:1000	Cell Signaling Technology	4691
Rabbit-anti-phospho-AKT - Thr 308	1:1000	SAB - Signalway Antibody	11055-2
Rabbit-anti-phospho-AKT - Ser 473	1:1000	Cell Signaling Technology	4060
Rabbit-anti-EGFR	1:500	SAB - Signalway Antibody	21073-1
Rabbit-anti-cofilin	1:500	SAB - Signalway Antibody	21164-1
Rabbit-anti-phospho-PDK1 - Ser241	1:1000	Cell Signaling Technology	3061
Rabbit-anti-NFkB-p65	1:1000	Cell Signaling Technology	4764
Rabbit-anti-phospho-Acetyl-CoA	1:500	Cell Signaling Technology	3661
Rabbit-anti-MEK1 - Thr292	1:1000	Ustate (Merck)	07-348
Rabbit-anti-phospho-IRS1 - Ser 636/639	1:1000	Cell Signaling Technology	2388
Rabbit-anti-OCRL	1:500	SCBT - Santa Cruz Biotechnology	393577
Rabbit-anti-SHIP2	1:500	SCBT - Santa Cruz Biotechnology	254335
Rabbit-anti-ACPI (LMWPTP)	1:500	SCBT - Santa Cruz Biotechnology	100343
Mouse-anti-βactin	1:1000	SCBT - Santa Cruz Biotechnology	477778
Rabbit-anti-Pan actin	1:1000	Cell Signaling Technology	9228
Secondary antibodies			
Goat-anti-mouse IgG IRDye 680LT	1:5000	LI-COR	926-68020
Goat-anti-rabbit IgG IRDye 800CW	1:5000	LI-COR	926-32211

Chapter 6

General discussion

Throughout our lifetime, most healthy cells in the body periodically divide and substitute themselves in a controlled manner. When this process gets out of control, abnormal cells accumulate to a mass, or what we usually call, a tumor. The noncancerous ones may stay quiet for a long time, neither invade nearby tissues nor spread to form new tumors in other parts of the body. On the contrary, malignant tumors can expand secretly, dispatch one “soldier” or “an army” through “underpasses”, and establish their “colonies” in the body. To this end, this thesis focused on the three fundamental features of tumors – growth, angiogenesis and metastasis. The characterization of the biological processes in cellular and molecular level may lead to new perspectives of tumor screening and treatment.

HOXA9 in premalignant lesions

Premalignant lesions are diseases or conditions with a risk of cancer development, a step before malignancy. Pathologically, premalignant lesions can be benign neoplasms, which do not invade normal tissues or disseminate to distant organs; it can be dysplasia, which is atypical growth of abnormal cells; sometimes it is even used for tumor *in situ*, as some will not progress to an invasive stage like other premalignant conditions. For example, colon polyps (colorectal adenomas) may develop to colorectal carcinoma (CRC); cervical dysplasia may develop to cervical cancer; monoclonal gammopathy of undetermined significance (MGUS) may develop to multiple myeloma or myelodysplastic syndrome (MDS) which possibly progress into leukemia.

Homeobox genes, which include the HOX gene clusters, regulate important pathways with relation to both embryogenesis and carcinogenesis [1]. Thus far, 39 HOX genes organized in four clusters (A to D) have been identified in humans. The evolutionary well-conserved mammalian HOX genes encode for transcription factors regulating the formation of tissues, structures and organs along the longitudinal body axis during embryology [1-3]. The role of HOX genes in malignant transformation was also explored in different forms of cancer [4-8]. HOXA9 overexpression as a result of the NUP98-HOXA9 translocation-derived fusion gene is detected in patients with the premalignant MDS as well as overt myeloid leukemia [9]. The NUP98/HOXA9 fusion transcript was reported to induce hematopoietic hyperproliferation as well as associated with poor prognosis in acute myeloid leukemia (AML), suggesting that it contributes to the transformation process of MDS to AML [10]. Our collaborating group has observed markedly high expression of HOXA9 in esophageal adenomas compared with normal esophagus when screening for the expression of HOX family members in gastrointestinal pathophysiology (unpublished data). In addition, HOXA9 also shows a pro-oncogenic effect in epithelial ovarian cancer, osteosarcoma, breast and oral squamous cell cancer [11-13].

The transformation of normal colonic epithelium to CRC follows a relatively ordered progression. The importance of premalignant lesions and their role in the adenoma–carcinoma sequence was described 30 years ago [14]. We found an elevated expression of HOXA9 in colorectal adenomas in comparison with healthy colonic tissue (Chapter 5). Moreover, an upregulation of HOXA9 has been described in CRC and it contributes to self-renewal and overpopulation of cancer stem cells [15–18]. We show that HOXA9 improves CRC cell proliferation and spheroid growth but inhibits cell migration. The following investigation of molecular consequences of HOXA 9 overexpression supports the phenotype changes. Forced HOXA9 expression increased growth-factor (IGF1, FLT3, WNT5a) action. IGF1 stimulates phosphorylation-dependent kinase cascades via the IGF-receptor, and the upregulation is found in CRC with growth-stimulatory effects [19]. HOXA9 induced upregulation of PTGS2 which is associated with adenomatous changes and its inhibition is well-established to counteract colorectal polyp formation [20, 21]. Genes associated with epithelial to mesenchymal transition (EMT) measured in this study showed little to no difference in expression as a result of HOXA9 overexpression, suggesting that HOXA9 is not involved in EMT induced migration in CRC. The reduced expression of the chemokine ligand 2 (CCL2) suggests the negative regulation effect of HOXA9 on CRC metastasis, as high levels of CCL2 are associated with high incidence of metastasis and poor outcome in CRC patients [22, 23]. Taken together, the upregulation of HOXA9 in colorectal adenoma show characteristics of promoting cell growth but inhibiting cell migration, indicating that its pro-oncogenic functionality only manifests at early stage of the CRC process and can be considered a marker of early stages.

Delineation of angiogenic effectors in melanoma

Solid tumors rely on vasculature to maintain growth of the original tumor and metastases. This is due to the requirement of nutrients and oxygen transferred from the vascular system for tumor cells survival. The angiogenesis process is a complex containing interactions between several cell types and extracellular matrix, as well as the participation of stimuli like cytokines and growth factors [24, 25]. This process keeps quiescent until transiently switched on in several physiological and pathological events like wound healing, chronic inflammation, etc. As for special cases like tumorigenesis, angiogenesis can be constantly activated to form vasculature for tumor progression, regulated by pro-angiogenic and anti-angiogenic factors [26–28].

Melanoma is malignant transformation of melanocytes and is characterized by rapid progression and early metastasis. Our previous study has reported that melanoma promotes endothelial cell survival under hypoxia through AKT/MAPK/ERK signaling [29]; moreover, our group also elucidated in melanoma an intrinsic anti-angiogenic regulator TIMP3

which inhibited directional endothelial cell migration [30]. Hypoxia is often a driver of tumor angiogenesis. Cells respond to hypoxic conditions by activating hypoxia-inducible factors (HIF) followed with vascular endothelial growth factor A (VEGFA) [31]. VEGFA is a pro-angiogenic factor guiding endothelial cells to avascular regions and promote mitogenesis [32, 33]. Endothelial cells have long been used in angiogenesis studies possibly because of the main function of sprouting and forming tubules for neovasculature. Pericytes, well known as supporting cells lying around endothelial tubes, are important in stabilizing endothelial cells and mediate maturation of microvessels [34]. Pericytes may also cooperate with endothelial cells to disassemble basement membrane through MMP2 for sprouting [35]. We found pericytes responding to melanoma conditioned medium with enhanced surviving and migrating capacity (Chapter 4). Even though the three melanoma cell lines we used have different growth, migration and invasion properties, they all displayed a similar effect on promoting pericyte survival and migration. The growth rate of pericytes was increased 10~50% by melanoma conditioned medium (CM), whereas the survival rate was 2~4 times higher with CM than with control medium. This contrast indicates that the survival effect was not only due to enhanced proliferation but more because of inhibited cell death (necrosis or apoptosis or both). The survival effect under hypoxia also existed with absence of serum in medium, demonstrating that some components produced by melanoma cells in CM sustained pericyte survival. These findings suggest that melanoma may be capable of communicating unilaterally with pericytes to promote angiogenesis, which is, if convinced, a step forward to the understanding of melanoma induced angiogenesis.

As the phenotype changes were observed, to further explore how and why, RNA sequencing was introduced to this study. The function clustering of differentially expressed genes demonstrates that cell movement, cell survival and death were among the most significantly involved biological processes in response to melanoma CM. The result explains the enhanced effect of survival and migration we observed in a molecular level, and will help on finding related downstream signaling pathways. According to gene expression change status, all three melanoma CM treated groups show a relative consistency of gene change directions in spite of different inherent properties of cell lines. This observation inspires us that melanoma cells may share one or several signaling pathways leading to the effect on pericytes. In other words, melanoma cells in general may produce one or several dominant determinants acting on pericytes. One interesting question would be: what is the effective factors in CM responsible for the phenotype?

To give an answer to this question, we found a series of upstream regulators predicted to be up-regulated based on measurements from our dataset and observations from the literature. Transforming growth factor-beta1 (TGFB1) was reported to remodel stroma for a positive simulation of tumor growth and survival [36]. Also belonging to the TGF

beta superfamily ligands, bone morphogenetic protein 4 (BMP4) induced differentiation and migration of endothelial cells and vessel formation [37, 38]. C-X-C motif chemokine ligand (CXCL) family show pro-angiogenic or anti-angiogenic functions according to small differences in protein sequence of family members [39]. CXCL6 and CXCL8 have pro-angiogenic properties playing a role in several types of tumor progression [40-43]. However these four genes displayed a lower expression level in melanoma cells than pericytes in our results. As pericytes could produce a relatively high amount of these factors by themselves, the hypothesis that these factors are modulators of pericyte effect may be invalid. A previous study reported that pericytes responded to oncostatin M (OSM) through activation of JAK/STAT signaling resulting in aggravating endothelial cell barrier dysfunction [44]. In our data a higher OSM expression was found in 1F6 than that in pericytes. A following western blotting and ELISA could be performed to verify the protein concentration in 1F6 CM. Although the high expression was not found in the other two melanoma cell lines BLM and MEL57, it is still worth testing if 1F6 produces enough OSM to make pericytes respond for an effect. Once the correlation was confirmed, we could next try some other melanoma cells. Fibroblast Growth Factor 1 (FGF1) is also one of the predicted upstream regulators, but unfortunately the secreted protein in melanoma CM was below detectable amount of ELISA. In this case FGF1 may be not the factor we are looking for.

A second solution to find dominant markers in CM is to fractionate CM components based on molecular weight. For pericyte survival under hypoxia, full fractions had a little improvement compared with small molecule fractions, whereas all fractions dramatically increased the survival in contrast with control medium. The findings point to a direction of seeking potential markers with molecular weight mainly below 10 kDa or possibly above 30 kDa. All CM including fractions produced from different melanoma cells had a similar effect on promoting pericyte survival, suggesting the three melanoma cell lines may secrete the same one or more components acting on pericytes. With respect to the effect on pericyte migration, the deviation between different melanoma CM appeared. Considering all three together, the most possible range with dominant markers may be below 30 kDa. For future plans mass spectrometry need to be performed to explore the exact molecules which pericytes respond to.

In this study we did not dig deeply in to the sequencing dataset for the downstream signaling pathways, but focused on finding the effective markers in conditioned medium. The further study plan will be to specify the principal signaling leading to observations of current experiments, and continue working on verification of potential markers using other techniques. As the anti-angiogenic therapy in tumors did not receive expected favorable outcome in certain cancers, finding other pro-angiogenic markers and blocking them effectively will be a promising direction for therapeutic development [45-48].

CREPT regulates melanoma migration and tumorigenesis

Metastases, in which tumor cells disseminate to a distant site, are crucial for malignant progression and the main cause of cancer deaths [49]. Tumor cells dissociating from primary sites must have the ability to migrate and invade through the basement membrane and extracellular matrix (ECM). To pass through tissues, tumor cells change their morphology and stiffness to fit in and interact with surrounding ECM structures [50]. These morphological changes, like cell polarization and formation of membrane extensions, are inseparable with filamentous actin and related cell-matrix attachments [51-53]. Integrins, which are transmembrane receptors and couple the cell to ECM components, regulate focal contact assembly and cell migration in melanoma [54]. Rho GTPase signaling contributes to cell movement by influencing cytoskeleton reorganization [55, 56]. After extravasation, metastatic tumor cells travel to a secondary site, adapt to the local microenvironment for survival, proliferate, and develop a vasculature to establish a new tumor [57, 58].

Regulation of nuclear pre-mRNA domain-containing (RPRD) proteins are identified as novel RNA polymerase II (RNAPII)-interacting proteins, which are evolutionarily conserved and ubiquitously expressed in human tissues. All three RPRDs (including RPRD1A, RPRD1B, and RPRD2) contain C-terminal domain (CTD) interaction domains. RPRD1A and RPRD1B associate with RNAPII phosphatase directly and interact with CTD heptapeptide repeats to recruit RNAPII for dephosphorylation of phosphor-S5 [59, 60]. Recently, an enhanced expression of RPRD1B (also referred to as CREPT) is reported in many human tumors, including gastric cancer, endometrial cancer, and colorectal cancer [61]. Data suggest that a new CREPT/c-myc/CDC25A pathway may result in cell growth and migration promotion [62]. In our study with melanoma cells and melanocytes, CREPT was found highly expressed in malignant cells compared to normal cells, indicating its oncogenic potential in melanoma (Chapter 3).

Increasing cell motility provides more possibilities for tumor metastasis. A study in gastric cancers revealed that CREPT increases cell migration by regulating E-cadherin, vimentin, N-cadherin, and matrix metalloproteinase 1 (MMP-1) expressions [63]. To assess the effect of CREPT on cell motility, we examined cell migration in 2D conditions and invasive capacity in 3D matrices, which mimics an *in vivo* environment. Since maintaining living cells inevitably causes cell division during migration assays, we tracked single cell movement to reveal cell motility. 2D and 3D migration results indicate that CREPT induces melanoma cell motility, migration, and invasion. The low expression level of CREPT in melanocytes provides an interesting possibility to study whether forced expression of CREPT in these cells would inflict a malignant transformation, which is currently under investigation in our group. Taken together, our findings show evidence

at the cellular level that CREPT promotes tumorigenesis-related biological processes, suggesting a non-negligible role of CREPT in the progression of melanoma.

Migrating cells have a polarized morphology with protrusions like lamellipodia and filopodia, which are the leading part in the direction of movement. These protrusions are driven by actin polymerization and filament assembly [64]. Focal adhesions connect actin cytoskeleton and extracellular matrix at the cell membrane, allowing actin networks to pull the cell forward [65]. The transcriptome sequencing analysis indicates that genes involved in the processes of “focal adhesion”, “actin polymerization”, and “stress fiber assembly” are regulated by CREPT. Further, immunofluorescence staining shows a CREPT-related enhancement of actin filaments and focal adhesion formation, which gives a subcellular interpretation of CREPT-regulated migration. Assembly and disassembly of focal adhesions dynamically occur during cell migration but are regulated by different mechanisms. Integrins aggregate and recruit adaptor proteins, like talin, tensin, and paxillin, to form adhesions connecting ECM structures and actin filaments. On the other hand, the disassembly process is triggered by microtubule extensions to focal adhesions [66]. In our study, the result of the dynamic equilibrium of focal adhesion formation. Focal adhesion protein levels and size were reported to be closely related to cell migration [67] while in this study, we did not observe a significant change in the mean size of focal adhesions with respect to CREPT differential expression. This result may be explained by the biphasic relationship between focal adhesion size and cell migration speed. It is reported that the mean size of focal adhesions is highly predictive of cell migration speed, however, the correlation is non-linear. Increased migration speed is accompanied by an increase in focal adhesion size until it plateaus, after which growing focal adhesions are associated with reduced migration speed. [68]. This phenomenon is also related to adhesion maturation and turnover. How and to what extent CREPT influences the focal adhesion dynamic process is still under investigation in our group.

Small GTPase protein RhoA is involved in the focal adhesion signaling pathway (KEGG: hsa04510) and regulates actin cytoskeleton organization. RhoA can activate Rho effector mDia1, which binds directly to the fast-growing barbed end of actin filaments and facilitates actin nucleation and elongation [69, 70]. In this study, we observed that CREPT upregulates RhoA activation and mDia1 expression. The results indicate a CREPT-RhoA-mDia1 signaling axis, which leads to actin organization regulation. One limitation is that we show an indirect interaction of CREPT and RhoA. How CREPT activates RhoA remains unknown, which would be an interesting question to study. To verify the role of RhoA in CREPT-induced cellular processes, we inhibited RhoA activation and consequently, actin filament/focal adhesion formation was reduced, and cell migration restrained. According to these findings, we conclude that CREPT promotes melanoma cell migration and actin filament/focal adhesion formation through RhoA activation.

CREPT stands for cell-cycle related and expression-elevated protein in tumor. As the name suggests, the function of modulating cell cycle has been verified in several tumor types, as well as the correlation with poor prognosis and the induction of tumorigenesis [71-73]. The effect of CREPT promoting cell growth is closely related to regulation of cell cycle related cyclins and kinases like Cyclin D1, Cyclin B1, Cyclin-dependent kinase 4 and 6 (CDK4 and CDK6) [61, 74, 75]. It is also indicated to be an upstream regulator of Wnt signaling pathway, acting as a transcription co-activator of the β -catenin·TCF4 (transcription factor 4) complex [76, 77]. In addition to improving proliferation, CREPT also reduces cell apoptosis by regulating the ROS/p53 pathway, and thus increases tumor growth [63]. Consistent with the published data, our results demonstrate that a high level of CREPT facilitates cell division and tumorigenesis in melanoma. The global gene expression profiling shows that CREPT-induced alterations of gene transcription is enriched in cellular growth and proliferation. Based on the literature and what we found in the current study, we summarized how CREPT functions in cell proliferation, apoptosis, actin polymerization and focal adhesion (Figure 1). A further study of examining the downstream signaling will extend the understanding of CREPT function in tumorigenesis. Promisingly, knockdown of CREPT increased cell sensitivity to treatment in endometrial adenocarcinoma, which suggests a therapeutic potential for targeting CREPT [74].

Novel tools in cell migration

During the process of tumor metastasis, the basic but decisive step is migration of tumor cells through the extracellular matrix (ECM) either towards lymph and blood vessels, or to a secondary site after survival in circulation [58]. To disseminate in tissue, cells require adhesion, proteolysis of ECM components and migration, which also occurs in normal physiological processes like embryonic morphogenesis and wound healing [78]. There are a diversity of strategies for cells movement, either individually (e.g. amoeboid or mesenchymal migration) or collectively (multicellular streaming, cluster, strand or sheet), which are based on cell-cell adhesion and cell-matrix interaction [79-81]. This activity can be simulated and observed by in vitro models and optical imaging to study cellular and molecular mechanisms.

Our group has previously established a ring-barrier assay to evaluate cell migration at two dimensions, which is a fast way to preliminarily assess cell motility and migration persistency [82]. To further delineate multiple aspects of migration including cell morphological alterations, cell-cell interaction, cell-matrix interaction, and matrix remodeling at three dimensions, we developed a microcarrier-based spheroid invasion assay (Chapter 2). Unlike conventional Transwell invasion assay or Boyden chamber assay

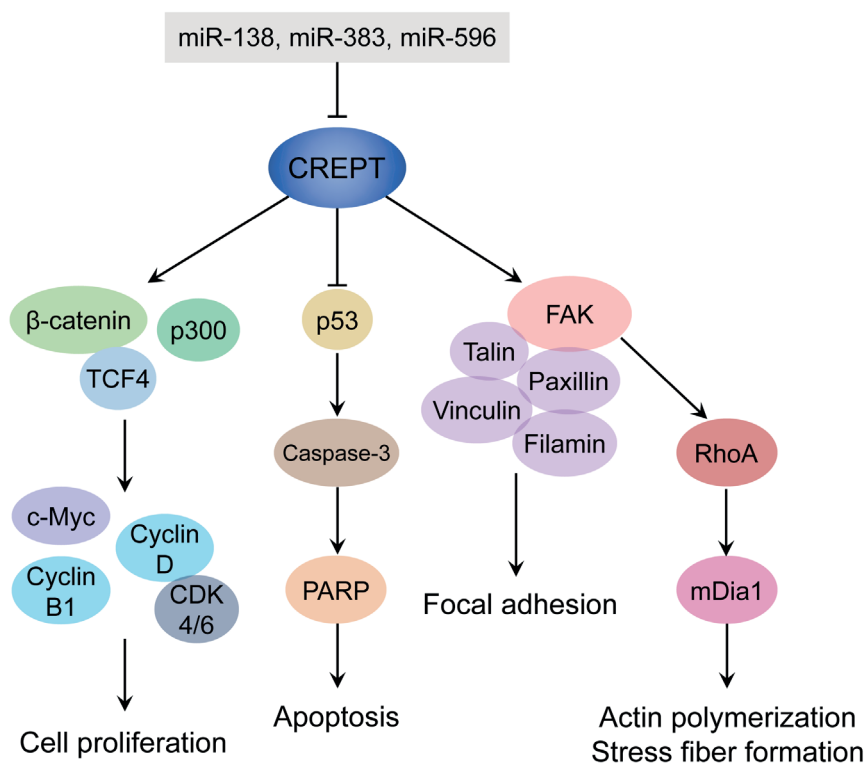


Figure 1. Summary of the function of CREPT in tumorigenesis.

which only record vertical invasions and are obscured in the whole invasive process, this method allows cells migrating in any direction and several migratory parameters can be detected. The application of microcarriers in spheroid generation overcome issues like cells do not aggregates or cells aggregate loosely [83-85]. Instead, microcarriers provide a support for adherent cells to make spheroids. Interestingly, introduction of carriers also enables co-culture of different cell types in close proximity [86]. This method has been used to study the effect of specific gene on cell migration and invasion [87-89]. It can also be adapted to investigate endothelial cells sprouting and vessel formation [90-92].

Although the microcarrier-based 3D invasion assay has a broad application, the presence of a carrier limits the use to study tumor cell behavior in a spheroid with an anoxic core. Moreover, to study infiltration of tumor cells into a spheroid of normal cells, or to study infiltration of immune cells into a tumor cell spheroid, the assay needs to be extended. A

multilayer spheroid can be created over time for this purpose by adjusting the matrix to inhibit migration away from the bead but allow growth. Notably, the described microcarrier-based method cannot be applied to non-adherent cells.

CONCLUSIONS

This thesis delineated the effects of intrinsic modulators and events during the process of malignancy, which may be associated with further development of therapeutic strategies. We highlighted the pro-oncogenic function of HOXA9 upregulation at the early stage of the CRC process – colorectal adenoma. The finding that HOXA9 drives adenoma growth but prevents further metastasis suggesting the role as a marker of premalignant lesion growth in CRC. To characterize core mediators of tumor angiogenesis, we determined the capacity of melanoma derived molecules to promote long-term survival of pericytes under hypoxic conditions and accelerate pericyte migration *in vitro*. We also identified the practicable range of effective components in melanoma conditioned medium, with molecular weight below 10 kDa for pericyte survival and below 30 kDa for pericyte migration. Further characterization and validation of specific molecules resulting in survival and/or migration could facilitate the development of treatment targeting pro-angiogenic markers for malignant melanoma. Moreover, we identified CREPT as a dominant regulator of the malignant progression in melanoma, providing a potential therapeutic target for melanoma treatment. The oncogenic role of CREPT in promoting cell migration, and invasion is dependent on the upregulation and activation of RhoA-induced actin organization and focal adhesion assembly. In addition, we described a powerful tool for cell invasion study, which enables quantitative evaluation of multiple aspects of cell invasion in 3D matrix. In all, this thesis identified pathophysiological determinants in the malignant process of colorectal cancer and melanoma. These novel mechanistic insights may guide further discovery of new rationales in tumorigenesis, and promote development for new therapeutic targets and strategies.

REFERENCES

1. McGinnis W., Krumlauf R. Homeobox Genes and Axial Patterning. *Cell*. 1992;68(2):283-302.
2. Pearson J.C., Lemons D., McGinnis W. Modulating Hox gene functions during animal body patterning. *Nat Rev Genet*. 2005;6(12):893-904.
3. Hueber S.D., Rauch J., Djordjevic M.A., Gunter H., Weiller G.F., Frickey T. Analysis of central Hox protein types across bilaterian clades: On the diversification of central Hox proteins from an Antennapedia/Hox7-like protein. *Dev Biol*. 2013;383(2):175-85.
4. Abe M., Hamada J.I., Takahashi O., Takahashi Y., Tada M., Miyamoto M., et al. Disordered expression of HOX genes in human non-small cell lung cancer. *Oncol Rep*. 2006;15(4):797-802.
5. Miller G.J., Miller H.L., van Bokhoven A., Lambert J.R., Werahera P.N., Schirripa O., et al. Aberrant HOXC expression accompanies the malignant phenotype in human prostate. *Cancer Res*. 2003;63(18):5879-88.
6. Liu Y.J., Zhu Y., Yuan H.X., Zhang J.P., Guo J.M., Lin Z.M. Overexpression of HOXC11 homeobox gene in clear cell renal cell carcinoma induces cellular proliferation and is associated with poor prognosis. *Tumor Biol*. 2015;36(4):2821-9.
7. Cantile M., Scognamiglio G., La Sala L., La Mantia E., Scaramuzza V., Valentino E., et al. Aberrant Expression of Posterior HOX Genes in Well Differentiated Histotypes of Thyroid Cancers. *Int J Mol Sci*. 2013;14(11):21727-40.
8. Cheng W.J., Liu J.S., Yoshida H., Rosen D., Naora H. Lineage infidelity of epithelial ovarian cancers is controlled by HOX genes that specify regional identity in the reproductive tract. *Nat Med*. 2005;11(5):531-7.
9. Nakamura T., Largaespada D.A., Lee M.P., Johnson L.A., Ohyashiki K., Toyama K., et al. Fusion of the nucleoporin gene NUP98 to HOXA9 by the chromosome translocation t(7;11)(p15;p15) in human myeloid leukaemia. *Nat Genet*. 1996;12(2):154-8.
10. Baril C., Gavory G., Bidla G., Knaevelsrud H., Sauvageau G., Therrien M. Human NUP98-HOXA9 promotes hyperplastic growth of hematopoietic tissues in Drosophila. *Dev Biol*. 2017;421(1):16-26.
11. Zhang Z.F., Wang Y.J., Fan S.H., Du S.X., Li X.D., Wu D.M., et al. MicroRNA-182 downregulates Wnt/beta-catenin signaling, inhibits proliferation, and promotes apoptosis in human osteosarcoma cells by targeting HOXA9. *Oncotarget*. 2017;8(60):101345-61.
12. Park S.M., Choi E.Y., Bae M., Choi J.K., Kim Y.J. A long-range interactive DNA methylation marker panel for the promoters of HOXA9 and HOXA10 predicts survival in breast cancer patients. *Clin Epigenetics*. 2017;9.
13. Wang K., Jin J., Ma T.X., Zhai H.F. MiR-139-5p inhibits the tumorigenesis and progression of oral squamous carcinoma cells by targeting HOXA9. *J Cell Mol Med*. 2017;21(12):3730-40.
14. Vogelstein B., Fearon E.R., Hamilton S.R., Kern S.E., Preisinger A.C., Leppert M., et al. Genetic Alterations during Colorectal-Tumor Development. *N Engl J Med*. 1988;319(9):525-32.
15. Kanai M., Hamada J.I., Takada M., Asano T., Murakawa K., Takahashi Y., et al. Aberrant expressions of HOX genes in colorectal and hepatocellular carcinomas. *Oncol Rep*. 2010;23(3):843-51.
16. Ko S.Y., Barengo N., Ladanyi A., Lee J.S., Marini F., Lengyel E., et al. HOXA9 promotes ovarian cancer growth by stimulating cancer-associated fibroblasts. *J Clin Invest*. 2012;122(10):3603-17.
17. Watanabe Y., Saito M., Saito K., Matsumoto Y., Kanke Y., Onozawa H., et al. Upregulated HOXA9 expression is associated with lymph node metastasis in colorectal cancer. *Oncol Lett*. 2018;15(3):2756-62.
18. Bhatlekar S., Viswanathan V., Fields J.Z., Boman B.M. Overexpression of HOXA4 and HOXA9 genes promotes self-renewal and contributes to colon cancer stem cell overpopulation. *J Cell Physiol*.

- 2018;233(2):727-35.
19. Rupp C., Scherzer M., Rudisch A., Unger C., Haslinger C., Schweifer N., et al. IGFBP7, a novel tumor stroma marker, with growth-promoting effects in colon cancer through a paracrine tumor-stroma interaction. *Oncogene*. 2015;34(7):815-25.
20. Baghaei R., Beiraghdar M., Sobhani A., Rafei R., Kolahi L., Foladi L. An investigation of the rate of cyclooxygenase-2 expression on the surface of adenomatous and colorectal adenocarcinoma polyps. *Adv Biomed Res*. 2015;4:200.
21. Das Gupta S., Das R.N., Ghosh R., Sen A., Chatterjee U., Saha K., et al. Expression of COX-2 and p53 in juvenile polyposis coli and its correlation with adenomatous changes. *J Cancer Res Ther*. 2016;12(1):359-63.
22. Borsig L., Wolf M.J., Roblek M., Lorentzen A., Heikenwalder M. Inflammatory chemokines and metastasis-tracing the accessory. *Oncogene*. 2014;33(25):3217-24.
23. Chun E., Lavoie S., Michaud M., Gallini C.A., Kim J., Soucy G., et al. CCL2 Promotes Colorectal Carcinogenesis by Enhancing Polymorphonuclear Myeloid-Derived Suppressor Cell Population and Function. *Cell Rep*. 2015;12(2):244-57.
24. Adams R.H., Alitalo K. Molecular regulation of angiogenesis and lymphangiogenesis. *Nat Rev Mol Cell Biol*. 2007;8(6):464-78.
25. Rocha S.F., Adams R.H. Molecular differentiation and specialization of vascular beds. *Angiogenesis*. 2009;12(2):139-47.
26. Hanahan D., Folkman J. Patterns and emerging mechanisms of the angiogenic switch during tumorigenesis. *Cell*. 1996;86(3):353-64.
27. Carmeliet P., Jain R.K. Angiogenesis in cancer and other diseases. *Nature*. 2000;407(6801):249-57.
28. Baeriswyl V., Christofori G. The angiogenic switch in carcinogenesis. *Semin Cancer Biol*. 2009;19(5):329-37.
29. Das A.M., Pescatori M., Vermeulen C.E., Rens J.A., Seynhaeve A.L., Koning G.A., et al. Melanomas prevent endothelial cell death under restrictive culture conditions by signaling through AKT and p38 MAPK/ ERK-1/2 cascades. *Oncoimmunology*. 2016;5(10):e1219826.
30. Das A.M., Seynhaeve A.L., Rens J.A., Vermeulen C.E., Koning G.A., Eggermont A.M., et al. Differential TIMP3 expression affects tumor progression and angiogenesis in melanomas through regulation of directionally persistent endothelial cell migration. *Angiogenesis*. 2014;17(1):163-77.
31. Simon M.C., Keith B. The role of oxygen availability in embryonic development and stem cell function. *Nat Rev Mol Cell Bio*. 2008;9(4):285-96.
32. Ferrara N., Gerber H.P., LeCouter J. The biology of VEGF and its receptors. *Nat Med*. 2003;9(6):669-76.
33. Ferrara N. Binding to the Extracellular Matrix and Proteolytic Processing: Two Key Mechanisms Regulating Vascular Endothelial Growth Factor Action. *Mol Biol Cell*. 2010;21(5):687-90.
34. Raza A., Franklin M.J., Dudek A.Z. Pericytes and vessel maturation during tumor angiogenesis and metastasis. *Am J Hematol*. 2010;85(8):593-8.
35. Virgintino D., Girolamo F., Errede M., Capobianco C., Robertson D., Stallcup W.B., et al. An intimate interplay between precocious, migrating pericytes and endothelial cells governs human fetal brain angiogenesis. *Angiogenesis*. 2007;10(1):35-45.
36. Berking C., Takemoto R., Schaidt H., Showe L., Satyamoorthy K., Robbins P., et al. Transforming growth factor-beta 1 increases survival of human melanoma through stroma remodeling. *Cancer Res*. 2001;61(22):8306-16.
37. Rothhammer T., Poser I., Soncin F., Bataille F., Moser M., Bosserhoff A.K. Bone morphogenic proteins are overexpressed in malignant melanoma and promote cell invasion and migration. *Cancer Res*. 2005;65(2):448-56.

38. Kim H.Y., Yang D.H., Shin S.W., Kim M.Y., Yoon J.H., Kim S., et al. CXXC5 is a transcriptional activator of Flk-1 and mediates bone morphogenic protein-induced endothelial cell differentiation and vessel formation. *FASEB J.* 2014;28(2):615-26.
39. Grepin R., Guyot M., Giuliano S., Boncompagni M., Ambrosetti D., Chamorey E., et al. The CXCL7/CXCR1/2 Axis Is a Key Driver in the Growth of Clear Cell Renal Cell Carcinoma. *Cancer Res.* 2014;74(3):873-83.
40. Wu S., Singh S., Varney M.L., Kindle S., Singh R.K. Modulation of CXCL-8 expression in human melanoma cells regulates tumor growth, angiogenesis, invasion, and metastasis. *Cancer Med-Us.* 2012;1(3):306-17.
41. Azenshtein E., Meshel T., Shina S., Barak N., Keydar I., Ben-Baruch A. The angiogenic factors CXCL8 and VEGF in breast cancer: regulation by an array of pro-malignancy factors. *Cancer Lett.* 2005;217(1):73-86.
42. Pold M., Zhu L.X., Sharma S., Burdick M.D., Lin Y., Lee P.P.N., et al. Cyclooxygenase-2-dependent expression of angiogenic CXC chemokines ENA-78/CXC ligand (CXCL) 5 and interleukin-8/CXCL8 in human non-small cell lung cancer. *Cancer Res.* 2004;64(5):1853-60.
43. Liu G.C., An L.P., Zhang H.M., Du P.G., Sheng Y. Activation of CXCL6/CXCR1/2 Axis Promotes the Growth and Metastasis of Osteosarcoma Cells in vitro and in vivo. *Front Pharmacol.* 2019;10.
44. Takata F., Dohgu S., Sakaguchi S., Sakai K., Yamanaka G., Iwao T., et al. Oncostatin-M-Reactive Pericytes Aggravate Blood-Brain Barrier Dysfunction by Activating JAK/STAT3 Signaling In Vitro. *Neuroscience.* 2019;422:12-20.
45. Miller K., Wang M.L., Gralow J., Dickler M., Cobleigh M., Perez E.A., et al. Paclitaxel plus bevacizumab versus paclitaxel alone for metastatic breast cancer. *N Engl J Med.* 2007;357(26):2666-76.
46. Brufsky A.M., Hurvitz S., Perez E., Swamy R., Valero V., O'Neill V., et al. RIBBON-2: A Randomized, Double-Blind, Placebo-Controlled, Phase III Trial Evaluating the Efficacy and Safety of Bevacizumab in Combination With Chemotherapy for Second-Line Treatment of Human Epidermal Growth Factor Receptor 2-Negative Metastatic Breast Cancer. *J Clin Oncol.* 2011;29(32):4286-93.
47. Kelly W.K., Halabi S., Carducci M., George D., Mahoney J.F., Stadler W.M., et al. Randomized, Double-Blind, Placebo-Controlled Phase III Trial Comparing Docetaxel and Prednisone With or Without Bevacizumab in Men With Metastatic Castration-Resistant Prostate Cancer: CALGB 90401. *J Clin Oncol.* 2012;30(13):1534-40.
48. Flaherty K.T., Lee S.J., Zhao F.M., Schuchter L.M., Flaherty L., Kefford R., et al. Phase III Trial of Carboplatin and Paclitaxel With or Without Sorafenib in Metastatic Melanoma. *J Clin Oncol.* 2013;31(3):373-9.
49. Chaffer C.L., Weinberg R.A. A perspective on cancer cell metastasis. *Science.* 2011;331(6024):1559-64.
50. Lauffenburger D.A., Horwitz A.F. Cell migration: a physically integrated molecular process. *Cell.* 1996;84(3):359-69.
51. Adams J.C. Cell-matrix contact structures. *Cell Mol Life Sci.* 2001;58(3):371-92.
52. Burridge K., Chrzanowska-Wodnicka M. Focal adhesions, contractility, and signaling. *Annu Rev Cell Dev Biol.* 1996;12:463-518.
53. Cramer L.P. Organization and polarity of actin filament networks in cells: implications for the mechanism of myosin-based cell motility. *Biochem Soc Symp.* 1999;65:173-205.
54. Siret C., Terciolo C., Dobric A., Habib M.C., Germain S., Bonnier R., et al. Interplay between cadherins and alpha 2 beta 1 integrin differentially regulates melanoma cell invasion. *Br J Cancer.* 2015;113(10):1445-53.
55. Wen S.J., Zhang W., Ni N.N., Wu Q., Wang X.P., Lin Y.K., et al. Expression of Rho GTPases family in melanoma cells and its influence on cytoskeleton and migration. *Oncotarget.* 2017;8(18):30112-22.

56. Klein R.M., Aplin A.E. Rnd3 Regulation of the Actin Cytoskeleton Promotes Melanoma Migration and Invasive Outgrowth in Three Dimensions. *Cancer Res.* 2009;69(6):2224-33.
57. Haass N.K., Smalley K.S., Li L., Herlyn M. Adhesion, migration and communication in melanocytes and melanoma. *Pigment Cell Res.* 2005;18(3):150-9.
58. Chambers A.F., Groom A.C., MacDonald I.C. Dissemination and growth of cancer cells in metastatic sites. *Nat Rev Cancer.* 2002;2(8):563-72.
59. Ni Z., Olsen J.B., Guo X., Zhong G., Ruan E.D., Marcon E., et al. Control of the RNA polymerase II phosphorylation state in promoter regions by CTD interaction domain-containing proteins RPRD1A and RPRD1B. *Transcription.* 2011;2(5):237-42.
60. Ni Z., Xu C., Guo X., Hunter G.O., Kuznetsova O.V., Tempel W., et al. RPRD1A and RPRD1B are human RNA polymerase II C-terminal domain scaffolds for Ser5 dephosphorylation. *Nat Struct Mol Biol.* 2014;21(8):686-95.
61. Lu D.D., Wu Y.Y., Wang Y.Y., Ren F.L., Wang D.J., Su F.Q., et al. CREPT Accelerates Tumorigenesis by Regulating the Transcription of Cell-Cycle-Related Genes. *Cancer Cell.* 2012;21(1):92-104.
62. Liu T., Li W.M., Wang W.P., Sun Y., Ni Y.F., Xing H., et al. Inhibiting CREPT reduces the proliferation and migration of non-small cell lung cancer cells by down-regulating cell cycle related protein. *Am J Transl Res.* 2016;8(5):2097-113.
63. Sun M., Si G., Sun H.S., Si F.C. Inhibition of CREPT restrains gastric cancer growth by regulation of cycle arrest, migration and apoptosis via ROS-regulated p53 pathway. *Biochem Biophys Res Commun.* 2018;496(4):1183-90.
64. Pollard T.D., Borisy G.G. Cellular motility driven by assembly and disassembly of actin filaments. *Cell.* 2003;112(4):453-65.
65. Ciobanasu C., Faivre B., Le Clainche C. Actin dynamics associated with focal adhesions. *Int J Cell Biol.* 2012;2012:941292.
66. Ezratty E.J., Partridge M.A., Gundersen G.G. Microtubule-induced focal adhesion disassembly is mediated by dynamin and focal adhesion kinase. *Nat Cell Biol.* 2005;7(6):581-U15.
67. Hooch S.C., Ritter A., Steinhäuser K., Roth S., Behrends C., Oswald F., et al. RITA modulates cell migration and invasion by affecting focal adhesion dynamics. *Mol Oncol.* 2019;13(10):2121-41.
68. Kim D.H., Wirtz D. Focal adhesion size uniquely predicts cell migration. *FASEB J.* 2013;27(4):1351-61.
69. Evangelista M., Zsigmond S., Boone C. Formins: signaling effectors for assembly and polarization of actin filaments. *J Cell Sci.* 2003;116(13):2603-11.
70. Rose R., Weyand M., Lammers M., Ishizaki T., Ahmadian M.R., Wittinghofer A. Structural and mechanistic insights into the interaction between Rho and mammalian Dia. *Nature.* 2005;435(7041):513-8.
71. Li W.M., Zheng G.X., Xia J.H., Yang G., Sun J.Y., Wang X.J., et al. Cell cycle-related and expression-elevated protein in tumor overexpression is associated with proliferation behaviors and poor prognosis in non-small-cell lung cancer. *Cancer Sci.* 2018;109(4):1012-23.
72. Zheng G.X., Li W.M., Zuo B.L., Guo Z.Y., Xi W.J., Wei M., et al. High expression of CREPT promotes tumor growth and is correlated with poor prognosis in colorectal cancer. *Biochem Biophys Res Commun.* 2016;480(3):436-42.
73. She Y., Liang J., Chen L., Qiu Y., Liu N., Zhao X., et al. CREPT expression correlates with poor prognosis in patients with retroperitoneal leiomyosarcoma. *Int J Clin Exp Pathol.* 2014;7(10):6596-605.
74. Wang Y., Qiu H., Hu W., Li S., Yu J. RPRD1B promotes tumor growth by accelerating the cell cycle in endometrial cancer. *Oncol Rep.* 2014;31(3):1389-95.
75. Ding L., Yang L., He Y., Zhu B., Ren F., Fan X., et al. CREPT/RPRD1B associates with Aurora B to regulate Cyclin B1 expression for accelerating the G2/M transition in gastric cancer. *Cell Death Dis.* 2018;9(12):1172.

76. Zhang Y., Liu C., Duan X., Ren F., Li S., Jin Z., et al. CREPT/RPRD1B, a Recently Identified Novel Protein Highly Expressed in Tumors, Enhances the β -Catenin-TCF4 Transcriptional Activity in Response to Wnt Signaling. *J Biol Chem.* 2014;289(33):22589-99.
77. Zhang Y.Q., Wang S.Y., Kang W., Liu C.X., Dong Y.J., Ren F.L., et al. CREPT facilitates colorectal cancer growth through inducing Wnt/beta-catenin pathway by enhancing p300-mediated beta-catenin acetylation. *Oncogene.* 2018;37(26):3485-500.
78. Friedl P., Wolf K. Tumour-cell invasion and migration: diversity and escape mechanisms. *Nat Rev Cancer.* 2003;3(5):362-74.
79. Sahai E. Illuminating the metastatic process. *Nat Rev Cancer.* 2007;7(10):737-49.
80. Christiansen J.J., Rajasekaran A.K. Reassessing epithelial to mesenchymal transition as a prerequisite for carcinoma invasion and metastasis. *Cancer Res.* 2006;66(17):8319-26.
81. Friedl P., Locker J., Sahai E., Segall J.E. Classifying collective cancer cell invasion. *Nat Cell Biol.* 2012;14(8):777-83.
82. Das A.M., Eggermont A.M., ten Hagen T.L. A ring barrier-based migration assay to assess cell migration in vitro. *Nat Protoc.* 2015;10(6):904-15.
83. Vinci M., Gowan S., Boxall F., Patterson L., Zimmermann M., Court W., et al. Advances in establishment and analysis of three-dimensional tumor spheroid-based functional assays for target validation and drug evaluation. *BMC Biol.* 2012;10:29.
84. Lee J.M., Mhawech-Fauceglia P., Lee N., Parsanian L.C., Lin Y.G., Gayther S.A., et al. A three-dimensional microenvironment alters protein expression and chemosensitivity of epithelial ovarian cancer cells in vitro. *Lab Invest.* 2013;93(5):528-42.
85. Dolznig H., Rupp C., Puri C., Haslinger C., Schweifer N., Wieser E., et al. Modeling colon adenocarcinomas in vitro a 3D co-culture system induces cancer-relevant pathways upon tumor cell and stromal fibroblast interaction. *Am J Pathol.* 2011;179(1):487-501.
86. Johns R.A., Tichotsky A., Muro M., Spaeth J.P., Le Cras T.D., Rengasamy A. Halothane and isoflurane inhibit endothelium-derived relaxing factor-dependent cyclic guanosine monophosphate accumulation in endothelial cell-vascular smooth muscle co-cultures independent of an effect on guanylyl cyclase activation. *Anesthesiology.* 1995;83(4):823-34.
87. Bakker E.R., Das A.M., Helvensteijn W., Franken P.F., Swagemakers S., van der Valk M.A., et al. Wnt5a promotes human colon cancer cell migration and invasion but does not augment intestinal tumorigenesis in Apc1638N mice. *Carcinogenesis.* 2013;34(11):2629-38.
88. Janmaat V.T., Liu H., da Silva R.A., Wisse P.H.A., Spaander M.C.W., Ten Hagen T.L.M., et al. HOXA9 mediates and marks premalignant compartment size expansion in colonic adenomas. *Carcinogenesis.* 2019.
89. Liu H., Seynhaeve A.L.B., Brouwer R.W.W., van I.W.F.J., Yang L., Wang Y., et al. CREPT Promotes Melanoma Progression Through Accelerated Proliferation and Enhanced Migration by RhoA-Mediated Actin Filaments and Focal Adhesion Formation. *Cancers (Basel).* 2019;12(1).
90. Dietrich F., Lelkes P.I. Fine-tuning of a three-dimensional microcarrier-based angiogenesis assay for the analysis of endothelial-mesenchymal cell co-cultures in fibrin and collagen gels. *Angiogenesis.* 2006;9(3):111-25.
91. Kniazeva E., Putnam A.J. Endothelial cell traction and ECM density influence both capillary morphogenesis and maintenance in 3-D. *Am J Physiol Cell Physiol.* 2009;297(1):C179-87.
92. Juliar B.A., Keating M.T., Kong Y.P., Botvinick E.L., Putnam A.J. Sprouting angiogenesis induces significant mechanical heterogeneities and ECM stiffening across length scales in fibrin hydrogels. *Biomaterials.* 2018;162:99-108.

Chapter 7

Summary

Samenvatting

SUMMARY

In general, cancer is an accumulation of abnormal cells with uncontrolled physiological behaviors, which causes millions of deaths worldwide. The cancer phenotype is the outcome of a combination of stimuli, inducers and suppressors, signal transduction pathways, and the resulting events, interweaving a function network. To this end, discovering more about the process of tumorigenesis and finding ways to block or inhibit tumor progression are, and will be, active research areas for a long time.

The tumorigenesis and progression of malignancy is intricate with composition of various genetic alterations and pathways regulating cell growth and death, differentiation, migration, invasion and interaction with tumor microenvironment. In **Chapter 1**, we briefly summarize the hallmarks in cancer and review several crucial features during tumorigenesis. The pathogenesis and development of melanoma and colorectal cancer are also outlined as two tumor models used in this thesis.

In **Chapter 2**, we describe a novel tool to explore the dynamics of adherent cells, including cell invasion in a three-dimensional model. This microcarrier-based 3D invasion assay enables quantitative evaluation of multiple aspects of cell invasion and is reckoned to be a fast and highly reproducible method helpful in cell biology studies.

In **Chapter 3**, we elucidated the oncogenic role of CREPT in positive regulation of melanoma cell proliferation, migration and invasion *in vitro*, providing a potential therapeutic target for melanoma treatment. The function in malignant processes is associated with RhoA-induced actin organization and focal adhesion assembly.

To characterize core mediators of tumor angiogenesis, we determined the capacity of melanoma derived molecules to promote long-term survival of pericytes under hypoxic conditions and accelerate pericyte migration *in vitro* in **Chapter 4**. We also identified the weight range of effective components in melanoma conditioned medium, with molecular weight below 10 kDa for pericyte survival and below 30 kDa for pericyte migration. Further characterization and validation of specific molecules promoting survival and/or migration could facilitate the development of treatment targeting pro-angiogenic markers for malignant melanoma.

In **Chapter 5**, we investigated the pro-oncogenic function of HOXA9 upregulation at the early stage of colorectal cancer transformation (colorectal adenoma). The close correlation with adenoma growth and reduction in migration suggests that HOXA9 is a marker and driver of premalignant lesion growth.

In **Chapter 6**, the significance and implications of the results in above chapters are discussed comprehensively together with future perspectives on how these findings contribute to further development of therapeutic strategies.

SAMENVATTING

Kanker, een opeenhoping van abnormale cellen met een ongecontroleerd fysiologisch gedrag, veroorzaakt wereldwijd miljoenen sterfgevallen. Het kankerfenotype is het resultaat van een combinatie van stimuli, inducerende en onderdrukkende factoren, signaaltransductieroutes en de daaruit voortvloeiende gebeurtenissen die een functie-netwerk vormen. Daarom zal nog langdurig onderzoek nodig zijn om meer te weten komen over het ontstaan en de ontwikkeling van tumoren en om manieren te vinden om tumorprogressie te blokkeren of te remmen.

Het ontstaan en progressie van maligniteit is ingewikkeld door de combinatie van verschillende genetische veranderingen en routes die celgroei en -sterfte, differentiatie, migratie, invasie en interactie met de micro-omgeving van tumoren reguleren. In **Hoofdstuk 1** hebben we de kenmerken van kanker kort samengevat en bespreken we de verschillende cruciale kenmerken tijdens tumorontwikkeling. De pathogenese en ontwikkeling van het melanoom en colorectale kanker zijn ook beschreven als de twee tumormodellen die in dit proefschrift beschreven onderzoek werden gebruikt.

In **Hoofdstuk 2** hebben we een nieuw hulpmiddel beschreven om de dynamiek van hechtende cellen te onderzoeken, inclusief celinvasie in een driedimensionaal model. Deze op microcarrier gebaseerde 3D-invasietest maakt kwantitatieve evaluatie van meerdere aspecten van celinvasie mogelijk en wordt beschouwd als een snelle en zeer reproduceerbare methode voor de ondersteuning van celbiologische studies.

In **Hoofdstuk 3** hebben we de rol van het oncogen CREPT in positieve regulatie van celproliferatie, migratie en invasie van melanoomcellen in vitro opgehelderd, wat een potentieel therapeutisch doelwit vormt voor behandeling. De functie van CREPT in tumoren is geassocieerd met RhoA-geïnduceerde actine-organisatie en focale adhesie-assemblage.

Om kernmediatoren van tumorontwikkeling te karakteriseren, bepaalden we in **Hoofdstuk 4** het vermogen van melanoom afgeleide moleculen om de overleving van pericyten, op lange termijn onder hypoxische omstandigheden, te bevorderen en pericytmigratie in vitro te stimuleren. We identificeerde een fractie met een molecuulgewicht van minder dan 10 kDa voor overleven van pericyte en minder dan 30 kDa voor migratie van pericyte. Verdere karakterisering en validatie van specifieke moleculen die overleving en/of migratie stimuleren zou de ontwikkeling van behandeling gericht op pro-angiogene markers voor kwaadaardig melanoom kunnen vergemakkelijken.

In **Hoofdstuk 5** hebben we de pro-oncogene functie van HOXA9-upregulatie in het

vroege stadium van de transformatie van colorectale kanker (colorectaal adenoom) onderzocht. De nauwe correlatie met tumorgroei en vermindering van migratie suggereert dat HOXA9 een marker en promotor van premaligne laesiegroei is.

In **Hoofdstuk 6** worden de betekenis en implicaties van de resultaten beschreven in bovenstaande hoofdstukken uitgebreid besproken samen met toekomstperspectieven die aangeven hoe deze bevindingen bijdragen aan de verdere ontwikkeling van therapeutische strategieën.

Appendix

List of abbreviations

PhD portfolio

List of publications

Acknowledgments

Curriculum vitae

LIST OF ABBREVIATIONS

2D	two-dimensional
3D	three-dimensional
ACTB	Beta-actin
AML	Acute myeloid leukemia
ANGPT1	angiopoietin 1
ANOVA	Analysis of variance
APC	adenomatous polyposis coli
BMP4	bone morphogenetic protein 4
CCL	chemokine ligand
CDK	cyclin-dependent kinase
CDKN2A	cyclin-dependent kinase inhibitor 2A
CIMP	CpG island methylation phenotype
CM	conditioned medium
CRC	Colorectal carcinoma
CREPT	Cell-cycle related and expression-elevated protein in tumor
CTD	C-terminal domain
CXCL	C-X-C motif chemokine ligand
DMEM	Dulbecco's modified Eagle's medium
DNA	Deoxyribonucleic acid
EC	Endothelial cell
ECM	extracellular matrix
EDTA	ethylenediaminetetraacetic acid
ELISA	enzyme-linked immunosorbent assay
EMT	epithelial-mesenchymal transition
FAK	focal adhesion kinase
FBS	fetal bovine serum
FGF1	Fibroblast growth factor 1
FGF2	fibroblast growth factor 2
GFR	growth factor reduced
GO	Gene ontology
HOX	Homeobox
IGF1	Insulin-like growth factor 1
KEGG	Kyoto Encyclopedia of Genes and Genomes
LLC	Lewis lung carcinoma

MAPK	mitogen-activated protein kinase
MDCK	Madin-Darby Canine Kidney
MDS	myelodysplastic syndrome
miRNA/miR	microRNA
MMP	matrix metalloproteinase
MMR	mismatch repair
MOMP	mitochondrial outer membrane permeabilization
MSI	microsatellite instability
mTOR	mammalian target of rapamycin
MTT	3-(4,5-dimethylthiazol-2-yl)-2,5-diphenyltetrazolium bromide
NC	Negative control
NCAM1	neural cell adhesion molecule 1
NF1	neurofibromatosis type 1
NG2	Neural/glial antigen 2
NHEM	Normal human epidermal melanocytes
NS	not significant
OSM	oncostatin M
PBS	Phosphate Buffered Saline
PC	Pericyte
PCR	Polymerase chain reaction
PDGFC	platelet-derived growth factor C
PI3K	Phosphoinositide 3-kinase
PlGF	placental growth factor
POT1	protection of telomeres 1
PTEN	phosphatase and tensin homolog
PTGS2	Prostaglandin-endoperoxide synthase 2
qPCR	quantitative polymerase chain reaction
RNA	Ribonucleic acid
RPRD	regulation of nuclear pre-mRNA domain-containing protein
SCF	stem cell factor
SEM	standard error of the mean
SF	serum-free
shRNA	short hairpin RNA
SRB	sulphophodamine B
STAT3	signal transducer and activator of transcription 3

TCF4	transcription factor 4
TERT	telomerase reverse transcriptase
TGFB1	Transforming growth factor-beta1
TNF	tumor necrosis factor
TP53	tumor protein p53
TPA	tetradecanoyl phorbol acetate
TRAIL	tumor necrosis factor-related apoptosis-inducing ligand
UV	ultraviolet
VEGFA	vascular endothelial growth factor A
XIAP	X-linked inhibitor of apoptosis protein

PHD PORTFOLIO

Name:	Hui Liu	
PhD period:	2015-2020	
Department:	Pathology	
Research school:	Molecular Medicine	
Promoter:	Prof. dr. Adriaan B. Houtsmuller	
Co-promoter:	Dr. Timo L.M. ten Hagen	
Courses and Workshops	Year	ECTS
Gene expression data analysis using R: How to make sense out of your RNA-Seq / microarray data	2019	2.0
Ingenuity Pathway Analysis (IPA) Workshop	2019	0.4
The data analysis in Python	2019	1.7
Basic Course on 'R'	2018	2.0
Basic and Translational Oncology	2017	1.8
The workshop on InDesign CS6	2017	0.3
The workshop on photoshop and Illustrator CS6	2017	0.3
Basic Introduction Course on SPSS	2016	1.0
Introduction to GraphPad Prism	2016	0.3
Scientific Integrity	2016	0.3
Survival Analysis	2016	0.6
Course on Laboratory Animal Science	2016	3.0
Biomedical Scientific English Writing	2016	2.0
Microscopic Image Analysis: From Theory to Practice	2016	0.8
Biomedical Research Techniques	2015	1.5
Conferences, Seminars and Symposiums		
Molecular Medicine Day, Rotterdam, NL	2016-2020	3.5
ASCB EMBO Meeting , San Diego, CA, US	2018	2.0
Daniel den Hoed Day, Rotterdam, NL	2016-2017	2.0
JNI Scientific Meetings, Rotterdam, NL	2016-2019	2.0
Lab Science Day, Rotterdam, NL	2015-2019	1.0
Journal Clubs	2015-2019	1.0
Teaching		
Supervising two bachelor students for the 6-month internship	2017-2018	4.0
Supervising new users for migration assays	2017-2019	2.0

LIST OF PUBLICATIONS

1. A microcarrier-based spheroid 3D invasion assay to monitor dynamic cell movement in extracellular matrix.
Hui Liu, Tao Lu, Gert-Jan Kremers, Ann L.B. Seynhaeve, Timo L.M. ten Hagen.
Biol Proced Online 2020; 22:3.
2. Forced expression of HOXA13 confers oncogenic hallmarks to esophageal keratinocytes.
Kateryna Nesteruk, Vincent T Janmaat, **Hui Liu**, Timo L.M. Ten Hagen, Maikel P Peppelenbosch, Gwenny M. Fuhler
Biochim Biophys Acta Mol Basis Dis 2020; 25:165776.
3. CREPT promotes melanoma progression through both accelerated proliferation and enhanced migration by RhoA-mediated actin filaments and focal adhesion formation.
Hui Liu, Ann L.B. Seynhaeve, Rutger W.W. Brouwer, Wilfred F.J. van IJcken, Yang Liu, Yingying Wang, Zhijie Chang, Timo L.M. ten Hagen.
Cancers (Basel) 2019; 12(1). pii: E33.
4. HOXA9 mediates and marks premalignant compartment size expansion in colonic adenomas.
Vincent T. Janmaat, **Hui Liu**, Rodrigo A. da Silva, Pieter H.A. Wisse, Manon C.W. Spaander, Timo L.M. Ten Hagen, Ron Smits, Marco J. Bruno, Gwenny M. Fuhler, Maikel P. Peppelenbosch.
Carcinogenesis 2019; 40(12):1514-24.
5. Externally triggered smart drug delivery systems demand chemotherapeutics with kinetics superior for local delivery. (submitted to *Biomaterials*)
Tao Lu, Dieter Haemmerich, **Hui Liu**, Ann Seynhaeve, Gerard van Rhoon, Adriaan Houtsmuller, Timo ten Hagen
6. Depletion of p42.3 gene inhibits proliferation and invasion in melanoma cells.
Hui Liu, Min Zhu, Zhongwu Li, Yan Wang, Rui Xing, Youyong Lu, Weicheng Xue.
J Cancer Res Clin Oncol 2017, 143(4): 639-48.
7. Immunohistochemical detection of the BRAF V600E mutation in melanoma patients with monoclonal antibody VE1.
Hui Liu, Zhongwu Li, Yan Wang, Qin Feng, Lu Si, Chuanliang Cui, Jun Guo, Weicheng Xue.
Pathol Int 2014; 64(12): 601-6.
8. Expression of thyroid transcription factor-1 in primary colorectal carcinomas and the metastases.
Hui Liu, Zhongwu Li, Weicheng Xue.
J Clin Exp Pathol 2013; 29: 1065-8. Chinese.

ACKNOWLEDGMENTS

Confucius said, “Since the age of 15, I have devoted myself to learning; since 30, I have been well established; since 40, I have understood many things and have no longer been confused.” I started learning much younger than 15, and when I was 30, my PhD period approaches to the end. I’m not sure if I at my 40s would be no longer confused about many things, but here, at the moment, I can say with excitement and gratitude, “I’m on the way!”

At the last part of the thesis, I would like to thank everybody who kindly helped me during my PhD life. Doing a PhD is much more challenging and inspiring than I expected five years ago, but it also allows me to find out my potentials, strengths and weaknesses to make a better me. I am so pleased to have the support from all of you to overcome difficulties and gain my fruit.

First, I would like to give the sincere gratitude to my promoter Prof. Adriaan B. Houtsmuller and co-promoter Dr. Timo L.M. ten Hagen. Dear **Adriaan**, thank you for being my promoter and supporting my PhD to reach the final point. I really enjoy the time when we have a discussion about my research and my thesis, especially with your interesting questions. It is so much fun! Your encouraging smile makes me feel that nothing is too difficult to be solved. Dear **Timo**, thank you for everything you did for me and for my project. I still remember the first time when I came to the Netherlands, I was a bit humble and trying to adapt to all new things because that was also my first time abroad. You told me, “Don’t be shy. You are in the Netherlands!” Actually, your actions encouraged me more. I think I improved in a “Dutch way” now, at least to some extent. These five years are not easy for me. There are so many hard times in the middle that made me think of giving up a project, but you always inspired me to have one more try. Your expertise and support meant a lot to me.

Next, I want to thank my inner doctoral committee, esteemed Prof. Maikel P. Peppelenbosch, Prof. Curzio R.M. Rüegg and Prof. Niels J. Galjart for helping me improve this thesis. I really appreciate your precious time on reviewing my manuscript and your approval to make it a final thesis. I hope there will be opportunities for collaboration in my further study.

I would like to thank China Scholarship Council (CSC) for financial support on my study in the Netherlands for four years. This freed me from the stress of living abroad so I can focus on my research to get a doctorate degree.

Now I want to give my heartfelt thanks to our LEO (formerly LECO) group and those who have worked here. Dear **Ann**, we started our “back to back” relationship since my very first day. You are so reliable that almost every time I turned to you about my questions, you gave a solution or pointed to a direction. I cannot even start my animal experiments without your help on the workprotocol and further technical support. It was great to go to the conference with you in San Diego. I clearly remember our pajama-pizza time, the cheesecakes, the trip, and the photo with Santa Claus! Dear **Tao**, it was so nice to have you in the office with whom I could talk in native language. We had quite a few off-hour conversations about your work, my work, your future, my future, almost everything. Thank you for listening to my complaints and comforting me by sharing your worse experience (hahaha). I think you are a good researcher and you will finally get a deserved position. Dear **Wei**, thank you for seeing through that I am slow to warm up to people and actively talking to me. I admire that you have such a clear life plan and keep moving towards the goal all the time. Your passion and subjective initiative inspired me a lot. I hope you are now living the life you want in Norway. Dear **Mesha**, thank you for teaching me how to do cloning. I witness the tortuous and long journey of your PhD life, but you always show your smile and look like you can handle it. I am happy that this will come to an end this year and congratulations on the birth of your baby girl! Dear **Loes**, my paranymph, you are such a helpful person that I am not worried about seeking your help even for some trivial matters. Thank you for everything you did and willing to do for me. I wish you all the best of luck for you PhD and more. Dear **Wenqiu**, thank you for the fun of many dinners and conversations. I cannot imagine how hard it is for you to keep apart from your daughters and come here alone for an academic development. Hope you can finish it and get together with your family soon. Dear **Raymond**, thank you for so many blots and cell work for my project. You saved my bench time so I could concentrate on some reading and writing. Dear **Reza**, I was impressed by your laugh and profound knowledge of pharmaceuticals. It would be nice to learn from you some techniques about liposome in the future. Dear **Mike**, it is so nice to have you around in the lab. To all the colleagues and students in LEO, thank you for the company and all the memories we have. It has been a lot of fun working with you.

Dear Dr. Gert-Jan Kremers and Dr. Gert van Cappellen, thank you for the strong support on confocal microscopy and image analysis. I have learned a lot from you.

Dear Prof. Zhijie Chang and your group, thank you for providing essential materials and technical support for my CREPT project. I really appreciate your patience and detailed revision on my manuscript which was improved a lot. Hope we have the chance to collaborate further in the future.

Dear Dr. Wilfred van Ijcken and Dr. Rutger Brouwer, thank you for your help on performing next-generation sequencing and data analysis for my projects.

Dear Sandeep, thank you for your help on analyzing cell migration data with machine learning, and trying to teach a CS newbie how to use these codes.

To everyone I have had the pleasure to collaborate with, dear Gwenny, Kateryna, Vincent and Joyce, it was very enjoyable working with you. The discussion about projects, ideas and techniques also brought new thinking to my research.

Dear Qiushi, thank you for the company and friendship. We had so many laughs and fun time whether it was in a trip or hotpots at home. Your cheerfulness affected me a lot!

To all the Chinese friends I met in the Netherlands, dear Bin Wu, Jingjing, Shihao, Guannan, Wenhao & Yao, Ya Gao, You Zhou, Meng Li, Lu Wang, Chaoping, Kai & Nan, Changbin, Ruoyu, Shanshan, Jinluan, Guoying, Jun Liu, Ling Huang, thank you for all the beautiful memories and all the fun together.

To my dearest big family, thank you for your unconditioned love and constant support. You are the strongest backing to let me move forward without any worries. I hope to get together more often, and I will come back!

Special thanks to my husband, Dr. Guang Yang, for literally everything. You worried about my worries and cheered for my cheer, even more than me. It has been really hard time since we decided not to stay together for our personal development, and I hope we can settle down in the near future. Good luck for both of us!

CURRICULUM VITAE

Hui Liu was born on December 2nd, 1989 in Liaocheng, Shandong, China. She completed the primary and secondary education at her hometown. In 2007 she went to Shanghai Jiao Tong University to start her bachelor program in Clinical Medicine. After five-year medical knowledge learning and clinical training, she obtained her Bachelor's Degree of Medicine in 2012. At the same year, she was recommended for admission to a post-graduate program of Oncology at Peking University. She completed her first project of detecting BRAF V600E mutation in melanoma patients through immunohistochemical staining at the Department of Pathology in Peking University Cancer Hospital & Institute (supervised by Prof. dr. Weicheng Xue and Dr. Zhongwu Li). Later she joined Prof. dr. Youyong Lu's lab to investigate the abnormal expression of p42.3 gene in melanoma and the related molecular mechanisms. After defending the thesis enclosed both projects about melanoma study, she obtained the Master of Science degree in 2015. Inspired by the challenging cancer research, she decided to pursue a PhD at Erasmus Medical Center, Rotterdam, the Netherlands under the support of China Scholarship Council. The PhD project was conducted at the Department of Surgery and the Department of Pathology under the supervision of Dr. Timo L.M. ten Hagen and Prof. dr. Adriaan B. Houtsmuller, focusing on investigating dominant factors of tumor growth, angiogenesis and metastasis in malignant melanoma and colorectal carcinoma.

